Western Australian School of Mines
Department of Exploration Geophysics

Redatuming to Improve Hard Rock Seismic Data

Kai Fu Kevin Ung

This thesis is presented for the Degree of
Doctor of Philosophy
of
Curtin University

September 2017

Declaration

To the best of my knowledge and belief this thesis contains no material previously published by any other person except where due acknowledgment has been made.

This thesis contains no material which has been accepted for the award of any other degree or diploma in any university.

Signature: 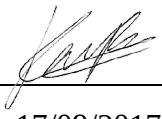

Date: 17/09/2017

Abstract

Data collected over hard-rock environments are generally distorted by complex wave propagations and contain a low signal-to-noise ratio (S/N). This is due to the complex near surface geology, which is also known as the regolith or overburden. The distortions induced by the near surface can be observed as diffractions, discontinuities or undulations in the reflection hyperbola of a seismic record in the shot domain. In general, redatuming is the virtual relocation of the acquisition surface, which produces an output that reflects the changes in this location. By doing so, seismic data can be significantly simplified by redatuming the acquisition surface to beneath the complex geology to remove any distortion from the near surface. Herein I presented, analyse and improve different wave equation redatuming techniques that improve seismic imaging in challenging near-surface conditions, such as those that can be found in many hard-rock settings.

I begin by studying finite difference redatuming under the category of model-driven techniques. Despite this method being theoretically the most accurate, it requires an input velocity model that accurately reflects the subsurface. In addition, issues related to spatial aliasing and finite difference noise can handicap this method. I performed a feasibility study to investigate the accuracy of this method when a detailed knowledge of the subsurface is unknown. I did this using a smoothed version of the input velocity model and a Root Mean Square (RMS) version. Both input produce an acceptable response, which is comparable with the result of using the accurate velocity model as an input, however, the RMS velocity redatuming output does lose accuracy in the far offsets and the undulation imprints can still be seen in the result.

Moving on from that, I look at Common Focus Point (CFP) redatuming, which is a data-driven technique to overcome some of the limitations of the previous method. With the CFP method, an input velocity model is not require, however, it relies on the presence of a reference reflector to redatum the acquisition surface to. This method is significantly faster and uses less computational power as it is computed by convolution with a focusing operator. This operator is the Green's function that represents the propagation between the recording surface and the output datum. There are several

possible approaches to estimate this operator, such as study of reflections and diffractions from the output datum. The original CFP focusing operators do not preserve the amplitudes of the redatumed data. I address this problem by introducing the obliquity factor used in Kirchhoff migration. To further attenuate the dipping artefacts introduced by this method, I added a simple mute process on the gathers before the summation to obtain the CFP gathers.

Since hard-rock seismic is generally distorted by diffractions from the complex overburden, I investigate the kinematics of diffracted waves for the purpose of acquiring the Green's function for CFP redatuming on synthetic data. Diffractions that were once considered as undesirable and destructive to seismic data have now become a potential source of useful information. I utilised this information to create the focusing operator, with the results being promising as the undulating imprints from the near surface are unravelled and a better representation of the reflector at a deeper subsurface is obtained.

Finally, I apply the CFP redatuming technique on two 2D surface seismic datasets collected in Western Australia and South Australia. The first data is from a sedimentary geology environment, which exhibits a low amplitude zone that is the subject of the redatuming. The second data is from a hard-rock environment with complex near surface geology, where the S/N was low throughout the data and reflection events are barely visible. The results from these datasets are encouraging despite suffering from poor data quality. The study shows the promise of CFP redatuming, as it uncovers reflectors and improve the continuity of reflection events in that area by removing any distortions caused by the subsurface above the new datum.

Acknowledgements

Firstly, I would like to express my sincere gratitude to my supervisor Associate Prof. Andrej Bona for the continuous motivation and support of my Ph.D study, his patient, motivation and immense knowledge. His guidance helped me in all the time of research and writing of this thesis. I could not have imagined having a better advisor and mentor for my Ph.D study.

Besides my supervisor, I would like to thank the rest of my thesis committee: Dr. Andrew Squelch and Dr. Mahyar Madadi for their insightful comments and encouragement. A special mention to my colleagues and staff in the Department of Exploration Geophysics, especially Aleksandar Dzunic, Javad Khoshnavaz, Sahadat Hossain, Pouya Ahmadi and Sasha Ziramov for their discussions and contributions in my work. I would also like to thank Robert Verstanding for proofreading my thesis.

This work has been supported by Deep Exploration Technologies Cooperative Research Centre (DET CRC) whose activities have been funded by the Australian Government's Cooperative Research Centre Program. I would like to acknowledge Pawsey Supercomputing Centre for the computational resources that was used throughout my thesis.

Last but not least, I would like to thank my family and partner for supporting me spiritually throughout writing this thesis and my life in general.

Table of Contents

Table of Figures

List of Tables

Chapter 1 Introduction

1.1 Mineral resources in Australia

Australia is host to a vast number of mineral commodities and these resources play a significant role in the economical wealth of the country. To date, mineral resources make up the largest export in the country. For example, by the end of 2012 Australia had the world's largest economic resources of gold, iron ore, lead, rutile, zircon, nickel, uranium and zinc and was ranked in the top six worldwide for known resources of bauxite, black and brown coal, cobalt, copper, ilmenite, lithium, magnesite, manganese ore, niobium, silver tantalum, tungsten and vanadium (McKay et al., 2014). In 2014, the mineral exports from Australia amounted to approximately $157 billon, which contributed to approximately 50 to 60 percent of all exported merchandise and goods (Britt et al., 2015). In the past, discovery of mineral deposits that were economically viable in Australia were made from outcropping or near outcropping geology that is exposed to the naked eye. These types of discoveries lead to low-cost exploration expenses. Figure 1-1 shows the comparison of discoveries and exploration expenditures in Australia from the period 1975 to 2011.

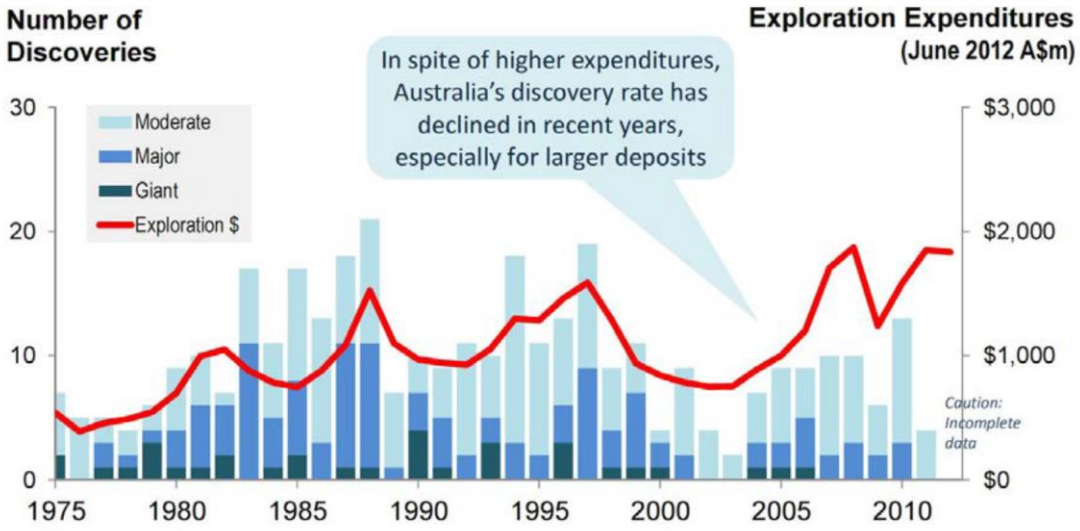

Figure 1-1: Comparison of exploration expenditure versus mineral discovery from year 1975 to 2011 (Schodde and Guj, 2012).

It is noted that during the 80s and 90s, there is a good correlation between the exploration expenses and the number of discoveries. However, over recent years there has been a significant decrease in the rate of discoveries, despite the increase in exploration expenses. This is due to the decrease in near-surface discoveries and the employment of expensive exploration techniques to uncover deeper-seated economically viable mineral deposits. Traditionally, non-seismic geophysical methods have been used to uncover mineral deposits by recording the physical properties such as density, magnetic susceptibility, radiometric signature and electrical properties. These techniques are generally used for near-surface exploration as they have limited spatial and depth resolution (less than 500m) and are deployed above the subsurface. For deeper-seated deposits, well logging is used where the physical properties are measured by lowering instruments into a hole penetrating the subsurface. This method is more costly and destructive to the environment. Figure 1-2 shows the depth where minerals were discovered from 1950 to 2010 for the Greenfield and Brownfield mine sites in Australia. Here we observe that despite having an increase in discoveries of deeper-seated deposits over the years, the main discoveries are still made at the near surface. This poses a concern as the near-surface search space will be depleted in the future.

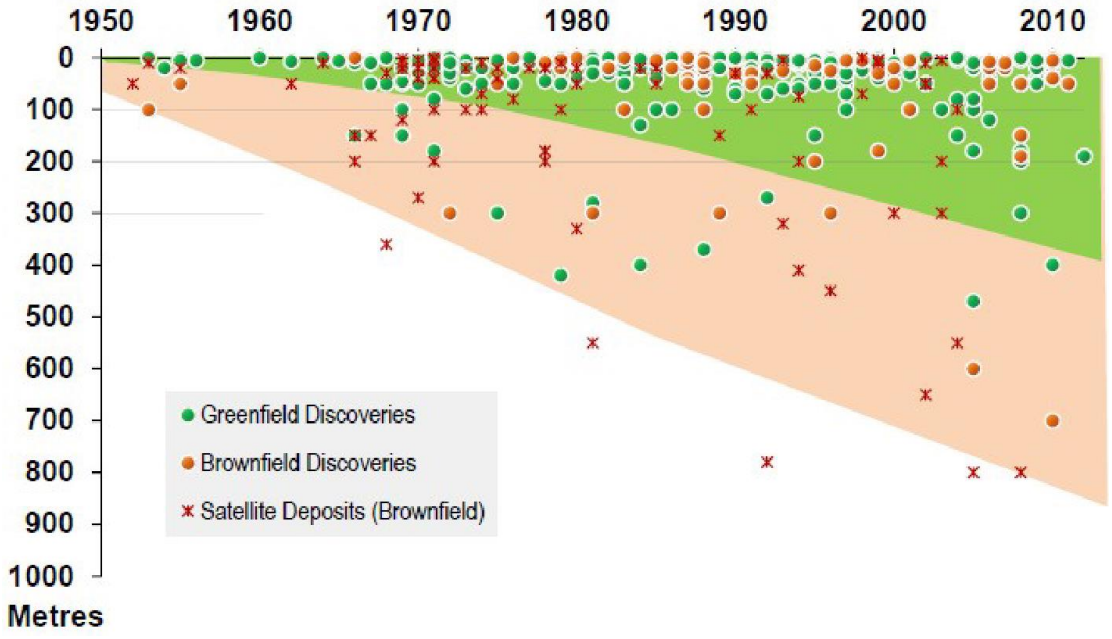

Figure 1-2: Depth of explored mineral deposits in Brownfield and Greenfield mine camps in Australia. Satellite deposits supplies ore to a central mill within an existing mining camp (Schodde and Guj, 2012). Despite making more discoveries in deeper regions over the years, primary discoveries are still done at the near surface.

With the depletion of near-surface mineral resources, it is apparent that new exploration tools must be developed to target deeper resources for the survival of exploration and mining industries in the future. To this end, the potential of the surface seismic method in the mineral industry for mine site characterisation and deeper target exploration has been growing over the past decade as it provides deeper penetration and a higher resolution compared to traditional non-seismic mineral exploration techniques.

1.2 Development of the seismic method for mineral exploration

The potential of using seismic methods as mapping tools in mineral exploration was first made known in 1980s by Green and Mair (1983) who studied seismic imaging in a complex fracture system at the Canadian Shield. Pretorius et al. (1989) showed the value of integrating both seismic and petrophysical methods to image key geological structures for mineral exploration. To date, there have been a number of 2D and 3D surface seismic and borehole seismic surveys performed in Canada, Europe, Australia and South Africa for mineral exploration and exploitation. In order for the seismic reflection method to target mineral deposits, three conditions are required: 1) the difference in acoustic impedance between target mineral and host rock must be sufficiently large to produce strong reflections; 2) the body of the target mineral should have a diameter larger than the width of the first Fresnel zone, and 3) the thickness of the target mineral should be more than a quarter of the wavelength to be resolved in seismic reflection (Salisbury et al., 2000).

Surface seismic methods in the past have been developed and used mainly in stratified sedimentary environments for hydrocarbon exploration where the geology is considerably flat and the physical properties of the lithology are homogeneous. Unlike in hydrocarbon exploration, mineral deposits are primarily found in hard-rock environments. This geological setting is covered by a diverse assemblage of igneous and metamorphic lithology with complex geological structures consisting of strong deformations such as faults, foldings, intrusions and fracture zones. This cover causes the scattering of seismic energy and introduces complex wave propagation to the recorded data. The acquisition and data processing of seismic reflection methods developed for oil exploration only found only limited use in mineral exploration in the

past due to a lack of knowledge of the environment. Preliminary challenges of using seismic reflection methods in mineral exploration includes the difficulty in detecting small targets, low reflection amplitudes, and challenges in interpretation due to a wide range of geological structures and velocities in the subsurface (Salisbury et al., 2003).

Salisbury and Snyder (2007) discussed some considerations to take into account to improve the quality of hard-rock seismic, which includes the use of denser acquisition a to overcome low S/N; a more complex processing workflow for imaging structures and locating small targets; the use of higher frequency for acquisition; the need to model the survey area in advance to determine the optimum location for receivers and to interpret data; and also laboratory testing to determine the impedance contrast of the target rock with the most common host rock. Urosevic et al. (2007) show the possibility of improving hard-rock seismic imaging through devising specialised data processing methodologies, which include velocity analysis and depth imaging techniques, in targeting specific mineral deposits in 2D seismic data. In their paper, Malehmir et al. (2012) summarised a few key points of recent development in hard-rock seismic methods from both industry and academia sources ranging from petrophysical studies to data acquisition, processing and imaging as well as 2D and 3D seismic modelling of mineral deposits and their host rock structures. The gradual increasing usage of seismic reflection methods for mineral exploration presents new opportunities for geophysicists and also brings about new challenges.

1.3 Research objectives

I start by pointing out the obvious—that the significant difference between soft-rock environments, where seismic has been used with great success for petroleum exploration, and hard-rock environments, where mineral deposits are commonly found, is in the complexities of their geology. Soft-rock environments are generally composed of various sedimentary rocks (shale, limestone, etc.), which are deposited in a near horizontal manner whereas hard-rock environments are made of strongly deformed assemblages of igneous and metamorphic rocks (granite, basalt, schist, etc.). These strong deformations can be present at both shallow and deeper parts of the subsurface in the hard-rock environments.

The term ‘near-surface cover’ is also known as overburden or regolith, which refers to any material overlaying the subsurface including interlayers or inclusions on loose or weathered material. These can influence the quality of the recorded seismic energy. Urosevic and Juhlin (2007) pointed out a number of near-surface issues when using reflection seismic methods in hard-rock environments. These include energy penetration, scattering, source generated noise, statics and coupling between sources and receivers that can lead to significant deterioration of seismic imaging. To avoid the near-surface issues, one can always bury the sources and receivers beneath the regolith and record from there; however, that is not an economically viable option.

The primary aim of this research is to improve seismic imaging for deeper target reflections by relocating the acquisition surface from the surface to a new virtual location beneath the near-surface complexities. This shall in effect produce a seismic image that is acquired at the new location in the subsurface, which is free from the near-surface effects. The term for this process is known as redatuming, which is defined by Berryhill (1979) as the upward or downward continuation of seismic data to redefine the reference surface on which the sources and receivers appear to be located. The simplest form of redatuming is known as static correction and is commonly used in processing to correct small elevation changes in the acquisition. In an environment with complex wave propagations, this method would be inaccurate as it uses the assumption of vertical rays. Therefore, a more accurate method is required, which in this case, is the wave equation redatuming technique.

Wave equation redatuming has long been used in the petroleum industry to improve seismic imaging by removing elevation statics or to mitigate the defocusing effects of certain geological bodies that cause deterioration of seismic energy, such as weathered zones or salt domes (Schuster and Zhou, 2006).

The main objectives of this thesis can be broken down into:

1. Investigation of both model-driven and data-driven wave equation redatuming techniques and the underlying principles in removing the complex propagation of seismic energy induced from the near-surface. This study is first done on synthetic dataset to determine the accuracy and feasibility of the methods.

2. Optimisation of the model driven redatuming technique to attenuate the artefacts and preserving the amplitude in the output. This is done by adding a simple mute in the process and using the Kirchhoff migration equation.

3. Field data often exhibit low S/N, which results in difficulties when applying wave equation techniques. Instead of treating diffractions as noise, I investigate an approach of using the kinematics of diffractions to estimate the Green's function needed for wave equation redatuming techniques which contains the imprints of the near surface to produce a more accurate result.

4. Application of the tested methods to field datasets to improve quality of imaging and to ascertain their use in real world applications.

1.4 Outline of thesis

In **Chapter 1**, a brief discussion on the importance of mineral resources for the Australian economy is discussed along with the review of the trend of mineral exploration. With the depletion of near-surface resources, a summary of recent studies on seismic reflection methods for deep exploration of mineral resources is presented along with the advantages and challenges. The research objectives are summarised at the end of the chapter, which focus on the adaption of wave-equation-based redatuming techniques for hard-rock environments where minerals predominantly deposit.

Chapter 2 is the literature review section where I first compare the wave equation redatuming and vertical ray tracing (static correction) redatuming techniques. Following that, a simple model is used to explain the general framework of the more accurate wave-equation-based redatuming process. Different methods of calculating the required Green's function operator are also presented. These methods can be classified into model-driven and data-driven methods.

Based on the literature review, I conclude that in hard-rock seismic environments, data-based wave equation redatuming techniques, such as Common Focus Point (CFP), is a more sensible approach as estimating a velocity model for the model-based method proves to be very challenging and time consuming. It is also readily extendible to 3-dimensional applications.

In relation to that, **Chapter 3** begins with the theory and methodology of the finite-difference redatuming technique, which is theoretically the most accurate method. In addition to this, I investigate the reciprocity theorem for different radiation patterns to allow for sources redatuming using the backpropagation method. This experiment is performed as a benchmark for the CFP redatuming output. A feasibility study is also performed to determine the accuracy of this method where a detailed knowledge of the subsurface is not known. This study will encompass the use of smoothed and RMS velocities as input model for the backpropagation method.

In **Chapter 4**, I explain in detail the concept of the CFP redatuming technique and apply it to a synthetic dataset. I also investigate the application of this method using an estimated focusing operator obtained through velocity analysis. In this chapter, I also discuss a novel approach in removing artefacts created from CFP redatuming technique through muting and amplitude preservation. In addition, I examine the kinematics of diffracted waves to estimate the Green's function for the CFP operator, which describes the propagation between the acquisition surface and the output redatumed surface.

Chapter 5 presents two case studies using the CFP redatuming technique on field data. The objective of applying the redatuming method here is to improve seismic imaging in low-resolution datasets.

Finally, in **Chapter 6**, the conclusions are drawn from the results of the previous chapters and recommendation for future research is presented.

Chapter 2 Literature review

Data processing plays an important part in improving the S/N of a recorded dataset. A well-processed data can facilitate the imaging to produce an accurate interpretation of the subsurface. Most of the existing seismic data processing algorithms, including imaging, are optimised based on the assumption that data are collected over a flat surface with very little variation to the structural and physical properties in the near surface. However, in reality this is rarely the case. Depending on the environment, land seismic acquisition can be met with significant variations in the elevations and complex near-surface geology that causes scattering of the seismic energy and distortion of reflection events. Distortions of reflection events can be observed as an unsmooth hyperbolic response or in some cases, discontinuities. This often leads to complicated processing with extensive assumptions on the velocities (i.e. velocities that are used for stacking, multiple removal, migration) being made. In addition to that, seismic data processed without consideration of the change in elevation and complexities in the near surface will result in a misleading interpretation of the subsurface. To compensate for this problem, processors often apply a process known as redatuming.

Redatuming is a time-varying shift that is generally applied during the pre-processing stage to transform data collected over an uneven surface to a flat surface. This process is also known as static correction. In this chapter, I discuss the limitations of conventional redatuming techniques in the presence of complex near-surface geology. Moving forward, I will introduce the wave equation redatuming technique that can be used to transform data accurately in the presence of complex geology. This technique is significantly more complicated when compared to static correction as it abides by the nature of wave propagation. An explanation of the general framework in using wave equation redatuming to transform the data is presented followed by different wavefield extrapolation techniques used for existing wave equation redatuming.

2.1 Static correction vs wave equation redatuming

In the simplest form, redatuming is known as static correction. This process is generally applied during the initial stage of processing to reference the data collected on an uneven surface to a flat surface. Distortions in seismic reflection methods due to variations in the acquisition elevation and the near-surface complexities can be significant and if not dealt with in the early stage can negatively impact standard processing sequences as they are not designed to account for this distortion. In addition, data that has not been compensated for these problems can also influence the imaging algorithm resulting in misleading interpretation. Generally, in the petroleum industry; variations in the acquisition elevation and near-surface geology are not significant and the use of static correction is sufficient to compensate for the distortion introduced. Static correction applies a vertical time shifts individually to each trace, which corrects for distortions caused by small variations in topographic elevation and near-surface complexities. A detailed overview of this method is discuss in a paper by Cox (1999).

However, there are limitations in using static corrections especially, in areas where the topography varies significantly or when complex near-surface geology is present, which introduces large emergence angle in the recorded data. Shtivelman and Canning (1988) explained that in the event where the emergence angle of the propagating wave is large, the use of static correction can further disorientate the reflection hyperbole, which will result in the degradation of wavefield-based processing, such as velocity analysis and stacking. This is because static correction use the assumption of vertical wave propagation in the computation. Figure 2-1 shows the difference between the true propagation path in the black line and the static corrected propagation path in the dash line in a situation where the emergence angle is large. For this problem, wave-equation redatuming methods, which take into consideration the true wave propagation paths, have been developed to accurately handle the transformation collected over significantly varying geology and topography. These methods use an approximation of one-way and two-way wave equations, which not only transforms the data to an ideal flat surface without introducing artefacts, but can also be used to simplify the data collected over complex near-surface geology. This can be achieved by virtually relocating the acquisition surface to a new datum beneath the complexities.

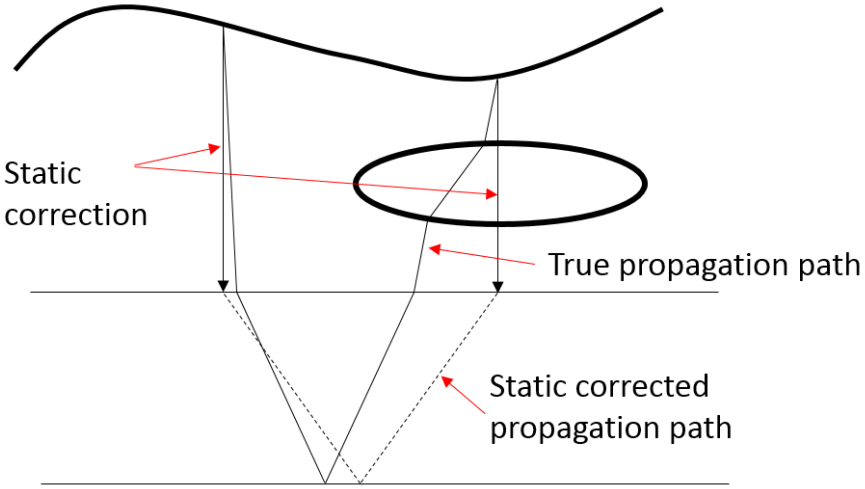

Figure 2-1: Comparison of true propagation path and assumed propagation path for static correction. Due to the vertical time shift applied for static correction, the assumption is not accurate for large elevation changes and also the presence of low velocity.

2.2 Wave equation redatuming framework

As mentioned above, wave equation redatuming is a numerical transformation of a surface-recorded data that takes into consideration the wave propagation path, through wavefield extrapolation, in such a way that the output observed is acquired at a different location. Theoretically speaking, this method virtually relocates the sources and receivers to a different location in the subsurface. By relocating the sources to a location in the subsurface, a portion of the downgoing wavefield will need to be eliminated whereas to relocate the receivers, a part of the upgoing wavefield will be removed. These upgoing and downgoing wavefields, known as one-way wavefield, are exact solution with moderate propagation angles, which is unlike a two-way wavefield data that accounts for both a downgoing and upgoing wavefield where, under linear assumption, is an exact solution that is valid for any propagation angle. The relationship between the two-way wave propagation and one-way wave propagation for a simple two-layer medium can be represented as:

$$\boldsymbol{X}(z_0, z_0) = \boldsymbol{W}^{-}(z_0, z_1)\boldsymbol{R}(z_1)\boldsymbol{W}^{+}(z_1, z_0), \tag{2.1}$$

where $\boldsymbol{X}(z_0, z_0)$ is the two-way propagation path between a source and receiver at datum z_0 that consist of the downgoing propagation operator, $\boldsymbol{W}^+(z_1, z_0)$, to the reflector at z_1, in which the wavefield is reflected by $\boldsymbol{R}(z_1)$ and then propagates upward to the surface, which is represented by $\boldsymbol{W}^-(z_0, z_1)$. This representation of the two-way propagation path of seismic data using the matrix notation was introduced by Berkhout (1982).

2.2.1 Two-way wavefield model representation of redatuming

Before diving into the complex wave propagation redatuming techniques, here is a simple representation of how redatuming operators, based on equation 2.1, are used to relocate the surface obtained data to a new datum in the subsurface. This illustration uses the **W R W** model formulated by Berkhout (1980). For a simple two-layer model (Figure 2-2), the propagation path of the seismic energy starts off at the source going downward, which is then reflected at a reflector and moves upward towards the receiver at the surface. The recorded two-way wavefield seismic data can be expressed in the matrix notation as follows:

$$\boldsymbol{P}(\boldsymbol{X}_S, \boldsymbol{X}_R) = \boldsymbol{D}(\boldsymbol{X}_R)\ \boldsymbol{W}(\boldsymbol{X}_R, \boldsymbol{X}_M)\ \boldsymbol{R}(\boldsymbol{X}_M)\ \boldsymbol{W}(\boldsymbol{X}_M, \boldsymbol{X}_S)\ \boldsymbol{S}(\boldsymbol{X}_S), \tag{2.2}$$

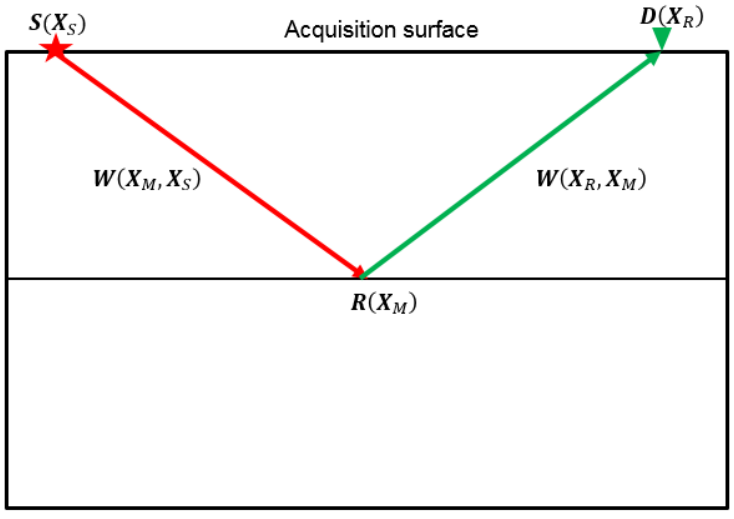

Figure 2-2: Propagation of seismic wavefield in a two-layer model. Seismic energy propagates downward before being reflected and propagate upward and is recorded at the surface.

where $\boldsymbol{P(X_S, X_R)}$ represents the response from the source wavelet, $\boldsymbol{S(X_S)}$, recorded by the receiver, $\boldsymbol{D(X_R)}$. $\boldsymbol{W(X_M, X_S)}$ represents the downgoing propagation of wavefield from the source at $\boldsymbol{X_S}$ to the reflector $\boldsymbol{R}$ at $\boldsymbol{X_M}$ whereas $\boldsymbol{W(X_R, X_M)}$ represents the upgoing propagation of wavefield from the reflector at $\boldsymbol{X_M}$ to the receiver at $\boldsymbol{X_R}$.

In general, the process of wave equation redatuming can be divided into two independent process. These processes are known as source redatuming and receiver redatuming. Source redatuming is done by removing the downgoing wavefield between the source at the recording surface and the new virtual source located at a new datum. By doing so, the observed seismic data can be interpreted as having the source buried at the location of the new datum and is recorded by the receiver at the surface. The one-way propagation matrix, $\boldsymbol{W}$, can be used in several ways. One use is in the recursive extrapolation scheme in the space-frequency domain that extrapolates the data from one location to another. This extrapolation accounts for both the lateral and vertical position while removing surface related multiples.

Redatuming of the source is illustrated in Figure 2-3. The extrapolation of the source downward to a new location involves a calculation of the wavefield propagation path between the input ($\boldsymbol{X_S}$) and new location ($\boldsymbol{X_{D1}}$), which is represented as $\boldsymbol{W(X_{D1}, X_S)}$. Here, redatuming is performed by removing the propagation path between the input source and the new source location. The matrix representing the propagation path of the redatuming of a single source is expressed as:

$$\begin{aligned}
&\boldsymbol{P}(\boldsymbol{X}_{D1}, \boldsymbol{X}_R) \\
&= \boldsymbol{D}(\boldsymbol{X}_R)\ \boldsymbol{W}(\boldsymbol{X}_R, \boldsymbol{X}_M)\ \boldsymbol{R}(\boldsymbol{X}_M)\ \boldsymbol{W}(\boldsymbol{X}_M, \boldsymbol{X}_S)\ [\boldsymbol{W}(\boldsymbol{X_{D1}}, \boldsymbol{X_S})]^{-1}\ \boldsymbol{S}(\boldsymbol{X}_S) \\
&= \boldsymbol{D}(\boldsymbol{X}_R)\ \boldsymbol{W}(\boldsymbol{X}_R, \boldsymbol{X}_M)\ \boldsymbol{R}(\boldsymbol{X}_M)\ \boldsymbol{W}(\boldsymbol{X}_M, \boldsymbol{X}_{D1})\ \boldsymbol{S}(\boldsymbol{X}_{D1}),
\end{aligned} \tag{2.3}$$

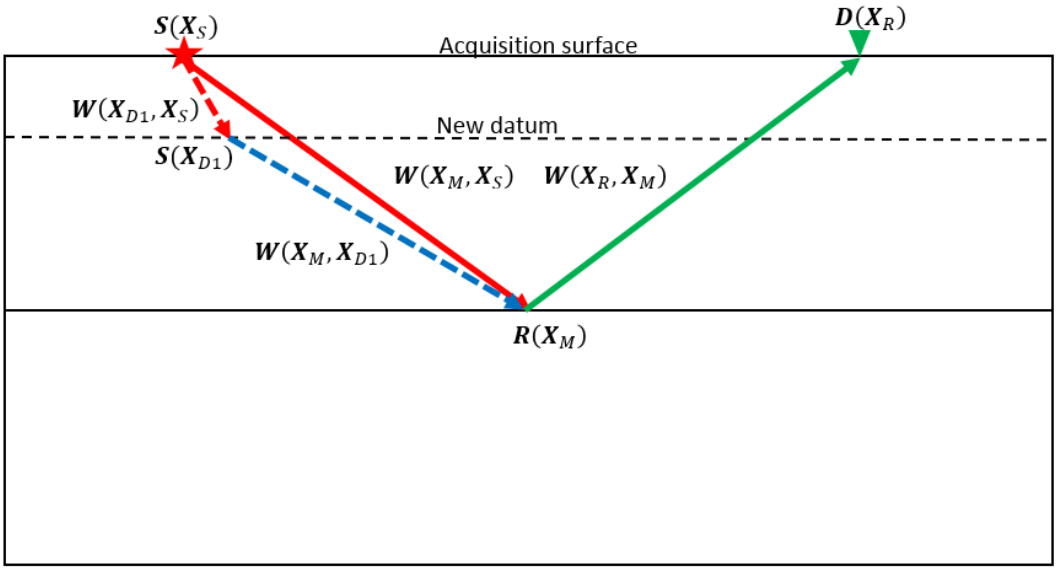

Figure 2-3: Source redatuming. The downgoing wavefield between the source at the surface and the new source at the used defined datum is calculated and removed from the data. By doing so, the recorded data can be interpreted as having the source at the new datum with the receiver at the surface.

After source redatuming, the output data will have a propagation path that follows the blue dash line going downward from the new source at $\boldsymbol{X_{D1}}$ and reflected upward following the solid green line to the receiver at the surface as shown in Figure 2-3. Receiver redatuming also follows the same concept as source redatuming; however, instead of calculating the downgoing wavefield, we will be calculating the upgoing wavefield between the new receiver location at the new datum and the receiver at the surface, the green dash line in Figure 2-4, then removing that from the data. From here, the complete matrix notation of source and receiver redatuming can be summarised as:

$$\begin{aligned}
&\boldsymbol{P}(\boldsymbol{X}_{D1},\, \boldsymbol{X}_{D2}) \\
&= \boldsymbol{D}(\boldsymbol{X}_R)\ [\boldsymbol{W}(\boldsymbol{X}_R, \boldsymbol{X}_{D2})]^{-1} \boldsymbol{W}(\boldsymbol{X}_R, \boldsymbol{X}_M)\, \boldsymbol{R}(\boldsymbol{X}_M)\, \boldsymbol{W}(\boldsymbol{X}_M, \boldsymbol{X}_{D1})\ \boldsymbol{S}(\boldsymbol{X}_{D1}) \\
&= \boldsymbol{D}(\boldsymbol{X}_{D2})\, \boldsymbol{W}(\boldsymbol{X}_{D2}, \boldsymbol{X}_M)\, \boldsymbol{R}(\boldsymbol{X}_M)\, \boldsymbol{W}(\boldsymbol{X}_M, \boldsymbol{X}_{D1})\ \boldsymbol{S}(\boldsymbol{X}_{D1}),
\end{aligned} \tag{2.4}$$

After applying both the source and receiver redatuming, the resulting data represents data that has its source and receiver located in the new datum in the subsurface instead of having the source and receiver at the surface. The new propagation path after source and receiver redatuming is represented by the blue dash line as shown in Figure 2-4. Figure 2-5 presents the comparison of propagation path before (solid line) and after (dashed line) redatuming. The computation of this upward and downward wave propagation path, between the new datum and the recording surface, can be achieved through numerous existing wavefield extrapolation operators that will be explained in section 2.3. The explanation here is done with a source and receiver pair; however, field seismic acquisition consists of an array of sources and receivers. Wave equation redatuming can be applied for post stack data with zero-offsets based on an extrapolation scheme or to pre-stack data where the same extrapolation algorithm can be used to redatum the sources and receivers in the common receiver gathers and common source gathers respectively.

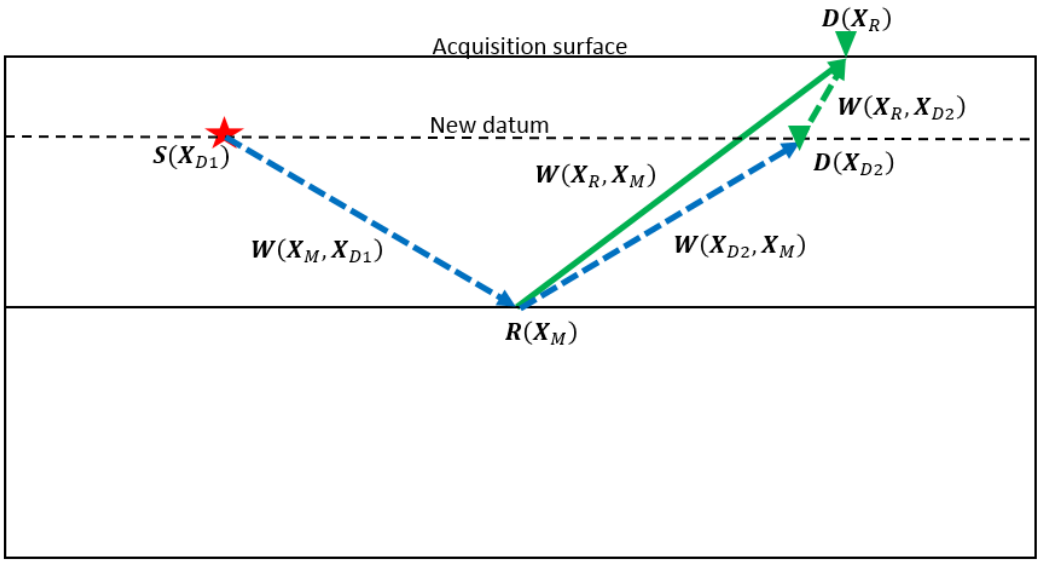

Figure 2-4: Receiver redatuming. The upgoing wavefield is calculated between the new receiver location and the receiver at the surface and is then removed from the data. This will result in a data observed as having being recorded at the new datum instead of the surface.

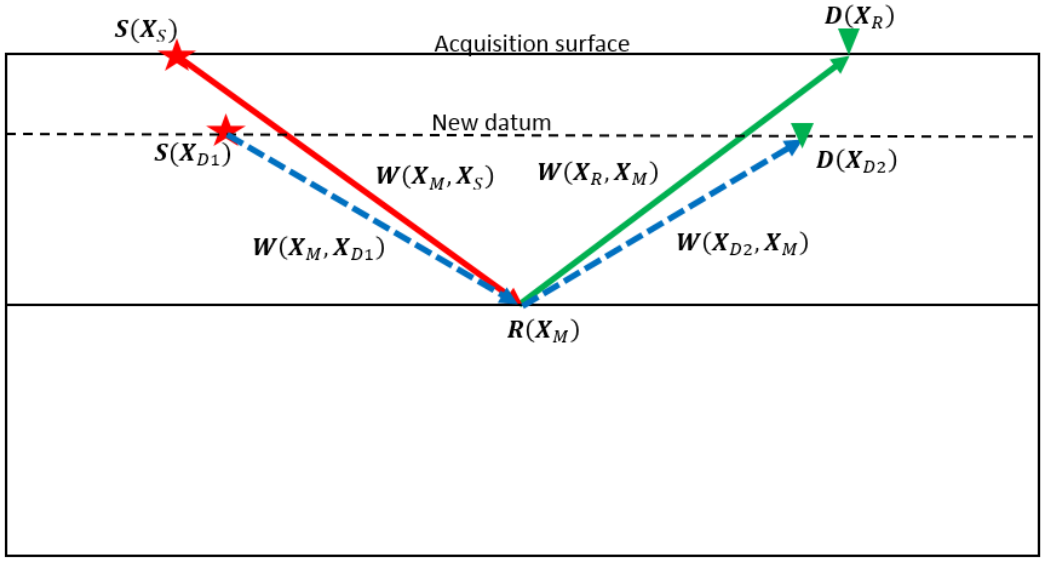

Figure 2-5:Solid lines represent the original propagation path recorded and the blue dotted lines represent the propagation path observed after performing source and receiver wave equation redatuming.

2.3 Wavefield extrapolation operators

Wave equation redatuming techniques have long been used in the oil and gas industry, often to remove elevation statics or to reduce defocusing effects due to complex geology and velocity in the subsurface (Tinivella et al., 2017; Barison et al., 2011; Bean and Martini, 2010; Larkin and Levander, 1996). This complex geology can come in the form of weathering zones or salt domes. The idea of wave equation redatuming, unlike static corrected redatuming, is to apply a time shift to the data in a manner consistent to the wave propagation path by estimating the Green's function of upward or downward wave propagation between the recording surface and the new user-defined surface. This process then attempts to compute the data from the initial recorded surface in such a way that it appears to be recorded at the newly defined surface. This significantly simplifies subsequent processing steps and ensures that processes that work with hyperbolic form, or even more complicated trajectories are consistent with the wave propagation and can be accurately applied. To date, there are a number of wavefield extrapolation methods which are used in wave equation redatuming. These can be categorised into model and data driven.

2.3.1 Model driven

Wavefield extrapolation method using an input velocity model can be used for post-stack and pre-stack data, which requires the separation of the extrapolation of sources and receivers. It can be categorised into three different methods: namely the Kirchhoff summation, phase shift, and finite difference methods. The method for Kirchhoff summation was first introduced by Berryhill (1979) for the use on post-stack data, which was applied to zero-offset data. He then later extended this method to pre-stack data (Berryhill, 1984) by applying the extrapolation algorithm to common source gathers and common receiver gathers. This method implements the Kirchhoff integral derived from the scalar wave equation to apply a downward or upward continuation to the data. The transformation of the wavefield from one datum to another, as illustrated in Figure 2-6, can be express in the frequency domain as:

$$P_j(w) = \sum_i A_{ij}\sqrt{-iw}P_i(w)e^{iw\tau_{ij}}, \tag{2.5}$$

where P_j is the recorded pressure field in the new datum, P_i as the input pressure data, A_{ij} describes the amplitude scaling term, and τ_{ij} being the travel time between the input location, i, and output location, j. This equation can also be express in time domain as:

$$P_j(t) = \sum_i A_{ij}D_{\frac{1}{2}} * P_i(t - \tau_{ij}), \tag{2.6}$$

where $D_{\frac{1}{2}}$ is a convolution operator corresponding to frequency domain multiplication by $\sqrt{-iw}$, which is used for a far-field approximation of the wavefield extrapolation. The Kirchhoff integral used for transforming the wavefield from one datum to another can be interpreted as calculating the weighted sum of delayed wavefield components of the data (Berryhill, 1979). The amplitude parameter, A, and time shift, τ, can be formulated from the Green's function describing the wave propagation between the new and old datum. Presently, this method has been developed for the use of a constant velocity environment. In complex velocity media, the computation of the Green's functions becomes significantly more complicated (Bevc, 1995).

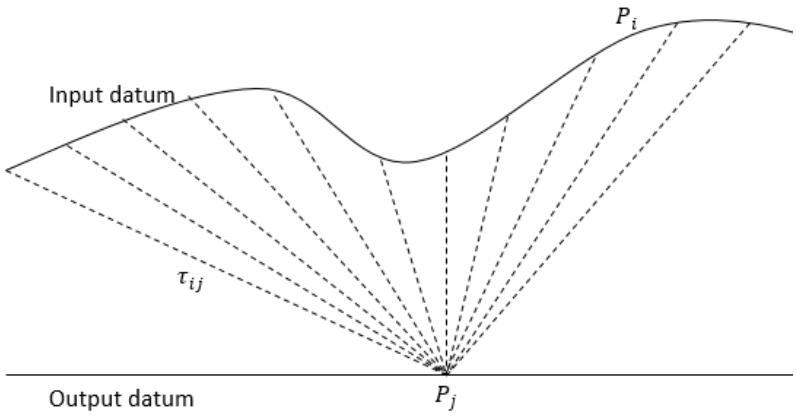

Figure 2-6: Schematic representation of the Kirchhoff downward extrapolation corresponding to implementation of equation 2.5. Each input trace $\boldsymbol{P_i}$ is filtered, time shifted according to $\boldsymbol{\tau_{ij}}$, scaled and summed into output trace $\boldsymbol{P_j}$.

Gazdag (1978) introduced the downward continuation of data using the phase shift method. Unlike the Kirchhoff summation method, which is performed in the space domain, this method is applied in the wavenumber-frequency domain. The wave-extrapolation formulation for downward or upward continuation of data can be written in 2-dimension as:

$$P(k_x, z = z_0 - \Delta z, w) = P(k_x, z = z_0, w)e^{ik_z \Delta z}, \tag{2.7}$$

The transform of data using this method can be described as a simple multiplication of the recorded data with the phase shift factor, which is the multiplication of the interpolated depth step, Δz, and the vertical wavenumber, k_z. The advantage of this method is the simple implementation and fast computation. However, by assuming k_z to be constant for depth intervals, the implementation has to be done in a recursive way in order to handle vertically varying velocities correctly, which is only stable for small lateral variations of velocities. In the event of complex laterally varying velocities, Gazdag and Sguazzero (1984) introduce an interpolation step after phase shift extrapolation of the wavefield to the desired datum known as the Phase Shift Plus Interpolation (PSPI) redatuming method, which can handle complex variations of lateral velocities. In this approach, a higher computational effort is required for better accuracy.

The finite difference method is theoretically the most accurate redatuming method, which is based on the idea of reversibility of the wave equation. The idea was drafted by Claerbout and Doherty (1972) where the wave equation between the old datum and new datum is computed using the finite difference equation, therefore making it the most computationally intensive method. The wave extrapolation is performed by computing the differential equation from the dispersion relation, which is later solved using the finite difference equation:

$$\frac{\partial P}{\partial z} = \frac{iw}{v}\sqrt{1 - \frac{v^2 k_x^2}{w^2}}P, \tag{2.8}$$

The finite difference wave equation derives the one-way wave propagation (Equation 2.8) to expand the input wavefield at any given point in space and time through numerical integration. In order to extrapolate the wavefield towards a certain location, all points in between need to be calculated and stored, making this method demanding in terms of computational memory.

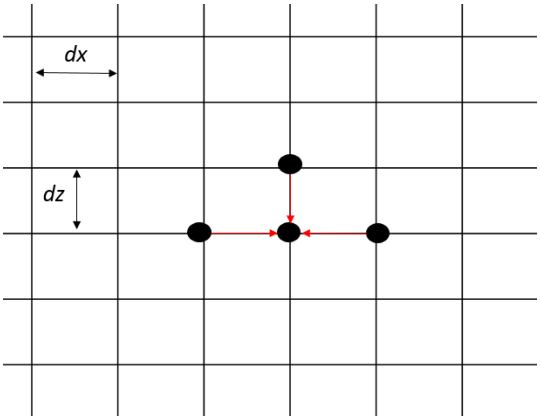

Figure 2-7: Schematic representing wavefield extrapolation using the finite difference method.

This method can handle both lateral and vertical velocity variations and in a complex velocity situation, and is limited to the availability of computational resources. In the event where computational resources is not a concern, a densely sampled velocity model can be used to define complex structures, such as dipping events, and strong lateral variation. Doing this would increase the computational time and memory as the solution to the wave equation would need to be solved at each grid point and the value

would need to be stored. The trade-off for having a densely sampled velocity model is that the finite difference method would need to solve the wave equation in each sample and store the value therefore taking up more computational resources. Joseph et al. (2016) studies the effects of grid size on computational time using the finite difference scheme on a two layer model and shows that a smaller grid size significantly increases the computational time for running the finite difference scheme. This does not pose a serious issue for a 2D survey; however, the same cannot be said for a 3D situation.

Bevc (1995) presented in his thesis a detailed comparison of these methods using a synthetic data to compute the upward and downward continuation of the data on a zero-offset seismic section. In this study, he noted that the Kirchhoff summation method generated the best result with minimal artefacts compared to the phase shift and finite difference methods. In addition to that, a regularly sampled grid is required for the computation of the finite difference and phase shift methods, which proves to be a great disadvantage compared to the Kirchhoff summation method. The Kirchhoff method has been widely used in for redatuming of 2D and 3D dataset. On the other hand, the finite difference and phase shift method are more commonly used for a 2D migration scheme.

All three of these methods suffer from a common problem. They require an accurate and sufficiently sampled input velocity model for their computation. For the Kirchhoff summation case, the amplitude factor and time shifts required to transform the data from one datum to another need to be known everywhere. In the event of a sparse dataset, artefacts and an incorrect amplitude of the real event will be generated in the output. For the phase shift method, calculation is done in the wavenumber-frequency domain therefore requiring calculation of the Fourier transform. This would require a regularly sampled input data. Lastly, for the finite difference method, in addition to requiring a regular sample model, the model requires denser samples when strong lateral variations are present. This is to avoid the generation of artefacts such as finite difference dispersion and spatial aliasing. This will in turn further increase the computational resources needed to perform this redatuming method.

2.3.2 Data driven

The significant shortcoming of model-based wave equation redatuming, which requires an accurate input velocity model, has introduced a new approach to redatum the sources and receivers, which can be derived from the data itself without the complicated process to acquire an accurate velocity model. This new redatuming technique is based on cross-correlation of seismic data with an operator. A number of contributions have been made in this area which includes Common Focus Point (Berkhout, 1997a, 1997b); Reverse time acoustic (Fink, 1992); Daylight imaging (Rickett and Claerbout, 1999); interferometric coda imaging (Wapenaar et al., 2002); and Virtual-source imaging (Bakulin and Calvert, 2004) just to name a few. Fundamentally, these methods are performed through a weighted correlation of the traces with a redatuming operator followed by a summation across all sources or receivers in the common receiver or source gather respectively. The difference between the mentioned methods is the choice of the weighted correlation used. A majority of cross-correlation redatuming relies on having either the sources or receivers buried in the subsurface (e.g. the vertical seismic profiling method) with some exceptions like the Common Focus Point (CFP), where both sources and receivers can be located on the surface to perform the redatuming.

The underlining theory of the cross-correlation method can be illustrated in Figure 2-8. If we have a source at the surface, **s**, and receivers in the subsurface, **g**', as shown in Figure 2-8, two events that are likely to be recorded are given by the operator:

$$A(\boldsymbol{s}'|\,\boldsymbol{s}) = e^{iw(\tau_{s's})}, \tag{2.9}$$

which represents the direct wave recorded at **s**' and:

$$B(\boldsymbol{g}'|\,\boldsymbol{s}) = e^{iw\left(\tau_{s's}+\tau_{x's'}+\tau_{g'x'}\right)}, \tag{2.10}$$

which represents the wave from the source that is reflected and recorded at receiver at **g**'. These two events share wave propagation from **s** to **s**', so the correlated data will be:

$$A(\boldsymbol{s}'|\,\boldsymbol{s}) * B(\boldsymbol{g}'|\,\boldsymbol{s}) = e^{iw\left(\tau_{x's'}+\tau_{g'x'}\right)}, \tag{2.11}$$

where $\tau_{s's}$ has been removed. However, in reality, the location of **s'** is not known. In addressing this problem, model-based redatuming utilises the stationary phase theory. This summation allows for a dominant response at the stationary point that corresponds to the propagation path, therefore resulting in the application of a correct time shift for redatuming (Schuster et al., 2004).

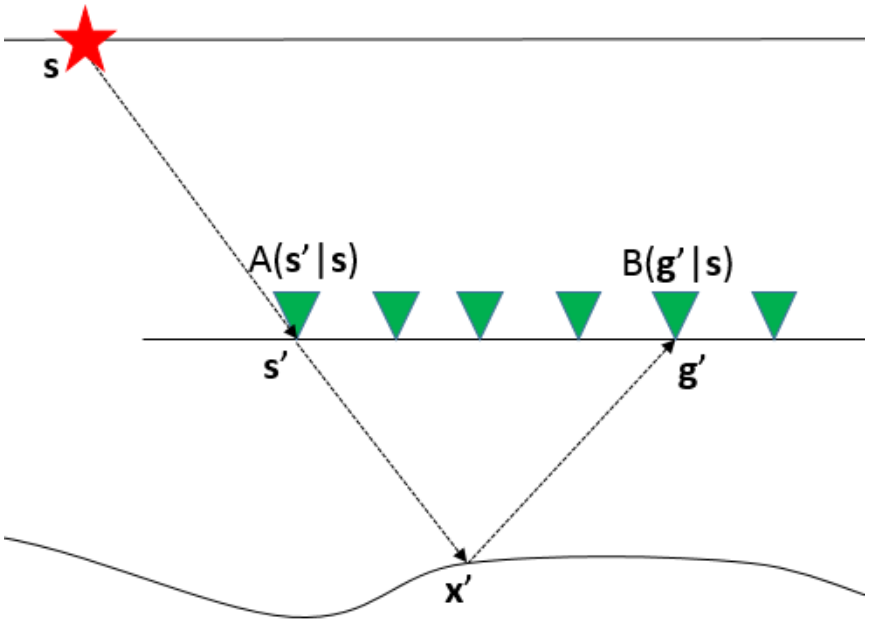

Figure 2-8: Propagation path from source at surface with buried receivers. Correlation method removes wave propagation which shares the same path between receivers at s' and r'.

Chapter 3 Model driven: Finite difference using backpropagation

The Finite difference wavefield extrapolation method is the most accurate technique for the redatuming of data when a detailed knowledge of the subsurface is known; however, it has not been popular among processors in the past due to the high computational resources required. In this chapter, I explore the use of this technique to overcome complex near-surface problems in seismic reflection. I will first introduce the underlying concept of finite difference for wavefield extrapolation, which is based on the reversibility of the propagation of the wavefield in the use of redatuming. Thereafter, I will discuss and examine the use of reciprocity theorem to redatuming the sources. Further, I shall present and examine the finite difference redatuming method on a synthetic data with an accurate velocity model followed by a feasibility study a using different input velocity model. This method is implemented using a two-dimensional, second-order finite difference solution of the two-way acoustic wave equation. It should be noted that this method is not the most practical approach in performing redatuming due to the requirement of a sufficiently accurate and densely sampled input velocity model and in this instance, is used as a benchmark for other wave-equation redatuming techniques examined in this thesis. Redatuming is computed with the use of one of Australia's most powerful computational resources, the Pawsey Supercomputing Centre.

3.1 Time reversal of the wavefield

The reversibility of time in wave physics is a phenomenon with many applications in areas such as medical imaging and therapy, the non-destructive evaluation of solid media to detect flaws, and underwater acoustics. A cinematographic example of this time reversal theory can be expressed as watching a film in reverse order where the frames are progressing in reverse chronology, which will give an impression of going back in time (last-in-first-out scenario). George Stokes was perhaps the first to appreciate the significance of time reversal theory where he considered the classical problem of reflection and transmission of energy through an interface separating two media (Hecht, 1987). Stokes verified that the recorded signal, p(**r,**t), and the time

inversion of this signal, p(**r**,-t) have the same solution to the wave equation and that this is true for all types of waves.

The mathematical and physical understanding of time reversal is complicated; however, several studies on the one-dimensional case (Sølna, 2002) as well as three-dimensional waves gives us a clear understanding on this unique theory. Fink (1996) describes the principles underlining the time-reversal theory in a time-reversal cavity experiment. In his experiment, an acoustic source is located inside an inhomogeneous medium with transducers surrounding the medium, as shown in Figure 3-1. The transducers record the propagating field, $p(\mathbf{r}_s, t)$, and then re-emit the recorded signal in a time-reversed manner $p(\mathbf{r}_s, T-t)$. He observed that the time-reversed signal focuses at the source location. Due to diffraction effects, details of dimensions smaller than the shortest wavelength are lost, thus fine details that can be imaged by high frequencies are lost causing degradation in field reconstruction.

The properties of time-reversal in random media include: (i) refocusing of scattered signals at a given deterministic time and (ii) statistical stability of the refocused pulse in an inhomogeneous or multi-scattering medium (Fouque et al., 2007). Time reversal, also known as backpropagation of signal, using the finite difference method can be easily implemented as it is just the inverse of forward modelling. Figure 3-2 shows the comparison of forward modelling versus backpropagation of a recorded data. In forward modelling, a single impulse source emits a wavefield that propagates in an expanding spherical manner throughout the medium away from the source. In backpropagation, the recorded wavefield signals are reverse in time and re-emitted into the medium at their respective recording location. With the focusing characteristic of backpropagation, the wavefield backtracks its propagation path which can be observed as energy collapsing in a spherical manner and focusing at the location of the source. In addition to this, the statistical stability property of the time-reversed signal implies that even in an inhomogeneous medium, where the propagation path of the wavefield can be complicated due to scattering, backpropagated signals are able to refocus near the source (Papanicolaou et al., 2004).

For redatuming purposes, this would mean that any complexities induced from a shallow depth can be removed using backpropagation when a detailed knowledge of

the complexities is known. In the time reversal cavity example (Figure 3-1), receivers are placed in all directions surrounding the source and result in a time-reversed signal that backpropagates perfectly following any scattering, reflection and refraction that was encountered in the forward direction. However, the real-world scenario does not allow for such luxury and the signal recorded is usually made with a limited angular aperture where a small number of waves propagated by the source are recorded. This therefore limits the backpropagated signal and the focusing quality while introducing artefacts to the data such as edge effects as illustrated in Figure 3-2.

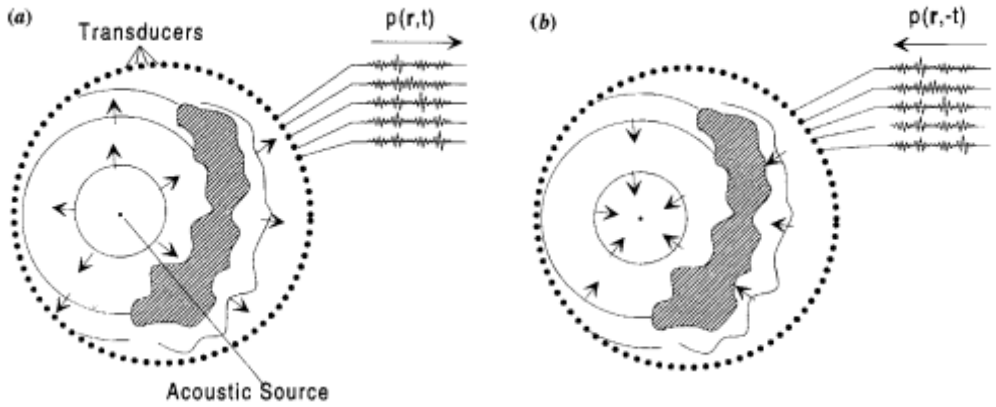

Figure 3-1: Time reversal cavity explanation by (Fink, 1996). (a) Recording of data: A closed cavity is filled with receivers to record the propagation of energy from a point like source in the cavity. (b) Time-reverse: Recorded pressure response is time reversed and re-emitted into the cavity at the point of recording. The time-reversed pressure field back propagates and refocuses exactly on the initial source.

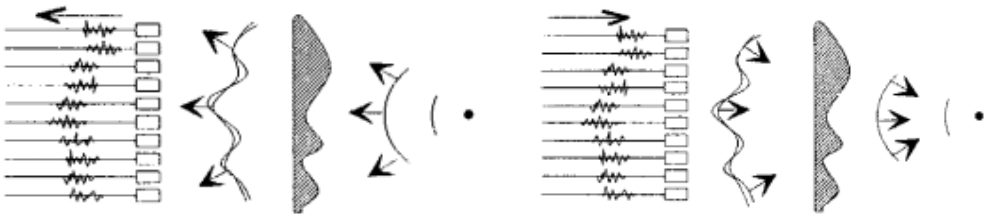

a) Forward modelling b) Backpropagation

Figure 3-2: Forward modelling versus backpropagation of a signal recorded with an array of receivers through an inhomogeneous medium (Fink, 1996). In forward modelling, the source emits a signal that travels through the medium and is recorded by the receivers. To perform backpropagation, the recorded signal is reversed in time and re-emitted into the medium. The backpropagation of signals will refocus at the source's location.

3.2 Backpropagation in redatuming

To illustrate the use of backpropagation to redatum the sources and receivers, I use a simple 3-layer velocity model, as shown in Figure 3-3. In this synthetic example, the acquisition consists of a split spread geometry of one source and 80 receivers with a spacing of 1 m at the surface where z=0 m. The velocity model includes an undulating interface with the purpose of introducing non-hyperbolic characteristics to the reflection event from the flat target reflector at 700 m. Figure 3-4 shows the forward propagation path of the seismic signal away from the source to the target reflector and back to the receivers at the surface. As the signal propagates downward, part of it is reflected and transmitted at the undulating interface. A change in the transmitted signal is observed as it further propagates downward due to the lateral and vertical changes of the velocity in the medium beneath the undulating interface, as observed at 0.27s. This signal then propagates upward as it is being reflected from the flat reflector. This upgoing signal then passes through the undulating interface again and is further distorted with undulating characteristics, as seen in the snapshot at 0.75 s. This would produce a seismic record that has an undulating reflection response from events deeper than the undulating interface. The recorded data at the surface is shown in Figure 3-5. The direct and reflected waves from the undulating and flat reflector are labelled with DW, R1 and R2 respectively.

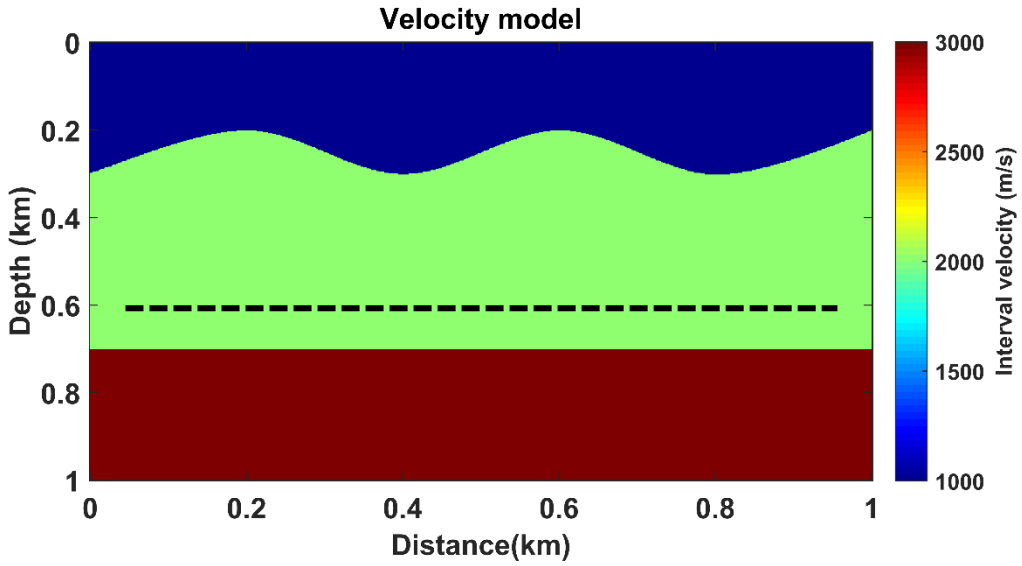

Figure 3-3: Interval velocity model to study the backpropagation technique in removing near-surface effects on recorded seismic data. Undulation seen in the first reflector is used to introduce non-hyperbolic nature to the recorded seismic data. Dash lines indicate the new receiver location after redatuming.

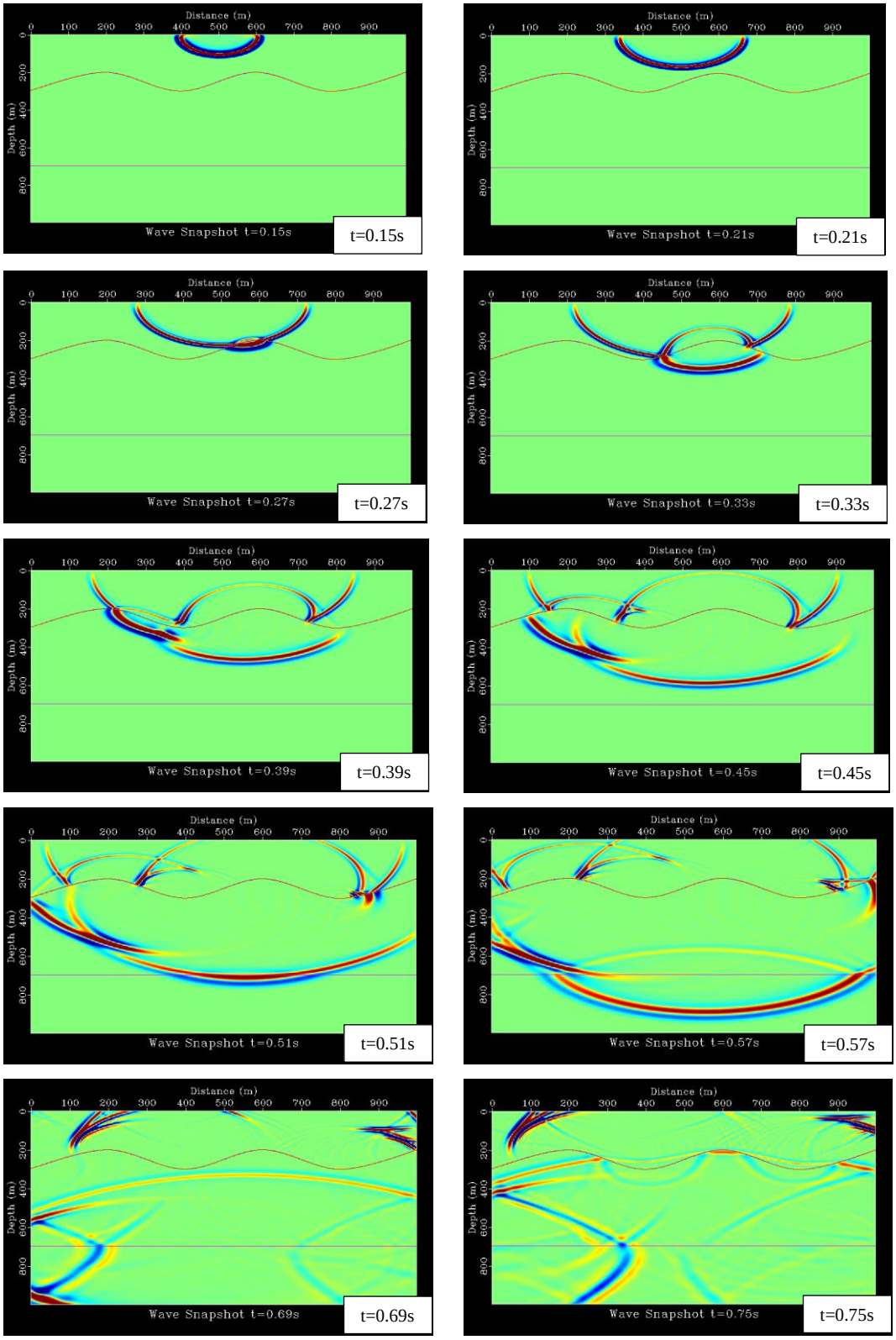

Figure 3-4: Forward propagation of seismic signal in the velocity model in Figure 3-3. As the wave expands and propagates through the undulation to the reflector and back, the hyperbolic nature of the reflector is contaminated by the effect of the undulation. This effect is clearly seen in t=0.81 s.

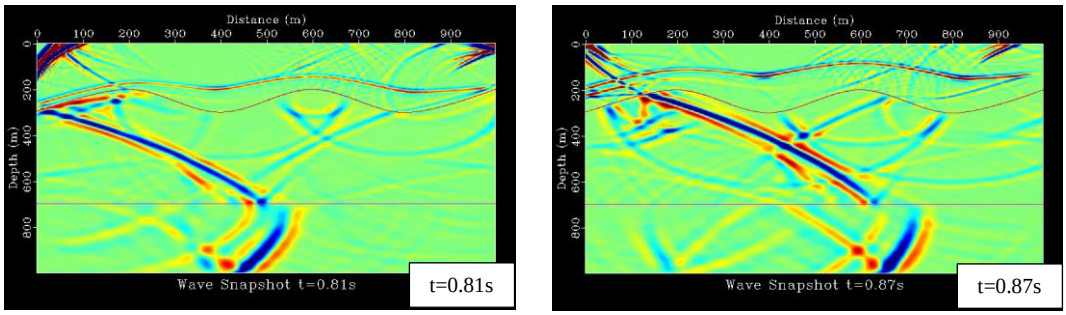

Figure 3-4: continued—wave propagation snapshots from 0.81 s to 0.97 s through the velocity model.

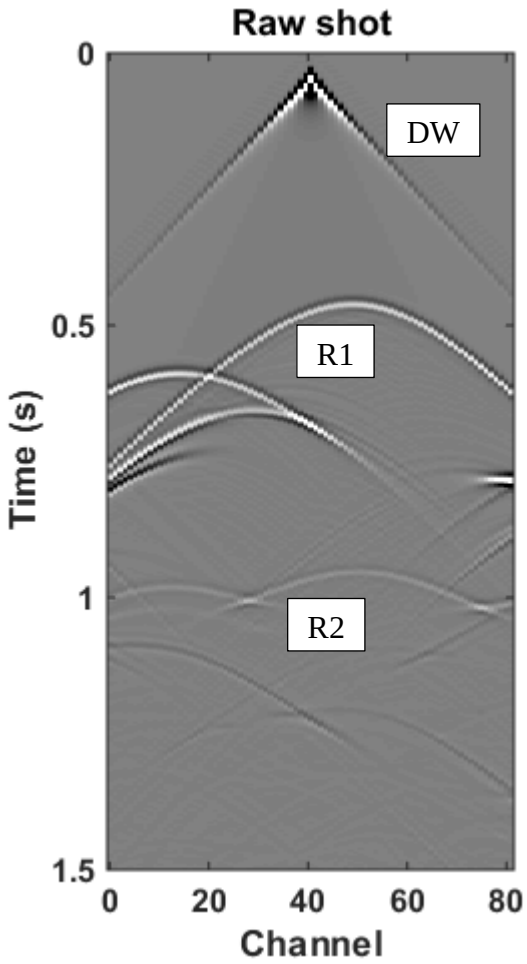

Figure 3-5: Seismic response corresponding to forward modelling using the velocity model in Figure 3-3. The notation DW, R1 and R2 represents the direct wave and the reflection response from the undulating and flat reflector respectively.

To perform the backpropagation, the recorded data as shown in Figure-3-5 needs to be time-reversed before re-emitting it back into the model. This means that each recorded trace needs to be flipped in the time domain, as shown in Figure 3-6. This time-reversed trace is then used as the input signal for a source located at their corresponding recorded location. The input velocity model for this backpropagation experiment is only required to contain the information of the undulating interface, as shown in Figure 3-7, as we are only interested in removing the effects of this structure in the recorded data. In order to reconstruct the flat reflector response after redatuming, the new acquisition surface will have to be above this target reflector. In this instance, the new receiver array location is located at 600 m depth and is 100 m above the flat reflector. This is shown in Figure 3-3 as the black dashed line. The progress of the backpropagated wavefield is shown in Figure 3-8 from 0.54 s to 0.87 s.

One can observe that as the reflection from the flat reflector backpropagates and passes through the undulating reflector, it unwinds the imprints that the undulating interface introduced earlier on. This transformation is seen between the times 0.72 s to 0.81 s during backpropagation. The recording of the backpropagation of the wavefield at the new receiver array location is shown in Figure 3-9(a) after the time is reversed. It is observed that the reflection response from the flat reflector after redatuming the receivers now shows a smoother hyperbolic characteristic as opposed to the data recorded from the surface. Artefacts seen above the targeted reflection event, R2, from the backpropagated data are from reflections off the boundaries of the velocity model and can be eliminated by using perfectly absorbing boundaries or by making the model large enough so that these reflections are not recorded. The procedure explained in this section only represents the receivers redatuming as we have only removed the imprints on the upgoing wavefield to the receivers and have not considered the imprints from the downgoing wavefield from the source. This is why the result does not accurately show the reflection response from the flat reflector if the effects from the undulating interface are completely removed as the peak of the hyperbola should be in the centre of the data in the split spread acquisition configuration.

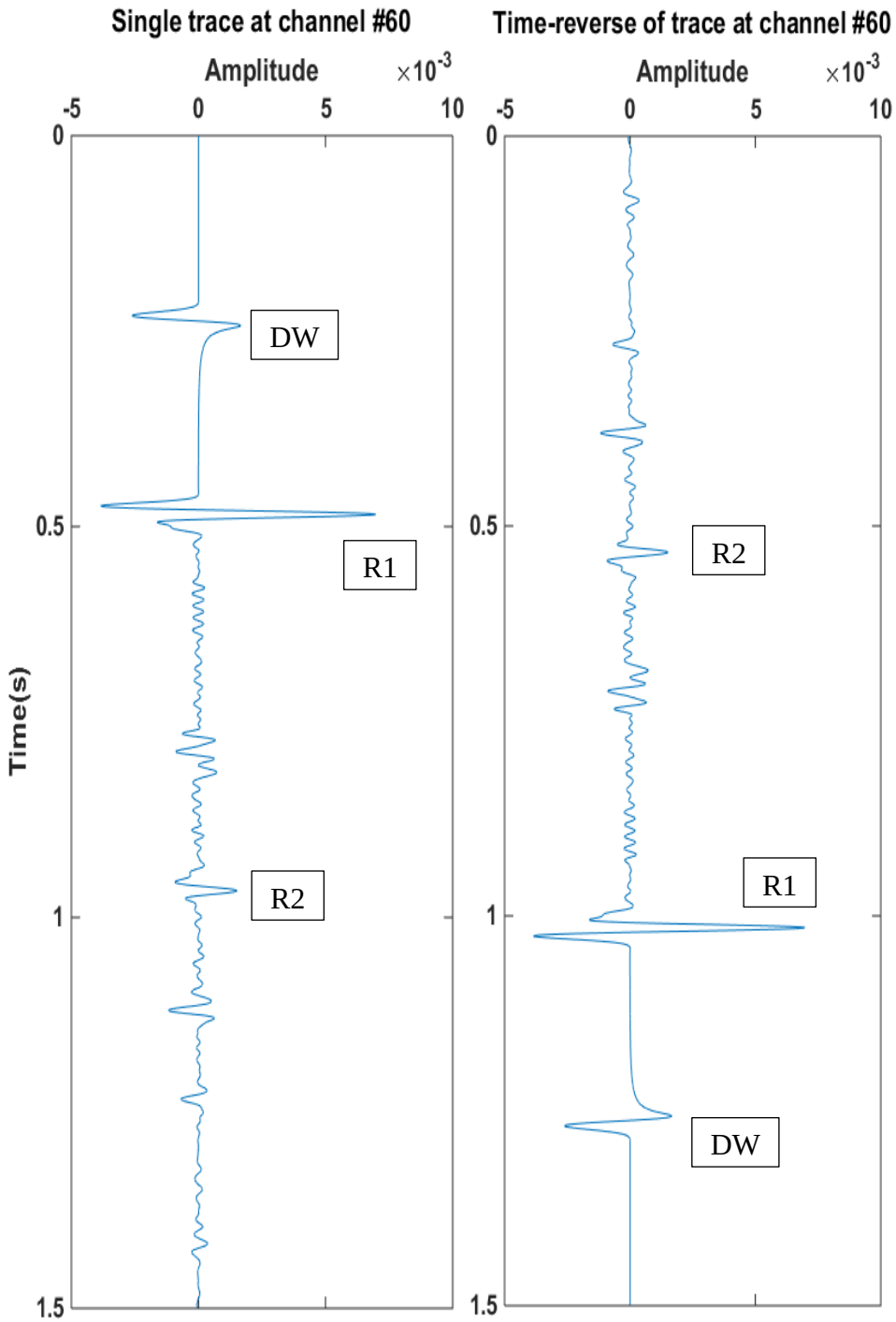

Figure 3-6: Trace at channel number 60. The figure on the left shows the recorded signal from forward modelling. The right trace shows the time reverse of the recorded signal for backpropagation redatuming. The time-reversed trace will be re-emitted into the velocity model and recorded at the desired datum. Response marked (DW) is the direct wave, (R1) is from the undulating reflector and (R2) is from the flat horizontal reflector.

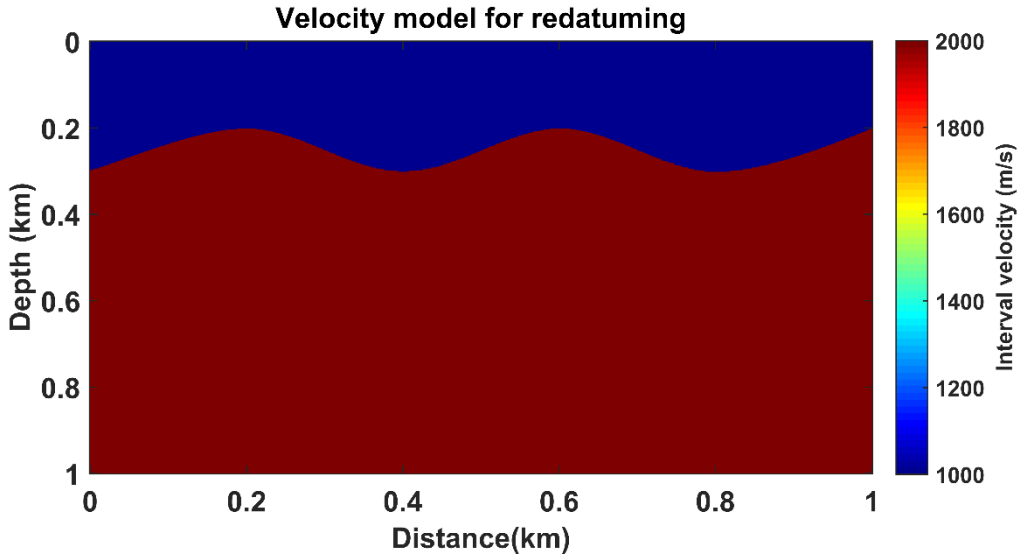

Figure 3-7: Velocity model used for redatuming via backpropagation. Recorded data will be backpropagated through this model and recorded at desired datum which in this case is at 600m depth to remove the undulation effect on the data.

For comparison to the backpropagation redatuming, a control data was acquired, see Figure 3-9(b), with the source on the surface and receiver array at the same location as used in the backpropagation redatuming. The first arrival on the controlled data corresponds to the direct arrival and the subsequent event is from the reflection off the flat surface. From these data, we can see that backpropagation of the data accurately transforms the target reflection to the correct position as if the receivers were located in the subsurface despite being recorded on the surface. In addition to that, the amplitude of the backpropagated data does attenuate at the far offsets. This is because we have a finite aperture of recording.

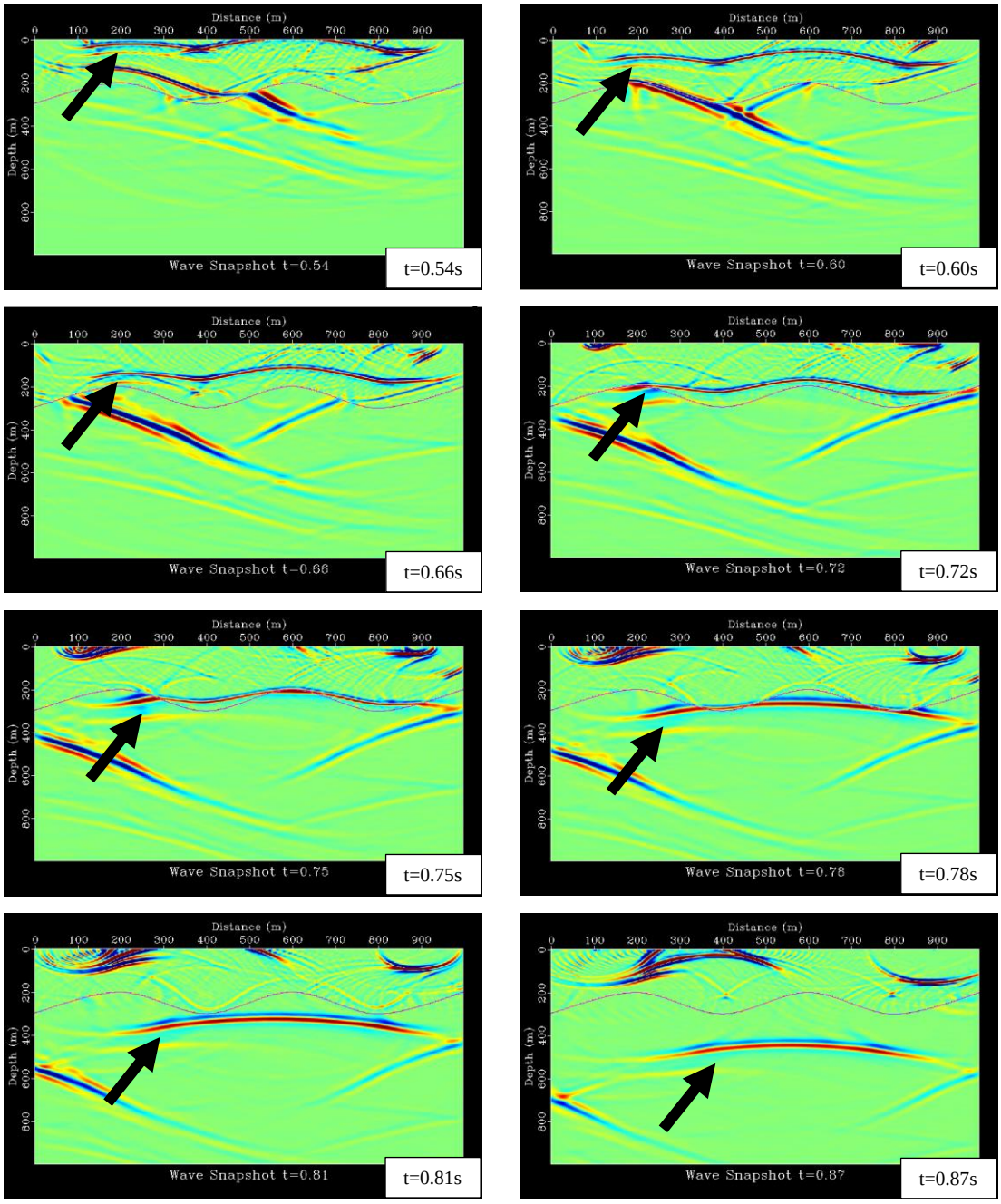

Figure 3-8: Backpropagation of recorded data. Reflection event 3, which is marked by the black arrow, backpropagates through the undulation and removes the imprint caused by it. This is due to the focusing of energy property of reverse-time. Instead of the wave expanding, it contracts and refocus leading to the removal of the undulation effect.

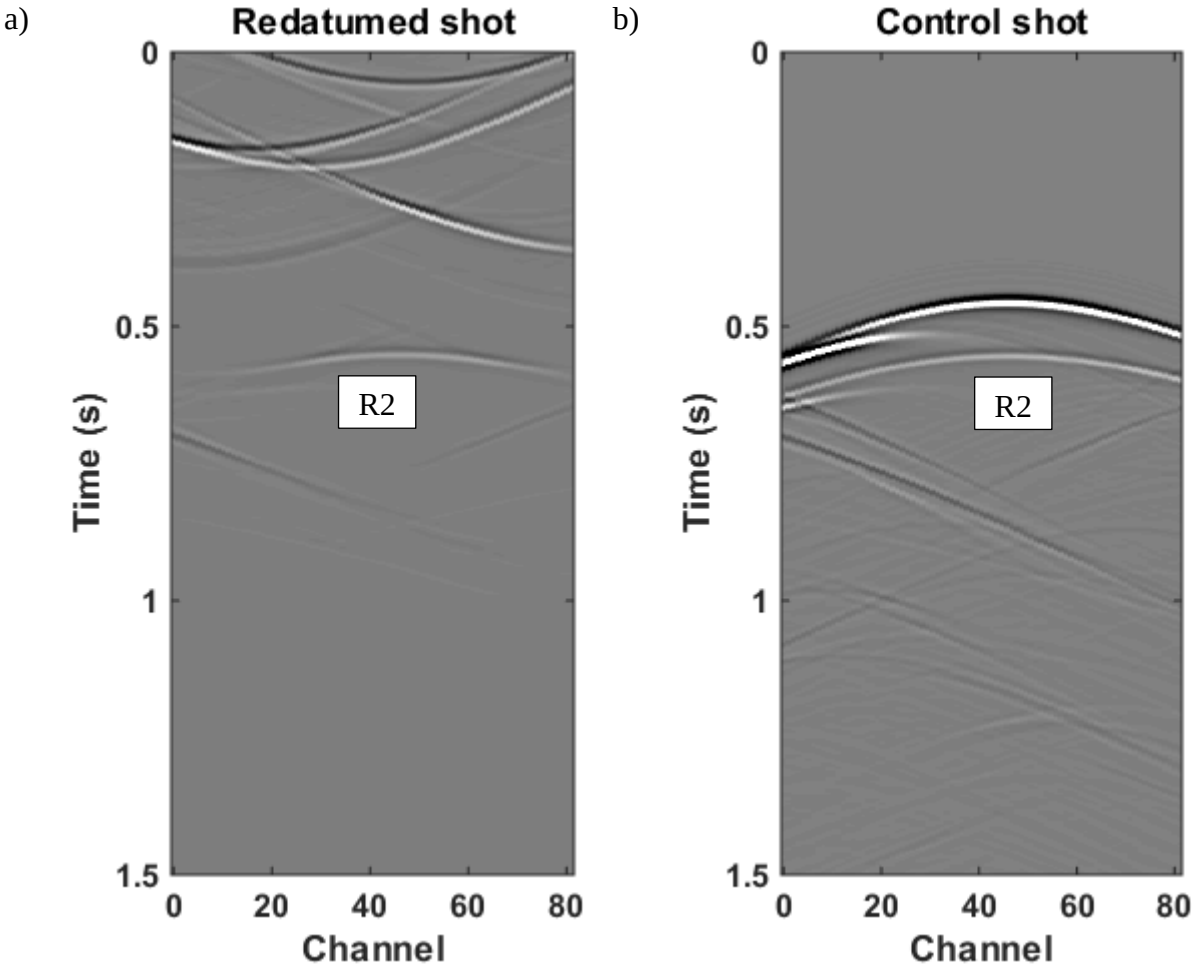

Figure 3-9: Seismic data corresponding to: (a) Result of redatuming the receivers to 600m in the model as shown by the dash lines in the velocity mode in Figure 3-3. (b) The control shot where the source is at the surface and the receivers located at the redatumed surface. R2 represents the reflection from the flat reflector in the velocity model.

3.3 Reciprocity theorem to redatum the sources

In the previous section, I have shown how receiver redatuming is performed using time reversal, which removes the contamination of the near surface in the reflected upgoing wavefield. Source redatuming using time reversal is more challenging as the waves now propagate downwards and away from the source, unlike in the receiver redatuming where waves propagates upwards and towards the receivers. To accommodate for these changes, the principle of reciprocity—as discussed in this section—plays an important part. The work done here has been submitted to ASEG-PESA 2015 24th International Geophysical Conference and Exhibition as an extended abstract (Ung et al., 2015).

The reciprocity principle has been used in many areas of physics when describing relationships between potentials satisfying either Laplace's equation or the wave equation. In seismic applications, the reciprocity principle states the intuitive notion that, interchanging the positions of the source and receiver will yield the same response. This principle is valid only if we interchange not only the locations of the source and the receiver, but also the corresponding radiation/sensitivity patterns (e.g., vertical source and geophone can be interchanged). To directly apply this principle to the field data is seldom possible, since the assumption of having the same radiation patterns of the source and receiver is rarely satisfied. In its simplest form, the reciprocity principle in elasticity can be expressed as:

$$G_{ij}(x_1, t; x_2) = G_{ji}(x_2, t; x_1), \tag{3.1}$$

where $G_{ij}(x_1, t; x_2)$ represents Green's function corresponding to a point force source in direction j at location x_2 and recorded at location x_1 at time t in direction i. The theoretical derivation of this principle dates back to Maxwell (1864). A derivation of the reciprocity principle is shown, among others, in the book by Aki and Richards (2002) or a paper by Achenbach (2006).

The use of the reciprocity principle in seismology can be found in many texts on seismic wave propagation. Examples are Knopoff and Gangi (1959), and Gangi (1970), who derived the reciprocity theorem in seismological setting and showed its

validity in experiments. White (1960) used the reciprocity relationships to obtain low-frequency radiation patterns of shear and compressional waves from relatively complex sources. Gupta (1966, 1965) used the reciprocity principle to obtain the radiation patterns of P and SV waves from horizontal and calculated the polar radiation patterns of P, SV and SH waves. van Borselen et al. (2013) use this principle in performing deghosting of marine seismic data. Fokkema and van den Berg (1993) provide an extensive overview of acoustic reciprocity and its application in seismic processing and interpretation, which includes wavefield decomposition, removal of surface-related wave phenomena, boundary imaging, domain imaging and seismic inversion. Berryhill (1984) and Mulder (2005) show that the principle of reciprocity can be used in datuming the sources.

Herein, we investigate the accuracy of the reciprocity theorem in the context of numerical modelling as it is important for the source redatuming, which is discussed later in the thesis.

3.3.1 Numerical validation

In this study, the SOFI3D finite difference full elastic forward modelling code (Bohlen, 2002) was used to model the wave propagation. This program allows for 3D viscoelastic, elastic and acoustic parallel modelling using Taylor or Holberg coefficients and can be used on a suitable multi-processor supercomputer (e.g., on the iVEC Pawsey Supercomputer). To study the degree of validity of this principle under real-world scenarios where the radiation pattern varies in different locations, a numerical test was devised. The model used in this section represents a volume of 200 x 200 x 200 meters with material parameters of global maximum P-wave velocity v_{p_max} = 5500 m/s and global minimum S-wave velocity v_{s_min} = 1500 m/s (Figure 3-10). A Ricker source wavelet is used with a centre frequency of 50 Hz.

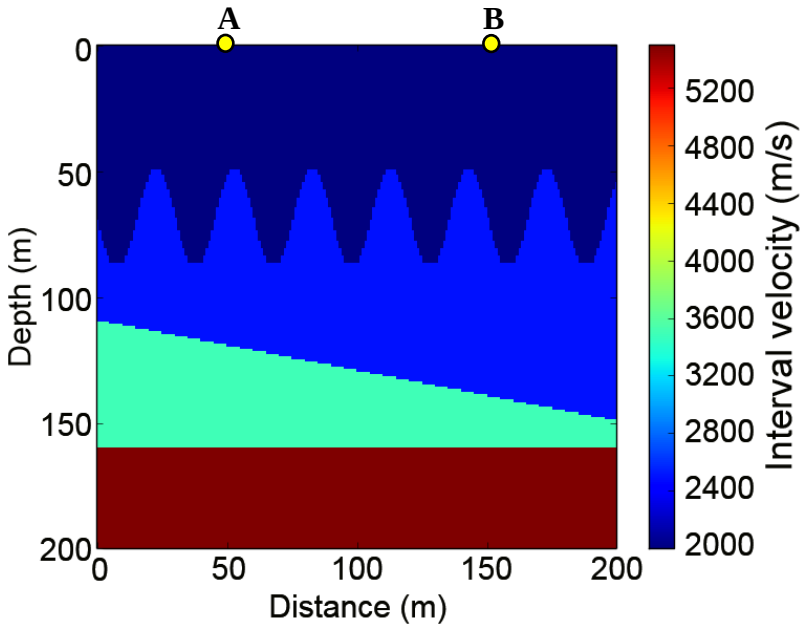

Figure 3-10: XY slice of the P-wave velocity model used for the reciprocity theorem test. To ensure for different radiation pattern between different locations, the model was designed to be asymmetric. The source and receiver were interchanged between location A and B as marked on the model.

Source-Receiver configuration:	Control		Reciprocity experiment	
	Source at A	Receiver at B	Receiver at A	Source at B
1	X direction	Y direction	Y direction	X direction
2	X direction	Z direction	Z direction	X direction
3	Z direction	Y direction	Y direction	Z direction

Table 3-1: Source and receiver configuration for reciprocity test.

These numerical experiments are performed by interchanging the location of the source and receiver at locations A and B, marked in Figure 3-10. The offset between the two locations is 100 m. The configuration of the source and receiver pair to examine the reciprocity principle under different radiation patterns is shown in Table 3-1. Figure 3-11 shows the reciprocity relations for source and receiver with different radiation patterns. It is observed that the recorded wavefield shows similar characteristics if the sources and receivers were interchanged despite having different radiation patterns at both locations. This difference in radiation patterns for the different locations does not introduce amplitude, phase and time difference of the propagated seismic energy.

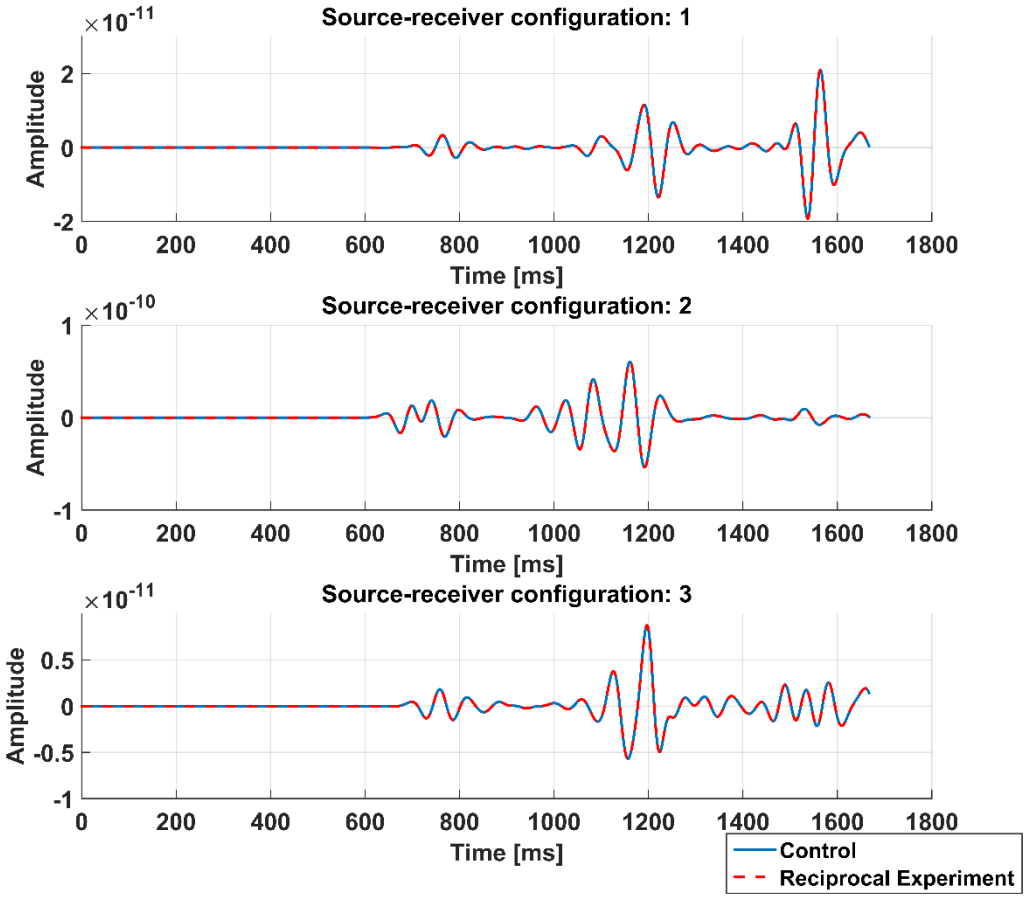

Figure 3-11: Reciprocity relations with the source and receiver at different location with different radiation patterns. Blue solid lines represent the control experiment and red dash line represents the corresponding reciprocity experiment according to Table 2-1.

The verification of this principle plays an important role in the finite difference redatuming as it allows for the interchange of source and receiver positions. This means that the propagation path can be reversed and similar step of backpropagation redatuming can be applied in transforming the recorded data to transform both the downgoing and upgoing wavefield from sources and receivers respectively. This simplifies the search for the extrapolation operator to remove the near-surface effects on the downgoing wavefield

3.4 Synthetic example of finite difference redatuming

In this section of the thesis, 2nd order acoustic wave-equation finite difference redatuming is applied to redatum the sources and receivers to a new location in the subsurface to remove the complex wave propagation introduced by the near surface. To achieve this, the velocity model as shown in Figure 3-12(a) is used. The velocity model is 1,000 m wide and 500 m deep. The first 200 m is filled with spherical "geology" with velocities ranging from 1,900 m/s to 3,700 m/s. The background velocity for this top layer is 2,000 m/s. These near-surface complexities are then cut off by an undulating interface, which is followed by a constant medium with a velocity of 3,000 m/s. The target reflector is flat and is located at a depth of 400 m with a velocity of 4,000 m/s for the medium below it. The model has a grid size of 0.5 m by 0.5 m. The purpose of designing a velocity model like this is to introduce significant scattering and a complicated wave propagation path to produce a non-hyperbolic and discontinuous reflection events from the horizontal interface at 400 m. Finite difference redatuming will then be used to relocate the sources and receivers to a new datum beneath the complexities to produce an image that is free from the complexities.

The synthetic dataset is modelled with a fixed receiver array. The receiver array consists of 60 channels with a spacing of 10 m located between 200 m and 790 m in the model. Sixty shots were fired at each receiver location. Both sources and receivers were placed on the surface. The corresponding synthetic data is shown in Figure 3-13 with the stack section in Figure 3-14. In the raw shot, a number of diffraction hyperbolas can be observed in the top 2 s. This then contaminates further reflection responses from deeper reflectors. As seen in Figure 3-13, the reflection from the flat reflector does not retain its hyperbolic nature and is not continuous. This makes subsequent processing steps like velocity analysis very challenging. The distortion by the near surface towards deeper reflectors can also be seen in the brute stack section, whereby the flat reflector is seen as undulating.

Finite difference redatuming is used to transform the recorded data virtually so that the sources and receivers appears below the complexities thus simplifying the reflection response from the target reflector. The new datum that the sources and receivers are relocated to is at a depth of 250 m as marked by the dotted line in Figure 3-12(a). As mentioned in the previous section, a detailed knowledge of the near surface is required to remove the effects that the near surface might introduce to the recorded data. The input velocity model for redatuming will only comprise of the complex geology part as shown in Figure 3-12(b). The step of finite difference redatuming can be summarised as:

1) Sort the data in the shot gather domain and apply a time reversal to each trace;
2) For each shot gather, emit the time-reversed trace at each receiver location the trace was recorded in to the velocity model with the near-surface geology;
3) Record the time-reversed trace at a desired datum and apply a time reversal to flip back the orientation of the data;

These steps only account for the receiver redatuming that transforms the upgoing wavefield. To handle the downgoing wavefield, we can take advantage of the reciprocity by repeating the above steps with the data sorted in the receiver gather domain and each time-reversed trace is emitted at the sources location in each common receiver gather.

a) b)

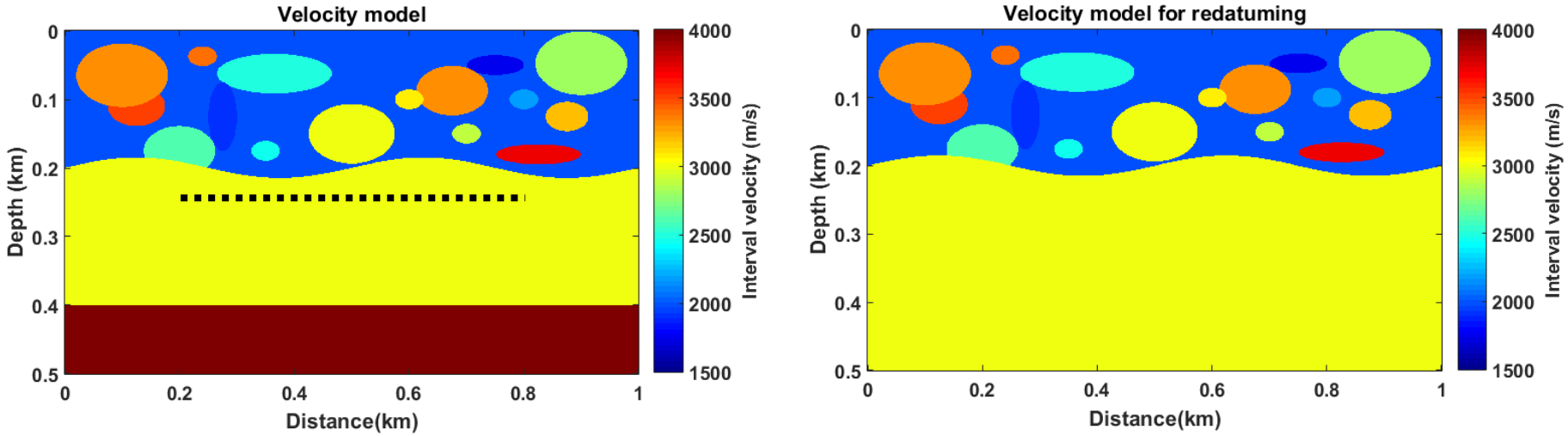

Figure 3-12: Input velocity models. (a) shows the initial velocity model used to acquire the synthetic data for the redatuming process. The near surface complexities are used to distort the response from the horizontal reflector, (b) is the input velocity model for the finite difference redatuming technique. The black dash line found in (a) is the location of the redatumed sources and receivers location which is 250m deep and 150m above the target flat reflector.

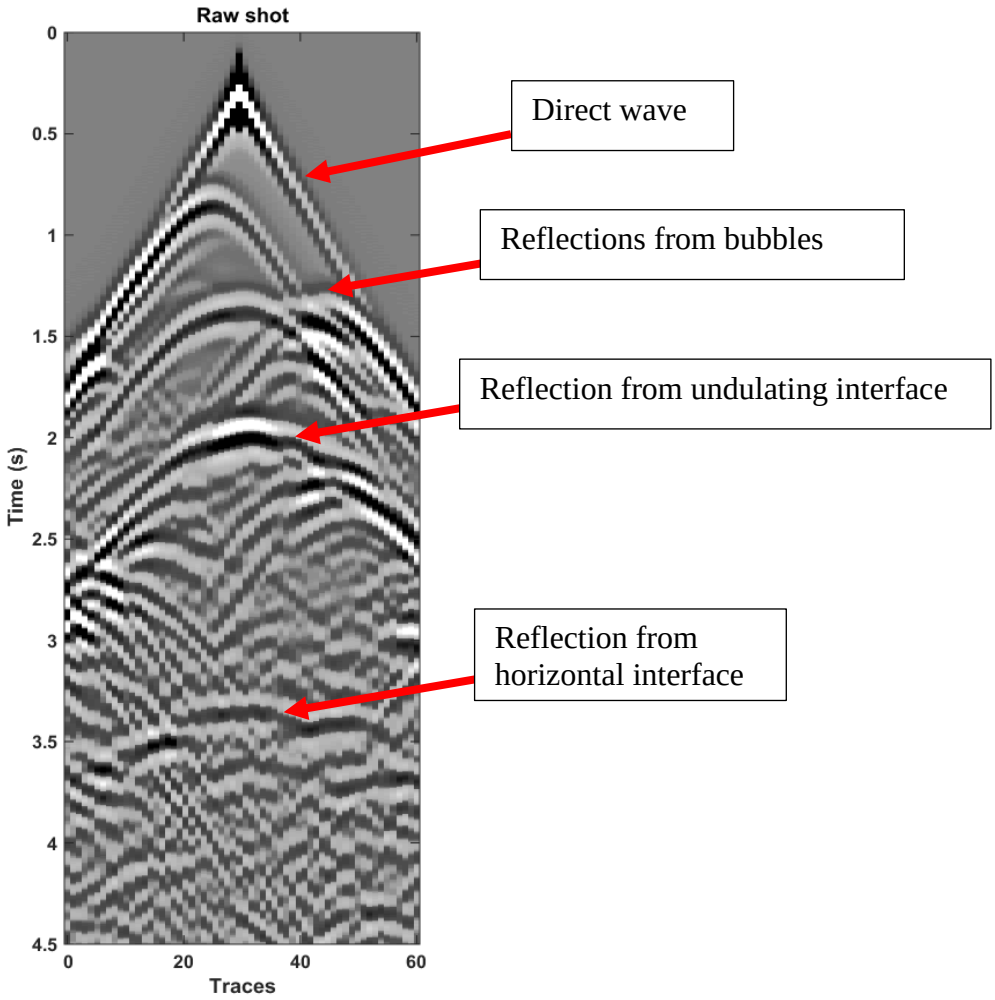

Figure 3-13: Synthetic raw shot generated from the input velocity model through finite difference forward modelling. This data is then time reversed and backpropagated in order to simplify the response from the horizontal interface.

The result of sources and receivers redatuming is shown in Figure 3-15(b) which is performed using the accurate velocity model (Figure 3-12b). The result of redatuming, which removes Green's functions that describe the upward and downward wave propagation between the new and old sources and receivers, effectively removes the imprints from the near-surface complexities. As observed in the redatumed data, a significant amount of finite difference noise is introduced in the background. The amplitude of this noise is very strong and matches the amplitude from the target reflection. In addition to that, linear events can be observed dipping towards the centre of the data. This is due to the edge effect as there is a finite limit to the recording aperture of the data, as discussed in the previous section. As compared to the example as shown in Section 3.2, the effects of the limited aperture are further emphasised by redatuming both the sources and receivers.

The linear noise causes the target reflection to be less smooth. To compensate for this, a simple f-k filter is used to remove the linear noise giving us a result as shown in Figure 3-15(c). By comparing the redatumed result with the initial data, we observe that the target reflection hyperbola is more continuous and is easily distinguishable after redatuming. Here redatuming using the finite difference method has successfully removed the complex wave propagation introduced by the complicated near-surface geology, which contaminated the initial synthetic data. In addition, a comparison with the control data, as shown in Figure 3-15(d), shows that the target reflector's reflection hyperbola is accurate in terms of velocity (shape of hyperbola) and timing. The stack section of the redatumed data after linear noise removal is shown in Figure 3-16(a). In comparison with the input brute-stacked data, the target reflector is more continuous and flat. The stack section of the controlled data is shown in Figure 3-16(b). The quality of the data can be further improved if computational resources and time is not an issue as one can always use a denser grid model for the computation, which will produce a better result. While in this synthetic test the results of finite difference redatuming is promising, often detailed knowledge of the subsurface is not known and obtaining one is always challenging especially if there are strong variations in the physical properties of the area.

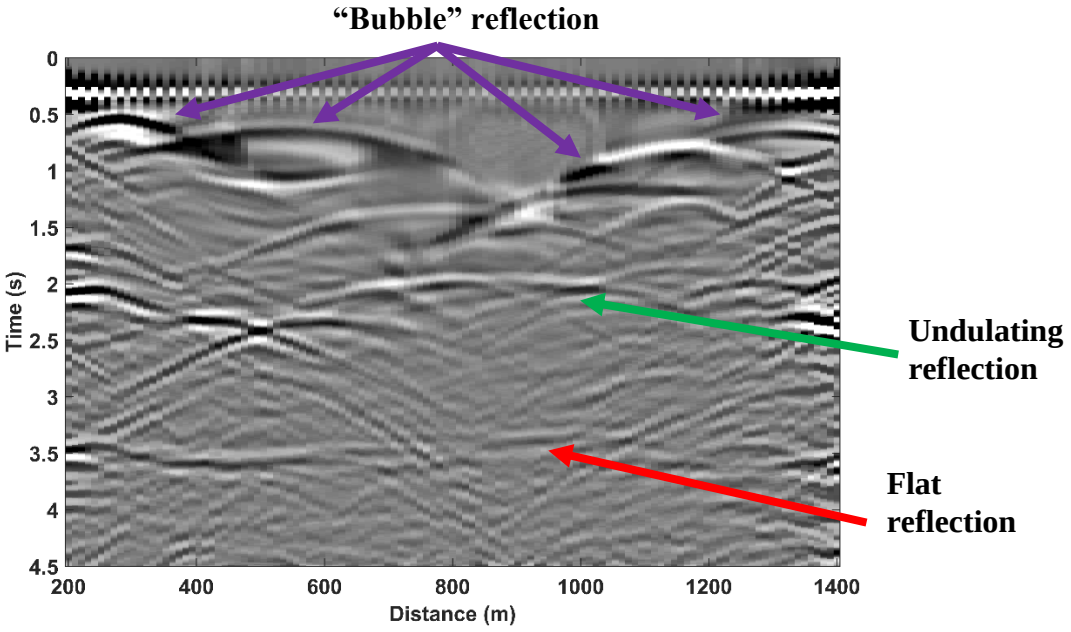

Figure 3-14: Brute stack from the forward modelling of input velocity model. The purple arrow shows the response caused by the bubble structure in the velocity model. The green line indicates the reflection response from the undulation and the red line is from the horizontal reflector. It is noted that the horizontal reflector has been contaminated by the complex near surface structures.

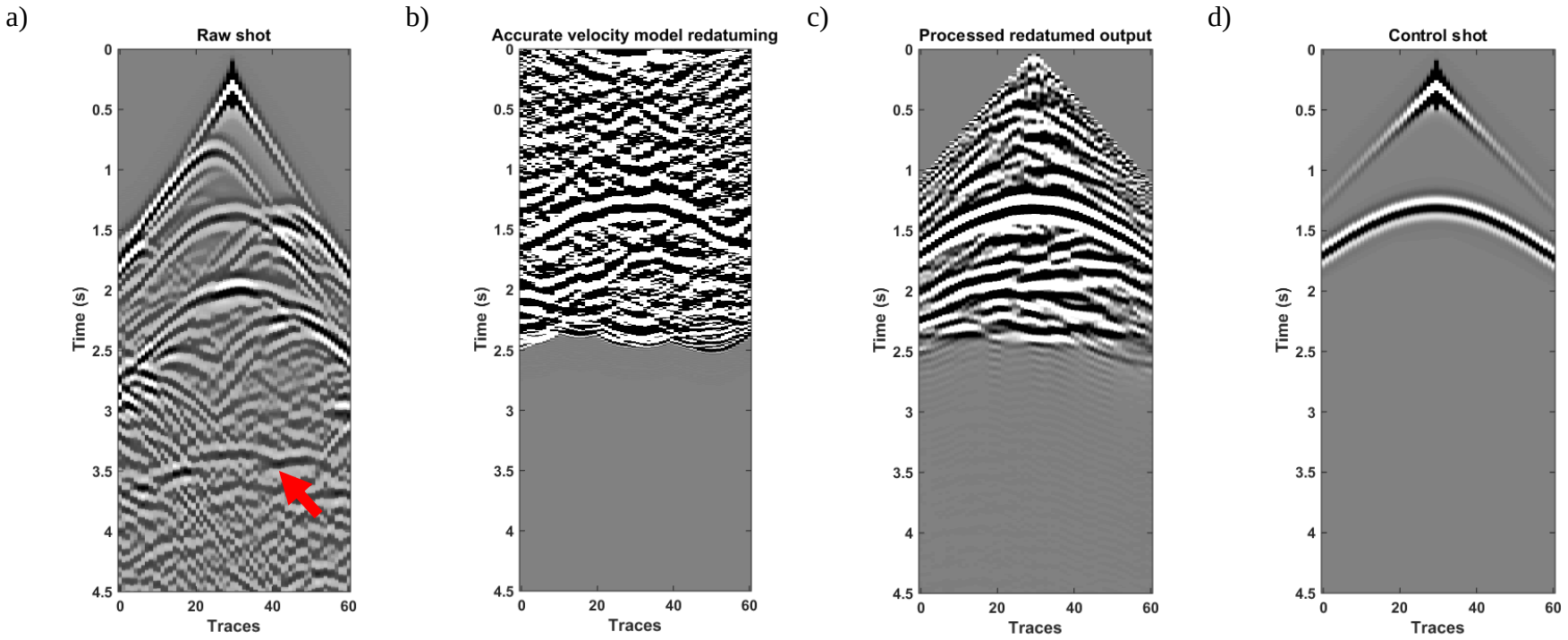

Figure 3-15: Common source gather with source in the middle of the receiver array. (a) is the input data response with the reflection from the flat surface marked by the red arrow, (b) is the output from finite difference redatuming, (c) is the processed redatuming output and (d) is response from the controlled test. The output from redatuming removes the imprints from the near surface and produces a smoother and continuous hyperbola that accurately represents the target reflector.

a) b)

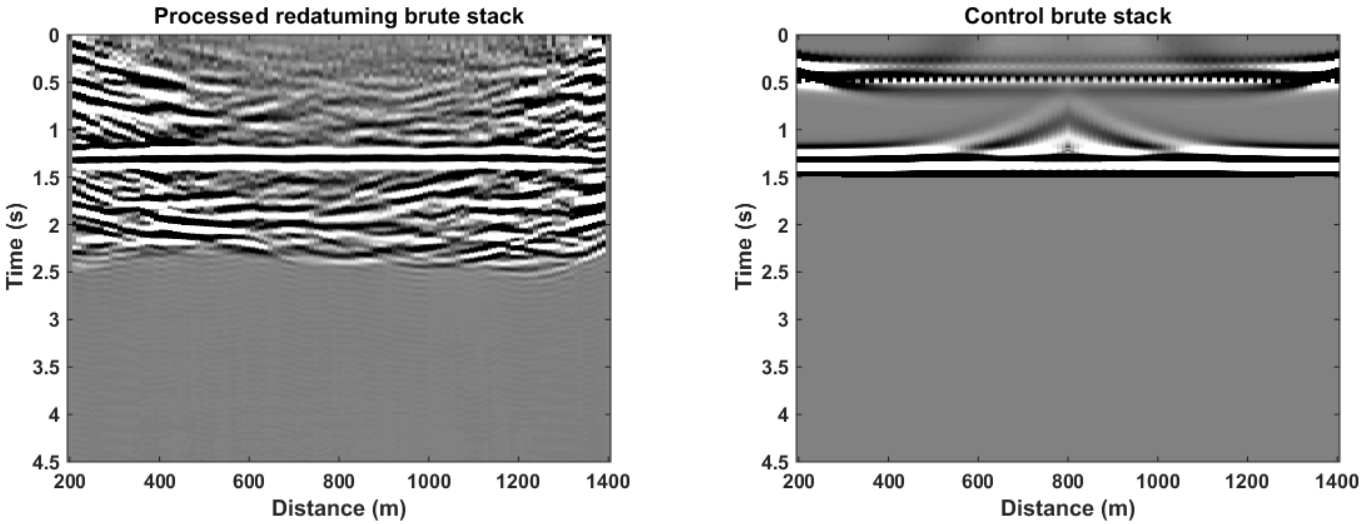

Figure 3-16: Brute stack of data of (a) linear noise removal output of finite difference redatuming using the accurate velocity model; and (b) control data. Target reflector after redatuming is straighter and has better continuity compared to the stack before redatuming in Figure 3-13.

3.5 Influence of the velocity model in backpropagation

Despite the finite difference method being the most accurate approach to performing wave equation redatuming, it requires the availability of an accurate input velocity model. Obtaining an accurate velocity model of the overburden can be very challenging, especially in hard-rock environments where there can be significant changes in velocity and geological structures. In light of this, this section of the thesis contains the feasibility study of the finite difference redatuming technique using two different degree of smoothed velocity model and a RMS velocity model as the input, which is shown in Figure 3-17. Smoothing of the velocity model was done using a multidimensional Gaussian filter across 60 samples for the milder and 120 samples for the stronger smoothing. The grid size of the model was set to 0.5 m by 0.5 m, which is the same as the initial model used to acquire the synthetic data in the previous part of this thesis. These two velocity models were computed based on the velocity model used in the previous section.

For comparison purposes, the new source and receiver locations for the redatuming output are the same as used in the previous section. The resulting gathers of redatuming using different input velocities are shown in Figure 3-18. The milder smoothed velocity model, as seen in Figure 3-18 (b) produces an output that closely resembles the redatumed result with an accurate velocity. However, it is observed that not all of the effect from the near surface is removed as the reflector is still undulating. As expected, using the stronger smoothed velocity model results in a less stable redatuming as the events looks more discontinuous. This is attributed to the lack of definition of the strongly smoothed velocity model. Simillar to the redatuming result using the mildly smoothed velocity model, the use of an RMS velocity model manages to reconstruct the reflector with some residual undulation.

The stack sections of the redatuming result are presented in Figure 3-19. All stacks are done using the same velocity with the data being redatumed using the midly smoothed (Figure 3-19(a)), strongly smoothed (Figure 3-19(b)) and RMS (Figure 3-19(c)) velocity model. It is observed that using the mildly and strongly smoothed velocity model for redatuming produces a continuous and strong reflector with a shift of 100 ms between them. This is because the strongly smoothed velocity model have a lower velocity. In contrast to this, when using the RMS velocity as input, the target reflector is not continuous and the event breaks off at the edge of the data. Despite having an unrealistically complex model for this study, we are able to remove the complexities introduced from the near surface with different degrees of accuracy from the input model. In a more realistic model, we would expect a decrease in the background artefacts and an overall better resolution redatuming result. In this method, the velocity estimation needs to be sufficiently accurate as there are no ways of determining the accuracy of the estimations from the output. In the next chapter, I will investigate the data driven method, which address these challenges.

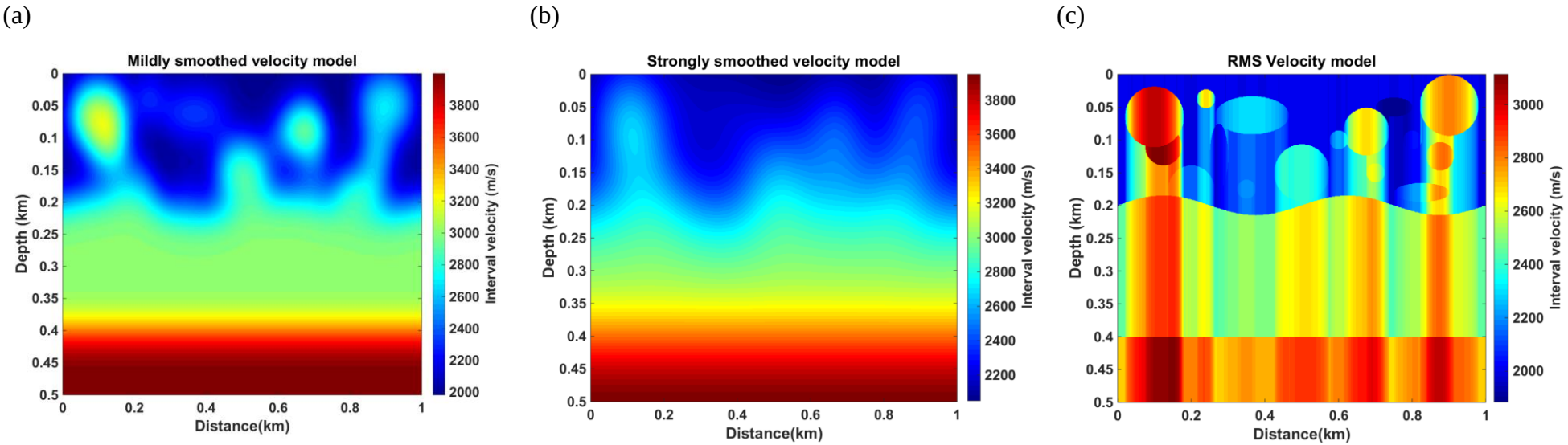

Figure 3-17: Feasibility study of finite difference redatuming technique using (a) midly smoothed, (b) strongly smoothed and (b) RMS velocity model as input.

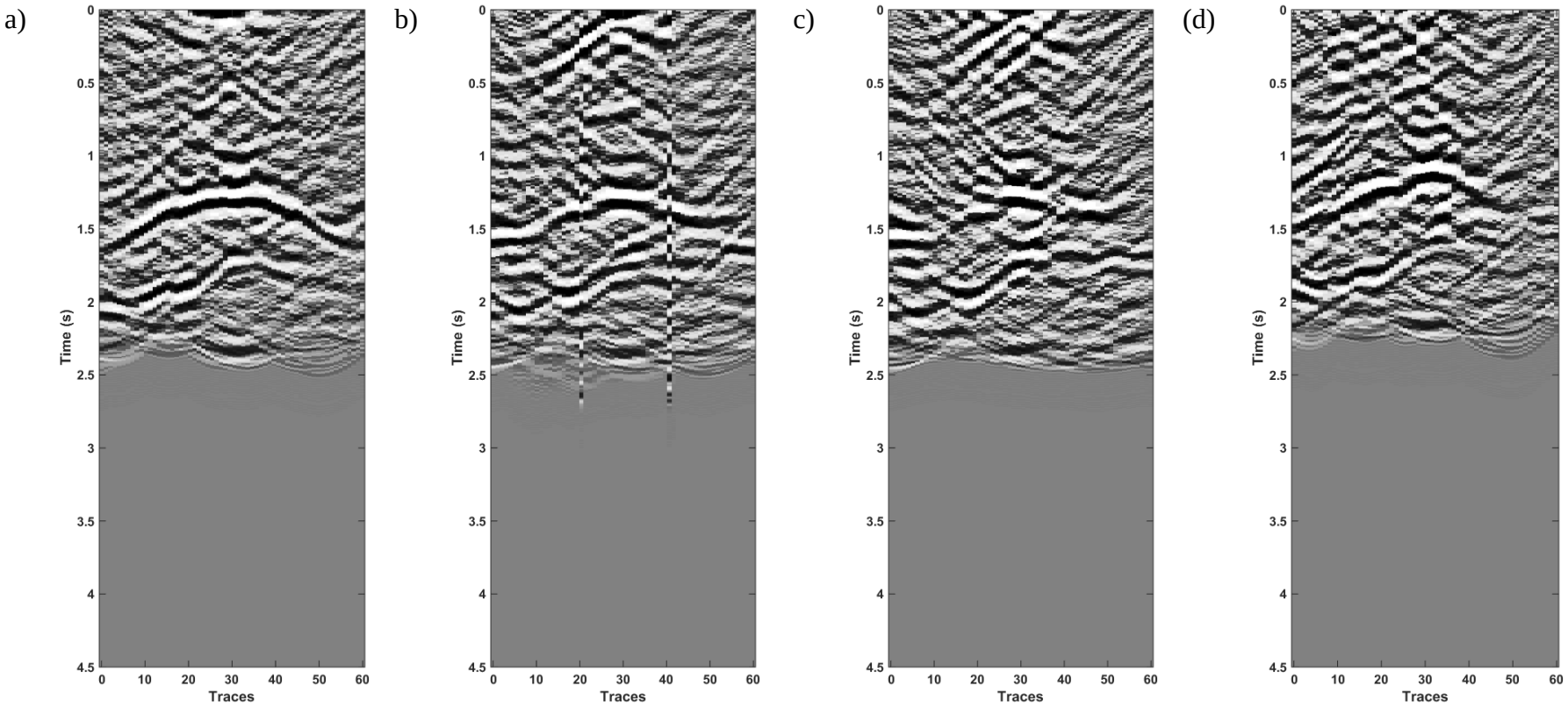

Figure 3-18: Common shot gather of redatumed output using (a) accurate velocity model, (b) mildly smoothed velocity model, (c) strongly smoothed velocity model and (d) RMS velocity model as input.

(a) (b) (c)

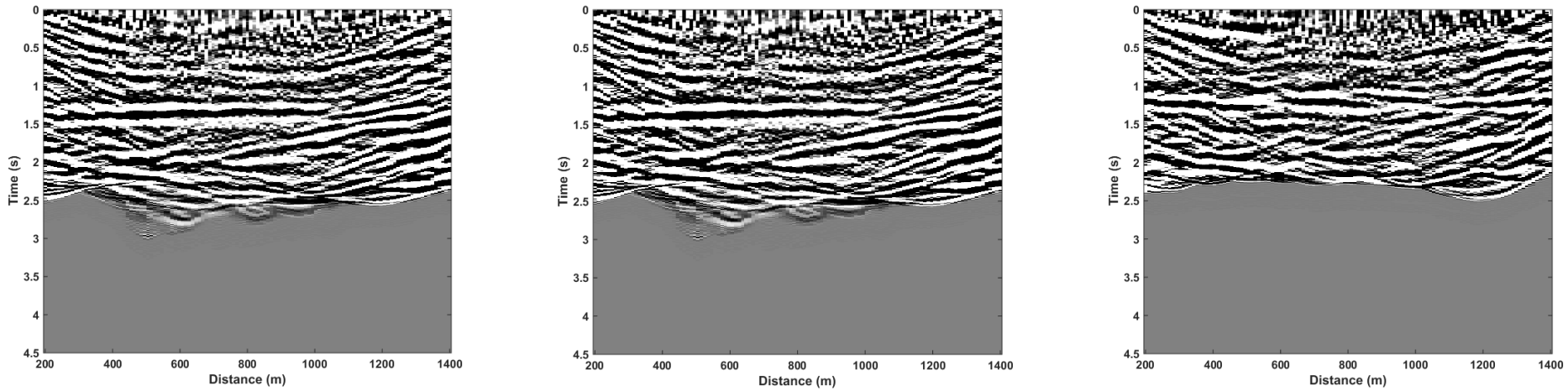

Figure 3-19: Stack section of finite difference redatuming output for (a) smoothed velocity model and (b) RMS velocity model as input.

Chapter 4 Data driven: Common focus point

In this chapter, I apply the data-driven redatuming technique known as the CFP method. The reason for investigating this particular method is because it allows for both sources and receivers to be redatumed to the subsurface by using only a Green's function. This Green's function describes the one-way response from the new source location to the source at the surface and is known as the focusing operator.

Unlike the technique presented in the previous chapter, the CFP method does not require the estimation of a velocity model and allows for iterative updating of the focusing operator to achieve a more accurate redatumed result. However, it is limited by the fact that a reference reflector is required as, unlike the finite difference redatuming technique, sources and receivers cannot be redatumed freely to any location in the subsurface,. It also allows the velocity estimation to be updated whereas the previous method does not.

4.1 Fundamentals of Common Focus Point redatuming

Like other data-driven redatuming methods, the CFP method uses cross-correlation when relocating the sources and receivers. Morton and Thorbecke (1996), Berkhout (1996) and Kabir et al. (1996) first used the CFP method on pre-stack migration to address the limitations of depth migrations, which is the inability to obtain an accurate velocity model. Berkhout (1997a, 1997b) then formulated the CFP redatuming using the Kirchhoff method for poststack data, which he later extended to prestack data based on two consecutive focusing steps. The result of these focusing steps is known as the CFP gathers. The importance of the CFP gathers was then presented by Kelamis et al. (1999) as a velocity-independent imaging tool used to better resolve and handle complex near-surface effects. Morton and Thorbecke (1996) define the CFP gathers with the Kirchhoff implementation as:

$$CFP(\boldsymbol{x_s}, \boldsymbol{x_m}, \tau) = \iint data[\boldsymbol{x_s}, \boldsymbol{x_r}, t = \tau + T(\boldsymbol{x_m}, \boldsymbol{x_r})]\boldsymbol{dx_r}, \tag{4.1}$$

where $\mathbf{x_s}$, $\mathbf{x_r}$, and $\mathbf{x_m}$ are the spatial coordinates of the sources, receivers and focus points respectively, t is the recording time and τ is the downward continued time. T is the one-way traveltime between two points in a particular medium. The CFP gather represents half of a migration process and is produced through convolution with a time-reverse focusing operator. The focusing operator is a Green's function that describes the one-way traveltime data, which is used to describe the downward or upward wave propagation between the surface location and the chosen grid point. The next step, focusing in detection, is similar to the previous focusing step. However, instead of combining all the shots, this step combines all of the receivers so that its response is focused at a specific location. The CFP method has been used for the removal of multiples (Berkhout and Verschuur, 2005), velocity model estimation (Cox and Verschuur, 2001) and velocity independent redatuming (Hindriks and Verschuur, 2001).

The two focusing steps used in the CFP method are known as 'focusing in emission' and 'focusing in detection', which relate to the sources and receivers redatuming respectively. Theoretically speaking, focusing in emission combines all the sources of a common receiver to simulate a virtual source in the subsurface, whereas focusing in detection combines all the receivers of a common source to simulate a virtual receiver in the subsurface. As both these focusing steps are not dependent on one another, they can be performed in any order of priority; however, it is important to note that these focusing steps are done in different domains: common receiver for focusing in emission and common shot for focusing in detection. For example, computing the redatuming result for one virtual receiver at the chosen focus point requires the data to be sorted into common source gathers, which are then convolved with a focusing operator relating to the focus point. The focusing operator corresponds essentially to a time-reversed Green's function that describes the downward or upward propagation of the wave between the recorded location and the new location at which the sources/receivers would be placed in the subsurface. In simpler terms, with the availability of a velocity model, the focusing operator can be seen as a time reversal of the data collected from the surface with the source in the subsurface at the chosen focal point, as shown in Figure 4-1.

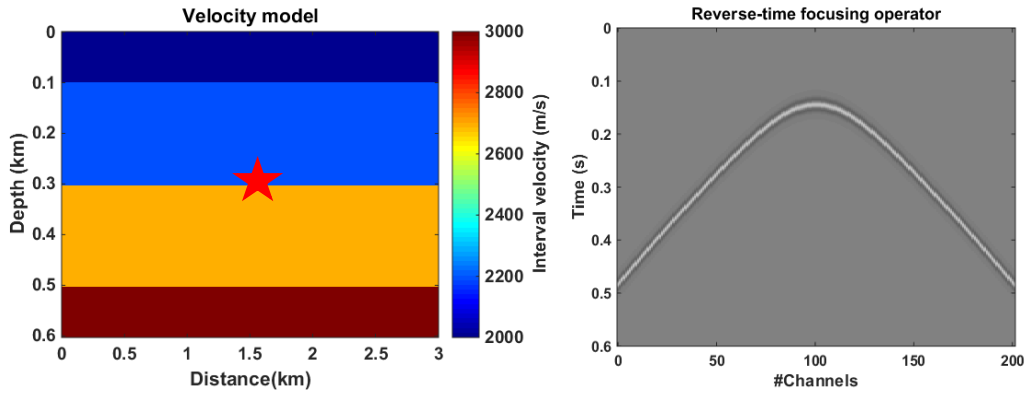

Figure 4-1: Obtaining a focusing operator from a velocity model. The focus point is marked by the star in the velocity model. The focusing operator can be obtained by placing a source at the location of the focus point and recording the response on the surface. By time reversing this response, we arrive at the focusing operator needed to be convolved to obtain a CFP gather in the redatuming process. The time-reverse focusing operator can be seen in the figure on the right.

The result of convolving every shot gather with a focusing operator then summing each shot gather into an individual trace and placing them side by side produces what are known as the CFP gathers, where the receivers have been redatumed. Physically, receiver redatuming corresponds to the transformation of the recording in such a way that the receivers has been virtual relocation to a new locating in the subsurface. Therefore, if an accurate focusing operator is used, the CFP gather obeys the principle of equal traveltime. This principle is defined by Kelamis et al. (2000), who state that if the focus point is chosen at a reflector and the correct focusing operator has been used to create the CFP gathers, then the selected reflection response in the CFP gather would have to exhibit the same data as the Green's function focusing operator. This provides a way of determining whether the focusing operator is accurate, as a time-corrected CFP gather with its focusing operator should produce an event that is perfectly aligned at zero time. This time-corrected CFP gather is known as the Differential Time Shift (DTS) panel.

Figure 4-2 shows the response in the DTS panel for a synthetic split-spread data generated in a homogeneous medium with a velocity of 2000 m/s with a flat reflector at a depth of 300 m. This reflector will produce a hyperbolic reflection response with a peak, t_0, of 0.3 s. By using this flat reflector as a reference for the focus point, we require an operator with t_0=0.15 s and a velocity of 2000 m/s in order to accurately obtain the CFP gather, as the focusing operator is a one-way traveltime response from the focus point to the surface as mentioned before. Figure 4-2(c) shows the DTS panel response for the accurate operator. The reflector response is seen as a flat horizontal event at time zero. Figure 4-2(a) shows a response when using an operator with t_0 of 0.1 s, lower than the accurate t_0, and a velocity of 2000 m/s. In the DTS panel, a concaving upward event with a peak at positive time is observed. Figure 4-2(b) shows a response when using an operator with t_0 of 0.2 s, higher than the accurate t_0, and a velocity of 2000 m/s. In the DTS panel, a concave downward event with a peak at negative time is observed. Figure 4-2(d) shows a response when using an operator with t_0 of 0.15 s and a velocity of 1500 m/s, which is slower than the accurate velocity. In the DTS panel, a concave up event with a peak at zero time is observed. Figure 4-2(e) shows a response when using an operator with t_0 of 0.15 s and a velocity of 2500 m/s, which is faster than the accurate velocity. In the DTS panel, a concave down event with a peak at zero time is observed.

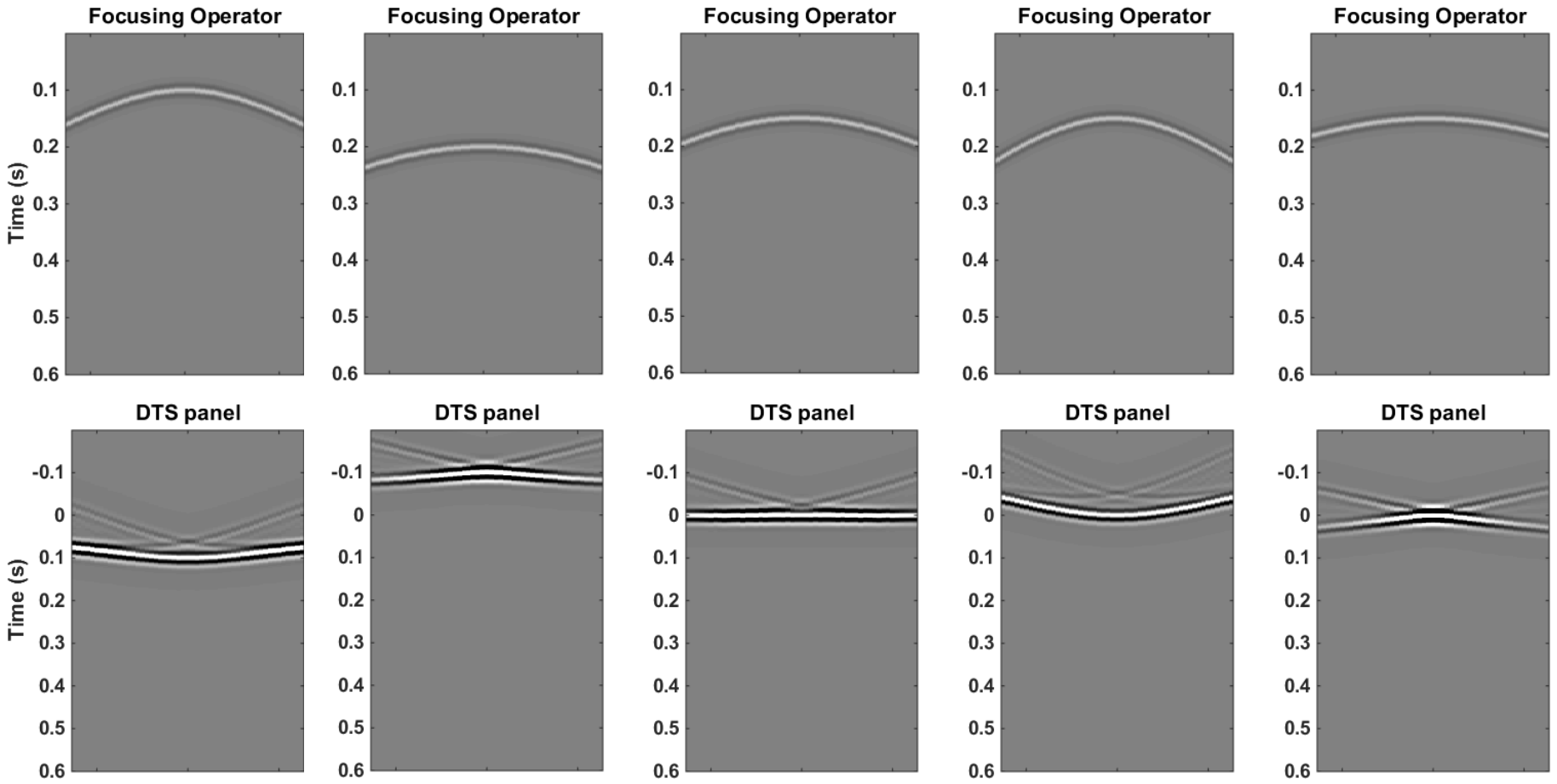

a) t_0 < accurate t_0 b) t_0 > accurate t_0 c) Accurate V and t_0 d)V < accurate V e)V > accurate V

Figure 4-2: Use of different operators and their time corrected CFP gathers, which is also known as the DTS panel. In the event where the operator is inaccurate, we note that the reference reflector is never flat and at zero time. With an operator with t_0 shorter (a) or longer (b) than the accurate t_0 produces a response shifter in positive or negative time respectively. If the velocity of the operator is too fast (e) or slow (d), a response that is concave downward or upward is seen, respectively. Only when the operator has an accurate t_0 and velocity, a horizontal event at zero time occurs, as seen in (c).

The beauty of using the CFP method for redatuming is that a velocity model is not needed and that the focusing operator can be easily updated using the principle of equal traveltime by referring to the DTS panel. The use of an incorrect focusing operator is corrected by adding half the traveltime of the event of interest in the DTS panel with the focusing operator. This process only takes a couple of iterations to produce an accurate result and is significantly faster when compared to updating a velocity model. Based on the discussion above, CFP redatuming can be summarised into these steps:

1. Determine a reference reflector on which the focusing point will be chosen.
2. Compute the initial focusing operator for the chosen focus point and convolve it with the data sorted in common source gathers in the 'focusing in detection' step. This will generate the CFP gathers that are sorted in the common receiver gathers with the receivers redatumed to the focus point and sources still at the surface.
3. Construct a DTS panel for each output gather and update the focusing operator until the principle of equal traveltime is satisfied. This is achieved when the target reflection event becomes flat at zero time in the DTS panel.
4. Repeat steps 2 and 3 on receiver redatumed CFP gathers sorted in common receiver gathers to redatum the sources to the focus point.

4.2 Synthetic example of common focus point redatuming

In this example, a synthetic velocity model with an undulating near surface is used to introduce distortions in seismic wave propagations from deeper events, as shown in Figure 4-3. Unlike in previous papers on CFP redatuming (e.g., Kelamis et al. (2002); Berkhout (1997a)), this model exhibits both vertical and lateral velocity variations in the near surface. The first three layers have a constant velocity of 2000 m/s, 2300 m/s and 2500 m/s respectively and are separated by an interface that is heavily undulated, which is used to represent the regolith that disrupts the seismic data. The fourth layer, with a velocity of 2700 m/s, is separated by a horizontal reflector at 500 m. This reflector is used as a reference for the CFP method to redatum the sources and receivers. The last interface acts as the target reflector and separates the final medium, which has a velocity of 3000m/s. The acquisition geometry for this synthetic data consists of a fixed array of 201 receivers with a 10 m spacing and with sources firing

at every receiver location. The location of the sources and receivers is marked in the velocity model in red (see Figure 4-3).

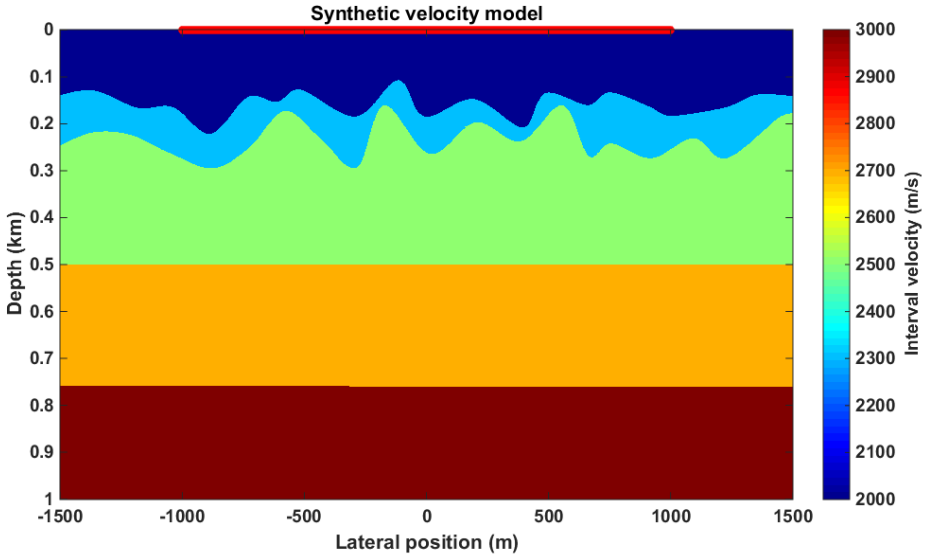

Figure 4-3: Velocity model with undulating reflectors to distort seismic data for CFP redatuming. The sources and receivers are relocated to a flat reflector reference at 500 m. The reflection response from the reflector at 750 m is the target reflection on which to test the CFP redatuming.

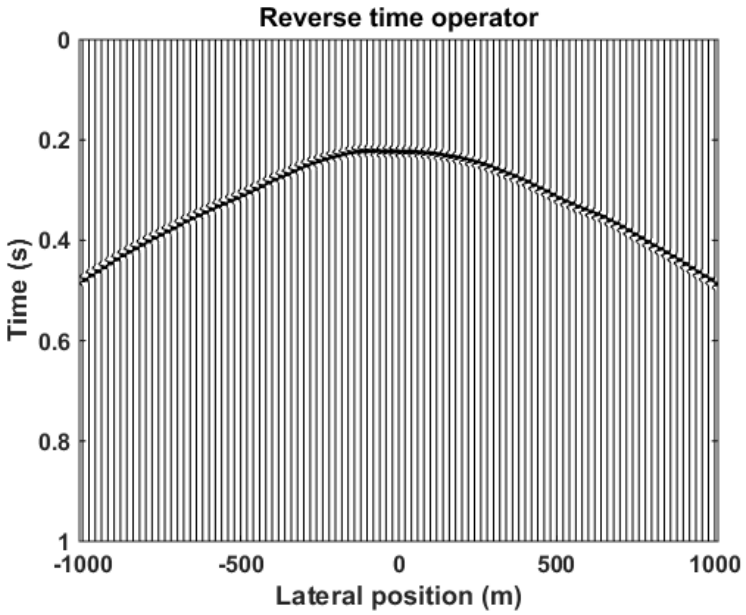

Figure 4-4: Reversed time focusing operator from the reference reflector at 500 m at x=0 m.

In performing CFP redatuming to relocate the receivers, the operator for the focus point at the reference reflector, x=0 and z=500 m, as shown in Figure 4-4, will first be convolved with the data in the source gathers domain. Here, the focusing operator is obtained by placing a source at the focus point with receivers at the surface and performing forward modelling. From the selected recording data, as shown in Figure 4-5 (a), (b) and (c), the target reflection represented by the last reflection event is not a smooth hyperbola as what is normally seen from a flat reflector. This reflection has been heavily contaminated by the undulation interface.

The results of this convolution are shown in Figure 4-5 (d), (e) and (f), which are then summed to form a single trace and placed beside each other to form the CFP gather, as shown in Figure 4-5 (g). This CFP gather represents the receiver redatuming, which is now sorted in the common receiver domain. The response of the reference reflector should be similar to that of the focusing operator to satisfy the principle of equal traveltime. The output can then be checked by convolving the CFP gather with the focusing operator to form a DTS panel that should result in a flat event at time zero. This is clearly shown in Figure 4-5(h), marked by the red arrow. This process to relocate the receivers to the reference reflector is the ‘focusing in detection’ step.

By choosing multiple focusing points on the reference reflector, the CFP gathers represent data sorted in the common receiver gathers with the sources at the surface and receivers in the subsurface at a depth of 500 m. To redatum the sources, the same process as above is repeated on the CFP gathers in the common receiver gathers, which then produce data sorted in the common source domain. The result represents sources and receivers that have been virtually relocated to a depth of 500 m on the reference reflector. In Figure 4-6, a comparison of the input data (left) and the redatumed result (right) with source at x=0 m is shown. The red line in the input data is where the data will be shifted to by the redatuming process.

It is clearly observed in the redatumed data that the target reflector hyperbola marked by the red arrow is now much smoother with the near-surface effects now removed. Much like the finite difference redatuming method, the output generated by CFP redatuming suffers from edge effects and the far offsets of the target hyperbola curve upward. However, there is less noise in the data overall and it does not suffer from the

finite difference artefacts. In addition, the linear events in the CFP redatumed data are noise caused by finite aperture artefacts, which can be easily removed in data processing.

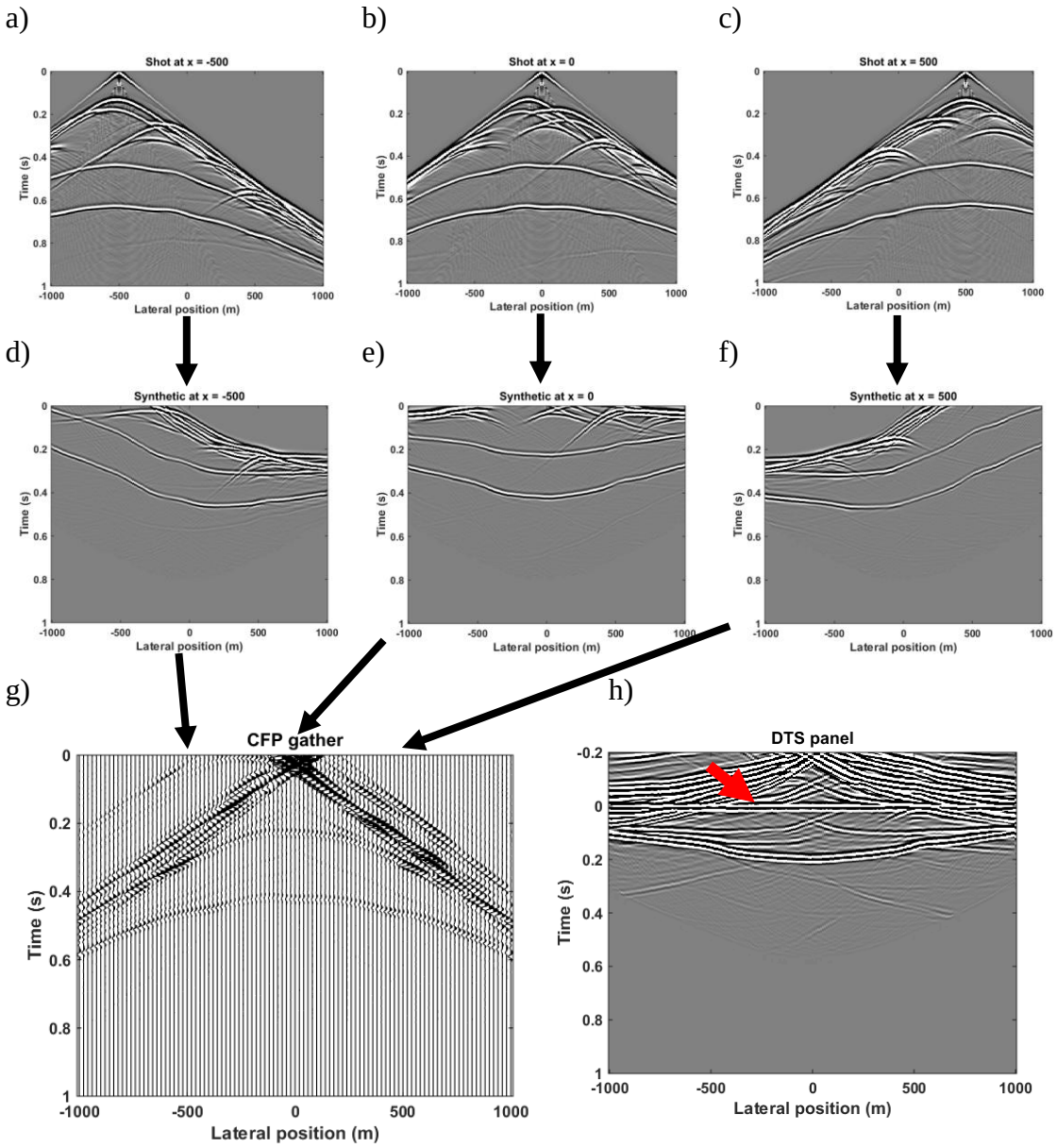

Figure 4-5: Synthetic data of shots at -500 m, 0 m and 500 m is shown in (a), (b) and (c), respectively. Convolution of data with a focusing operator at Figure 4-4 is shown in (d), (e) and (f). Summation of the convolution results is shown in (g). The accuracy of the focusing operator is examined by convolving the CFP gathers with the focusing operator, which results with the DTS panel shown in (h). Flat events marked by the red arrow indicates that the correct focusing operator has been used.

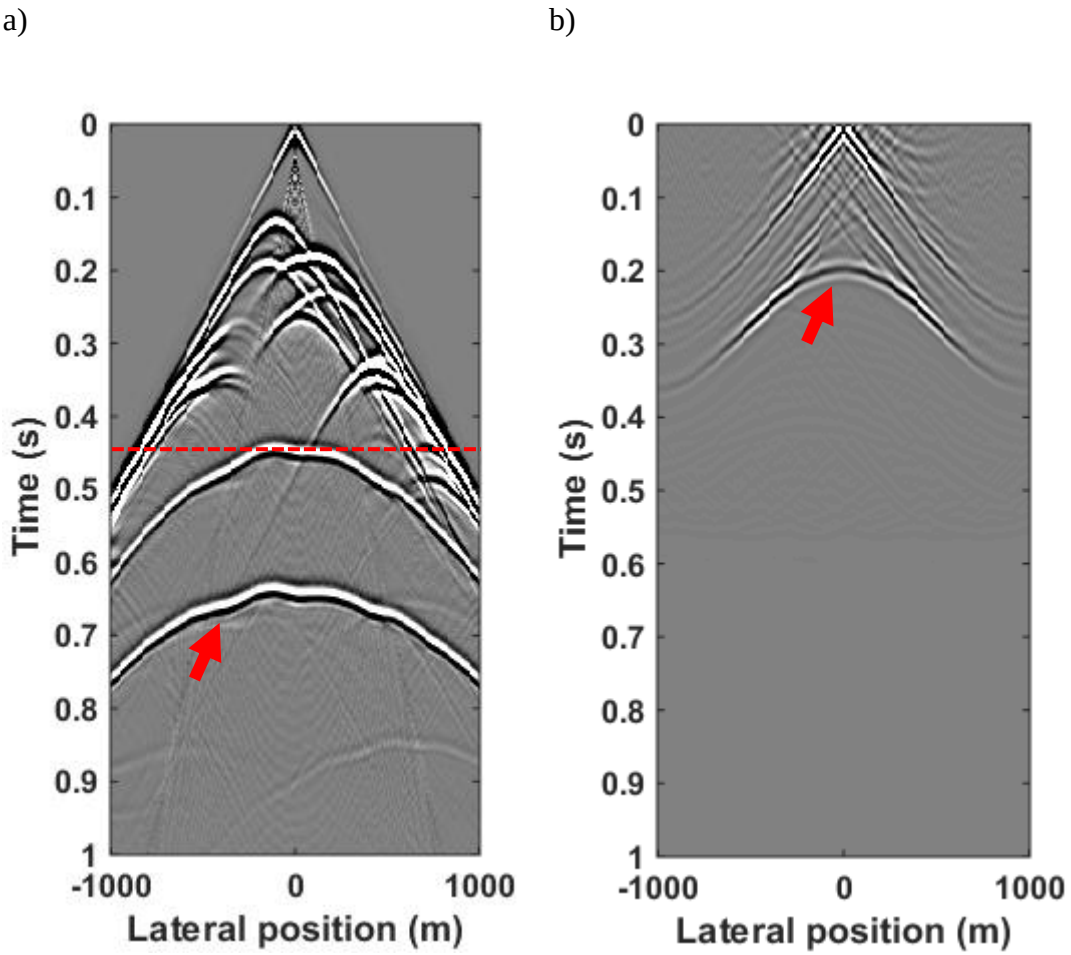

Figure 4-6: Comparison of (a) input data and (b) CFP redatuming of both source and receiver results. The sources and receivers have been shifted virtually to the reflector with a peak at t=0.44 s, marked as the red dash line in (a). The red arrow marks the target reflector.

4.2.1 Muting in the Differential Time Shift panel

Other artefacts observed in the CFP redatumed results are the low-amplitude upward curving events above the direct wave, as seen in Figure 4-7(a). These artefacts are introduced by reflection events that are above the reference reflector in the input data. The removal of these artefacts can be done by muting data above the flat event at time zero in the DTS panel during the first pass of redatuming and then transforming it back to the CFP gathers. The transformation of the DTS panel back to the CFP gathers can be achieved by deconvolution with the inverse focusing operator. Figure 4-7(b) shows the result of before and after DTS panel muting. It is clear that the artefacts above the direct arrival are removed after redatuming.

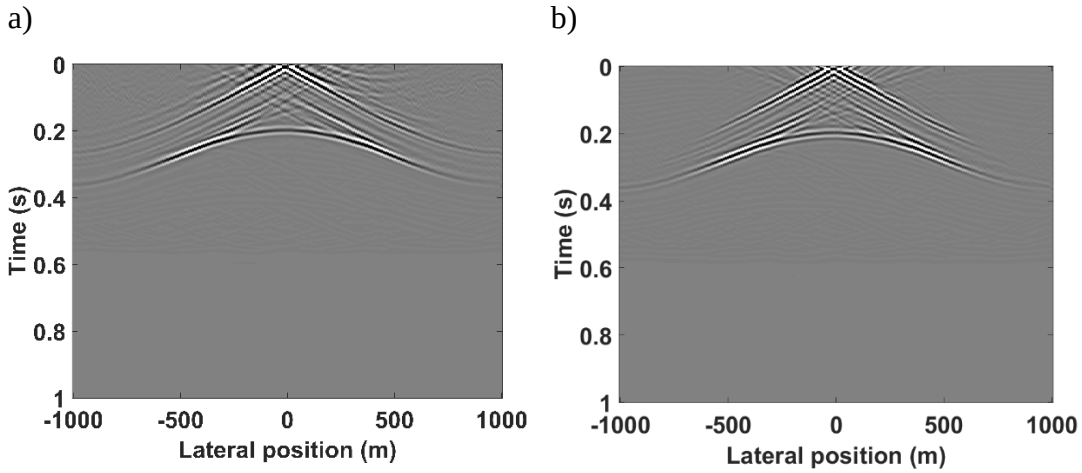

Figure 4-7: CFP source and receiver redatuming a) without and b) with muting of the DTS panel above the flat event at zero time. Upward curving artefacts above the direct arrival are removed after we apply the mute as seen in (b).

4.2.2 Amplitude preservation in CFP redatuming

In addition to having accurate kinematics for the focusing operator, an amplitude factor should also be considered in the computation of the redatuming. Kelamis et al. (2002) and Morton and Thorbecke (1996) mention the need to apply an amplitude factor to avoid high-amplitude artefacts in the far offsets when using a constant amplitude operator. In this redatuming example, we observe that the amplitude at the peak of the target reflection hyperbola is weaker than the amplitude at the slope of the hyperbola (see Figure 4-8(a)). This is mainly due to the constructive interference with the linear noise resulting from CFP redatuming. To compensate for this, we use equation 4.2 from Kirchhoff migration equation, which defines amplitude as:

$$A = \frac{\cos(\theta)}{d_r * V}, \tag{4.2}$$

where $\cos(\theta)$ is the obliquity factor and θ is the angle of incidence, d_r is the reflection point and V is the stacking velocity. As observed, the CFP redatuming results using the amplitude corrected focusing operator (Figure4-8(b)) show the amplitude of the reflection event decreasing from near offset to far offset as expected.

Another way of approaching the question of whether we need to modify the amplitudes during the CFP redatuming, is that we can reformulate the method in terms of redatuming using Kirchhoff wave propagation modelling or Kirchhoff migration.

Kirchhoff modelling is based on the Haugens principle, which can be loosely translated into receiver redatuming setting, as follows. Each receiver becomes a source emitting the recorded signal backward in time. The emitted wavefield of each reversed receiver is computed as a convolution of the time-reversed signal with a kernel, given by (Schneider 1978, eq. 5).

$$U(r,t) = \frac{1}{2\pi}\int \frac{\cos\theta}{d_r V}\frac{\partial}{\partial t}U\left(r_0, t - \frac{d_r}{V}\right)\mathrm{d}r_0, \tag{4.3}$$

where I omitted the second term divided by d_r. Thus, to redatum the receivers we need to time reverse the received signal, differentiate it, and then convolve it with the amplitude factor (eq 4.2).

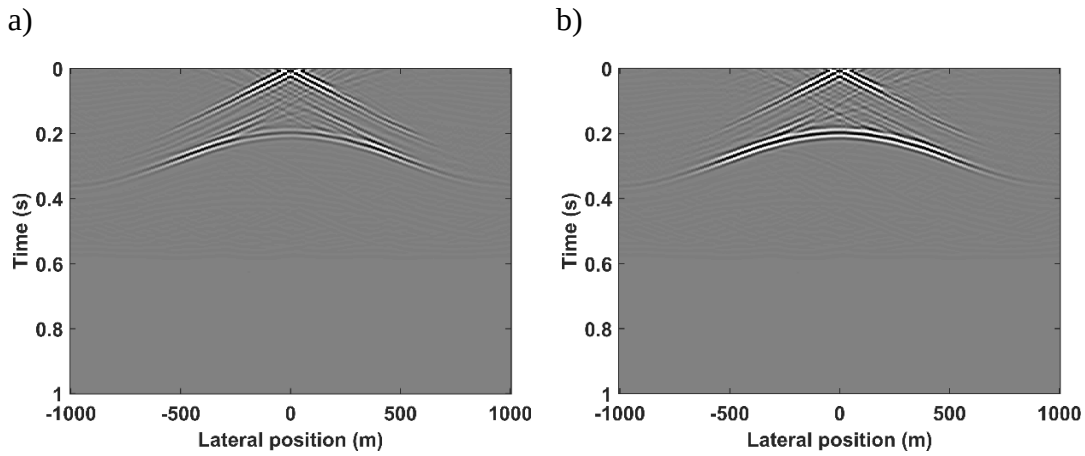

Figure 4-8: CFP sources and receivers redatuming (a) without and (b) with amplitude factor in the focusing operator.

4.3 Estimating the focusing operator using common midpoint gathers

In a real-world scenario, an accurate velocity model that describes the recorded data is often difficult or challenging to acquire, especially for land seismic data. However, this does not limit the ability of CFP redatuming to be performed with accuracy. With the presence of a strong reference reflector, the focusing operator can be estimated in a number of ways. The most common method to determine the focusing operator is by looking at the zero offset section of a seismic data recording (Kelamis et al., 2000). This would give an indication of the propagation time at the peak of a reflection hyperbola. With this information, a one-way Green's function can be produced with an estimated velocity. By time reversing this reflection hyperbola, the focusing operator is obtained. This first operator does not have to be accurate. By using the DTS panel, one can continuously update the focusing operator until it satisfies the principle of equal traveltime. Only a few iterations are needed to update the operator to achieve a good redatuming result.

Here, the focusing operator is estimated by picking the reference reflection events in the Common Midpoint (CMP) domain. Figure 4-9 shows the arrangement of a CMP data, whereby in a constant velocity medium, the ray path of a wave propagation reflects off the midpoint between the distance of the source and receivers. As the focusing operator is only the one-way wave propagation to the chosen focus point, which is the location of the redatumed sources and receivers, we need to divide the picked traveltime by half to obtain an approximation to the focusing operator.

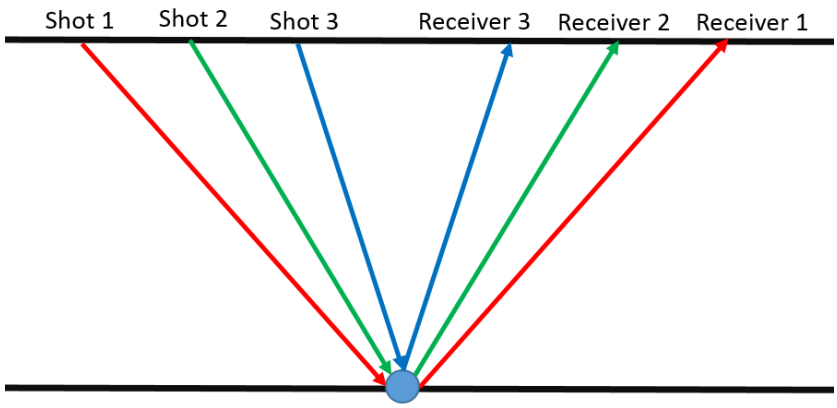

Figure 4-9: Two-way ray tracing of the CMP domain data. Dividing the time by half in the CMP domain will yield a one-way traveltime reflection hyperbola.

Using this focusing operator estimation technique, I pick the reference reflection in the CMP domain of the synthetic data obtained from the velocity model in Figure 4-3. The picks are shown in Figure 4-10. These picks are then halved and reversed in time to obtain the focusing operator needed for the CFP redatuming process. Figure 4-11(a) shows the result of CFP redatuming using an estimated operator from the CMP gathers. Comparing this result to the redatumed result using the accurate focusing operator shows that it is still contaminated with the undulation effects, as shown in Figure 4-6(b). This is because the assumption of a constant medium between the reference reflector and the acquisition surface does not hold for lateral and vertical varying velocities in the near surface. Despite that, after one iteration in updating the focusing operator estimated from the CMP domain, the result improves significantly and the undulation effects are removed as shown in Figure 4-11(b).

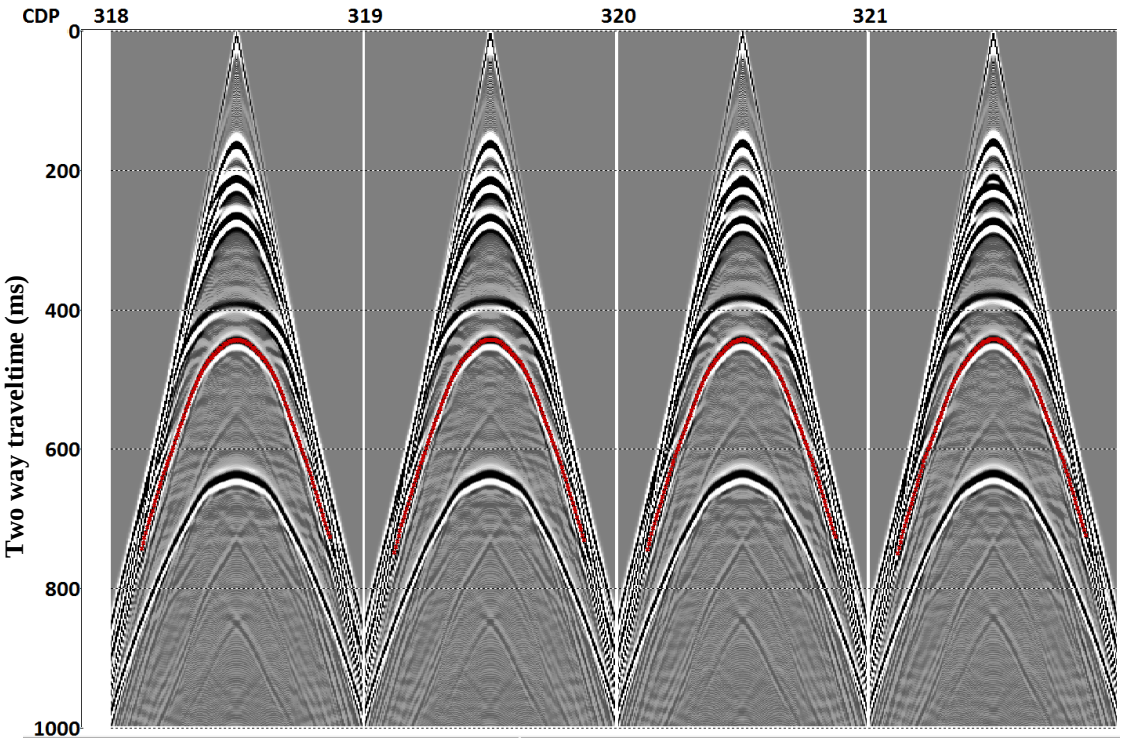

Figure 4-10: Picking of the reference reflector in CMP domain for synthetic data produced by the velocity model in Figure 4-3.

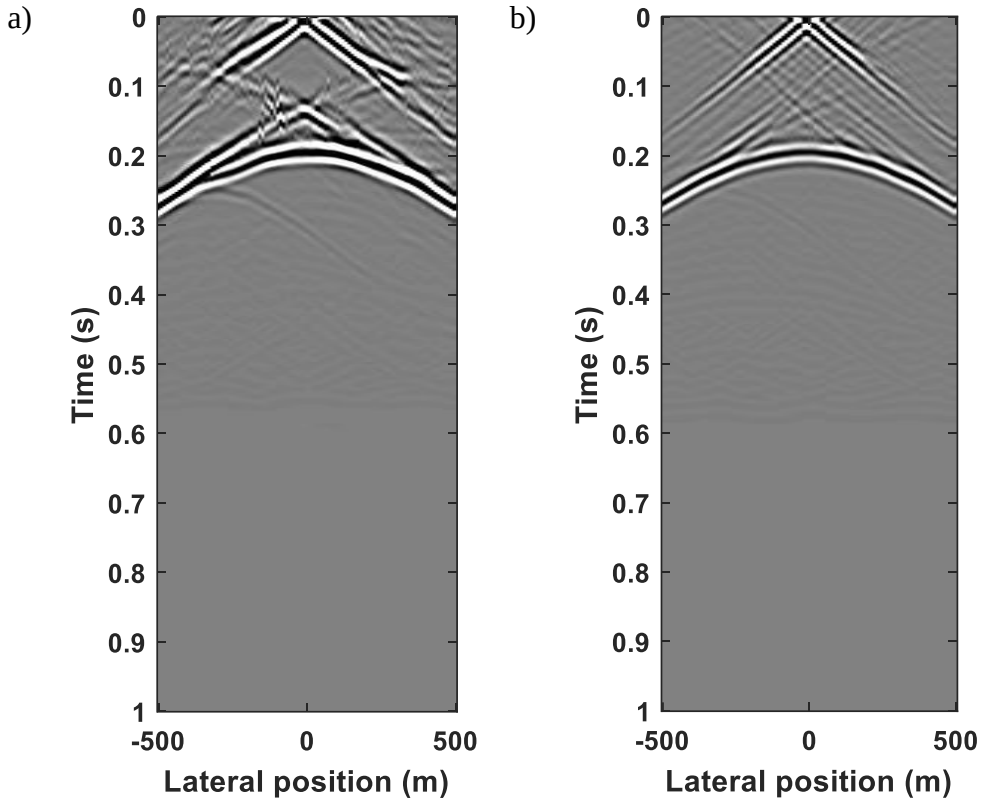

Figure 4-11: CFP redatuming result using a focusing operator (a) estimated from CMP gathers and (b) after one update iteration.

4.4 Diffraction imaging in estimating Green's Function

Despite the promising results when using the focusing operator estimated in the CMP domain, sometimes there may not be a sufficient number of strong reflectors at the desired location to redatum. Due to this limitation, in this section I study the feasibility of CFP redatuming by estimating the focusing operator using the kinematics of diffractions.

Diffractions occur when the seismic wavefront encounters a sharp geological discontinuity, such as faults, pinchout, unconformity, and so on, where the seismic wavelength is larger than the geology (Yilmaz, 2001). Under these circumstances, the seismic energy is scattered and diffracted rather than reflected or refracted. These features can be easily identified in the common offset section or on a CMP stacked section as a weaker amplitude hyperbolic event. The purpose of this section is to introduce the possibility of using the kinematics of diffractions as a means to estimate the Green's function for CFP redatuming.

In seismic processing history, diffractions are often regarded as noise in the data and are removed by the migration process. However, recent studies have proved that the kinematics of diffraction contain useful information in delineating small-scale subsurface inhomogeneities that have a size smaller than or equal to the wavelength of incident seismic wave (Mahapatra and Mahapatra, 2009). Other studies of diffraction imaging by Fomel et al. (2007), Berkovitch et al. (2009) and Klokov and Fomel (2012), just to name a few, have been used successfully to delineate diffractors from reflection events for imaging and velocity estimation purposes. In hard-rock environments where complex geology is abundant, the presence of diffractors may prove to be useful in providing the necessary kinematic information for estimating the Green's function for CFP redatuming.

4.4.1 Estimating Green's Function from diffractions

Seismic data from complex geological settings are often contaminated by diffractions. In this environment, seismic data contains low signal-to-noise where reflection events are weak, which make it challenging to estimate the focusing operator much less applying the redatuming method. Therefore, instead of treating the diffractions as noise, we can use them to construct a sufficiently accurate focusing operator that is needed for CFP redatuming.

Consider picking a diffraction event in the zero-offset seismic section; the two-way time equation representing the diffraction hyperbola (as illustrated in Figure 4-12) here can be expressed as:

$$t(x) = \sqrt{t_0^2 + \frac{4(x - x_0)^2}{V^2}}, \tag{4.3}$$

where $t(x)$ is the two-way travel time in a zero-offset section for a source-receiver pair located at (x,0), $t_0 = \frac{2h}{v}$ is the traveltime for a source and receiver located vertically above the diffractor, h is the depth of the diffractor and V is the RMS velocity. Since the diffraction ray path in the zero-offset section is directly from the source/receiver location to the diffractor, dividing the two-way time calculated using equation 4.3 gives the Green's function, which describes the one-way propagation

between the diffractor and the source and receiver locations. This can be used as the focusing operator with the focus point being the diffractor location.

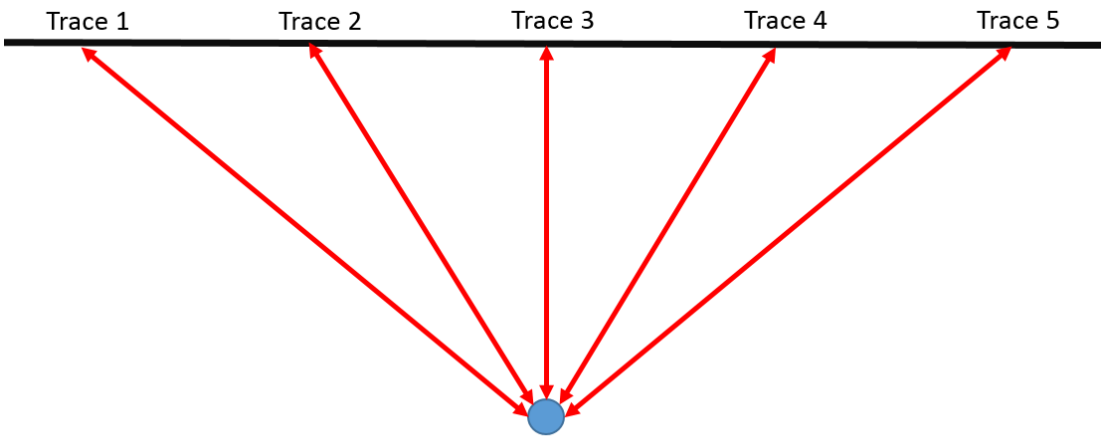

Figure 4-12: Illustration of diffraction ray path from zero-offset seismic section.

4.4.2 Synthetic example of CFP redatuming using diffractions

In this example, a modified version of the velocity model, as shown in Figure 4-3, is used where five sharp edges are introduced. The location of these edges are located at depth of 500 m with a lateral spacing of 500 m, as shown in Figure 4-13. These edges will introduce diffractions to the seismic data. The zero-offset section of data collected using this velocity model is shown in Figure 4-14.

Picking the diffractions is relatively easy as they are clearly distinguished in the zero-offset section from the primary reflections. Figure 4-15 (a) shows the picks of diffractions, even along the strong primary reflection amplitudes, which mask the peak of the diffractions and (c) where picks are only done in area where diffractions are visible. Figure 4-15 (b) shows the extrapolation of the picked diffraction hyperbola for image in (a) and in the case of (d) the interpolation and extrapolation of picks in (c) using equation 4.2. The purpose of this is to determine whether the diffraction areas, which are covered by the strong primary reflection, can be substituted by picking along the primary reflectors as part of the diffraction hyperbola in order to obtain a better CFP redatuming result.

After picking these five diffraction hyperbolas, I performed a linear interpolate between two diffraction picks to generate focusing operators that can be used to redatum sources and receivers to locations without diffractors. The linear interpolation of these focusing operators is shown in Figure 4-16 (a) for picks along the primary reflections and (b) for picks that are interpolated for areas of primary reflections. Picks that are done with part of the primary reflection exhibit more imprints of the undulating, due to the effects from the near surface on the primary reflector, compared to picks of diffractions that are interpolated across the primary reflection area.

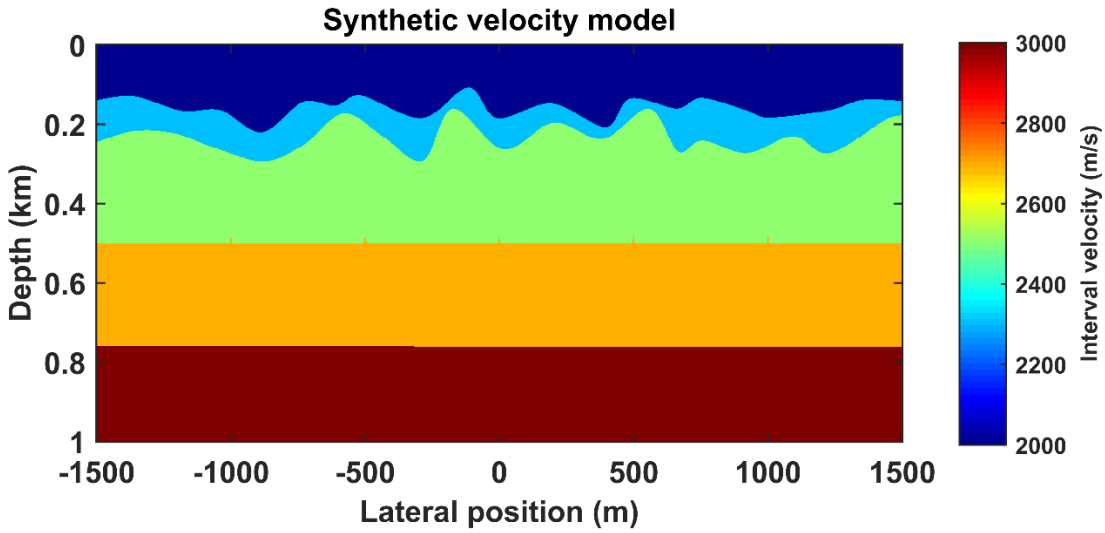

Figure 4-13: Velocity model with five diffractors located at 500m depth at lateral positions of -1000m, -500m, 0m, 500m and 1000m. These sharp edges will produce diffractions in the synthetic data.

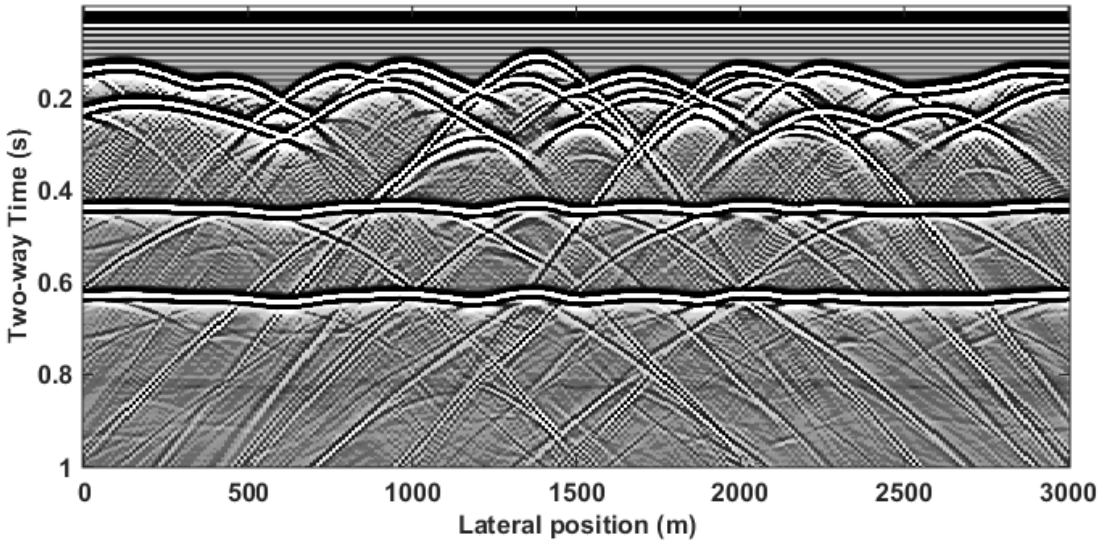

Figure 4-14: Zero-offset section representing the velocity model in Figure 4-13. Five diffractions can be clearly observed at the locations of the diffractors as marked in the velocity model.

The CFP redatuming result using diffraction picks with part of the primary reflections and picks of only the diffraction, where areas that are masked by the primary reflection are interpolated, as show in Figure 4-17 (c) and (d) respectively. Although both of these picks unravel the undulation imprints very well, we observe that the picks with the interpretation towards the area where primary reflection masked the diffractions produce a more accurate result when compared to the picks that include the primary reflection in areas where it covers the diffractions. This is clearly observed when comparing the redatuming result of these two picks with the result using the accurate focusing operator, see Figure 4-17(b), with shot at 0 m. The redatumed result for picks at x=-750 and 250 m are from operators interpolated between two picked diffractions. When the result is compared to the input data, as shown in Figure 4-17(a), the target reflector between 0.6 s and 0.7 s has been shifted up by about 0.4 s and the undulation imprints on it have been significantly reduced. The focusing operator estimated here can also be improved through the use of the DTS panel as previously mentioned.

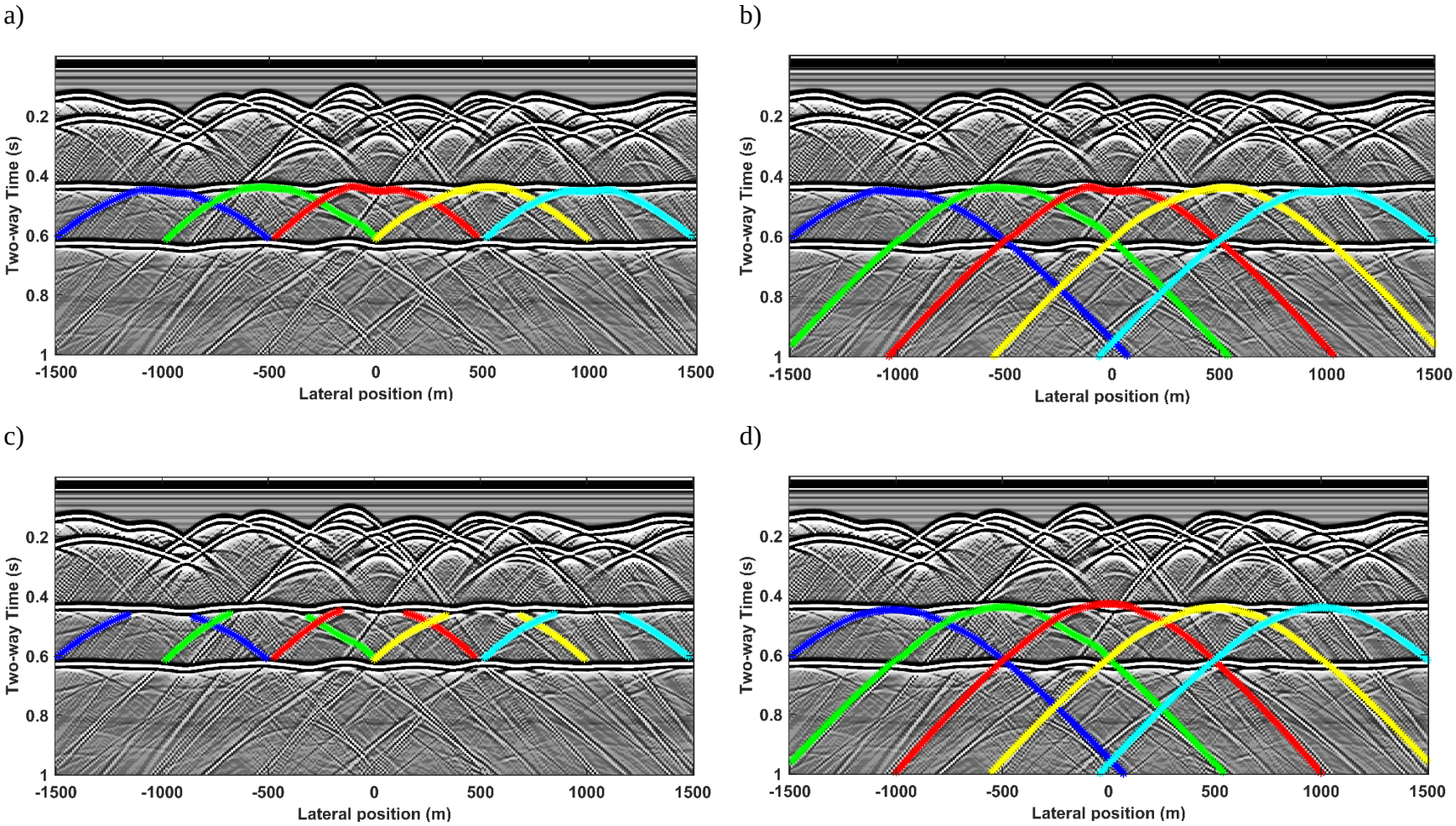

Figure 4-15: Picking of diffraction events on the zero-offset seismic section a) with picks including primary reflections that cover the peak of diffraction and c) at visible areas only of the diffractions that are not masked by primary reflections. b) shows the extrapolation of tail diffractions from picks at a), and d) shows the interpolation and extrapolation of picked diffractions at (c) for areas masked by strong primary reflectors, using equation 4.3.

a)

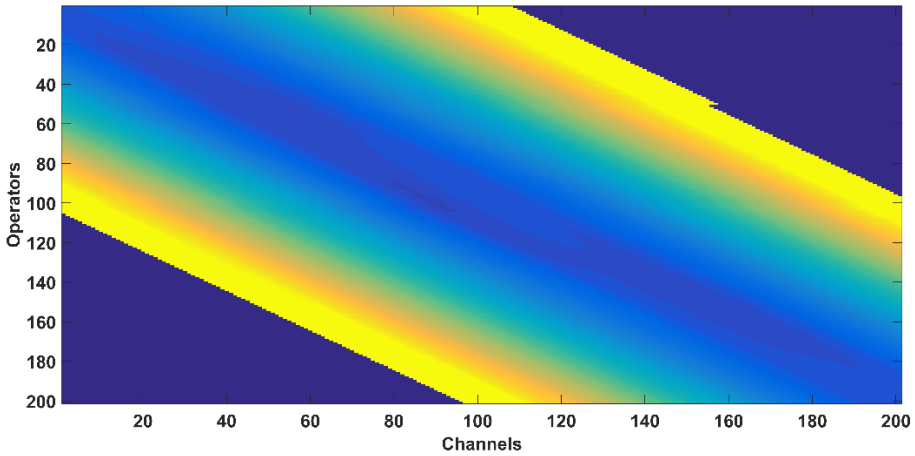

b)

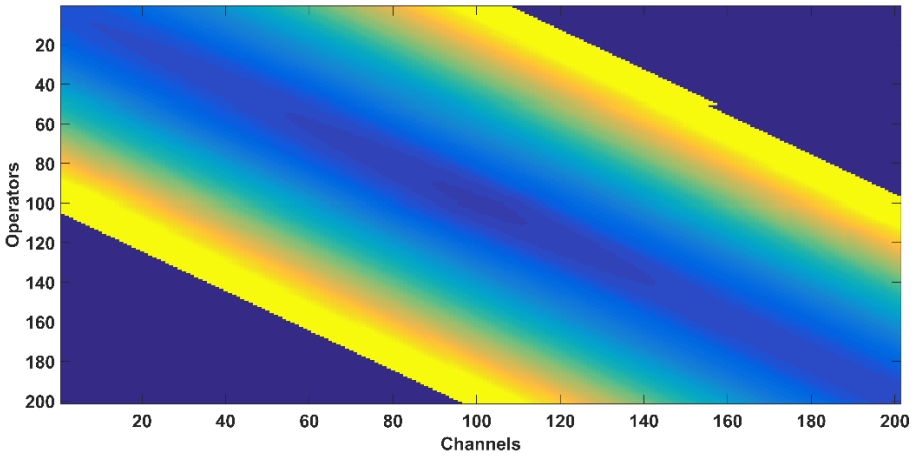

Figure 4-16: Interpolation of diffractions across to neighbouring diffractors for a) picked along visible diffractions and primary reflections and b) picks done only on diffraction events and interpolated across the primary reflections area for CFP redatuming purpose.

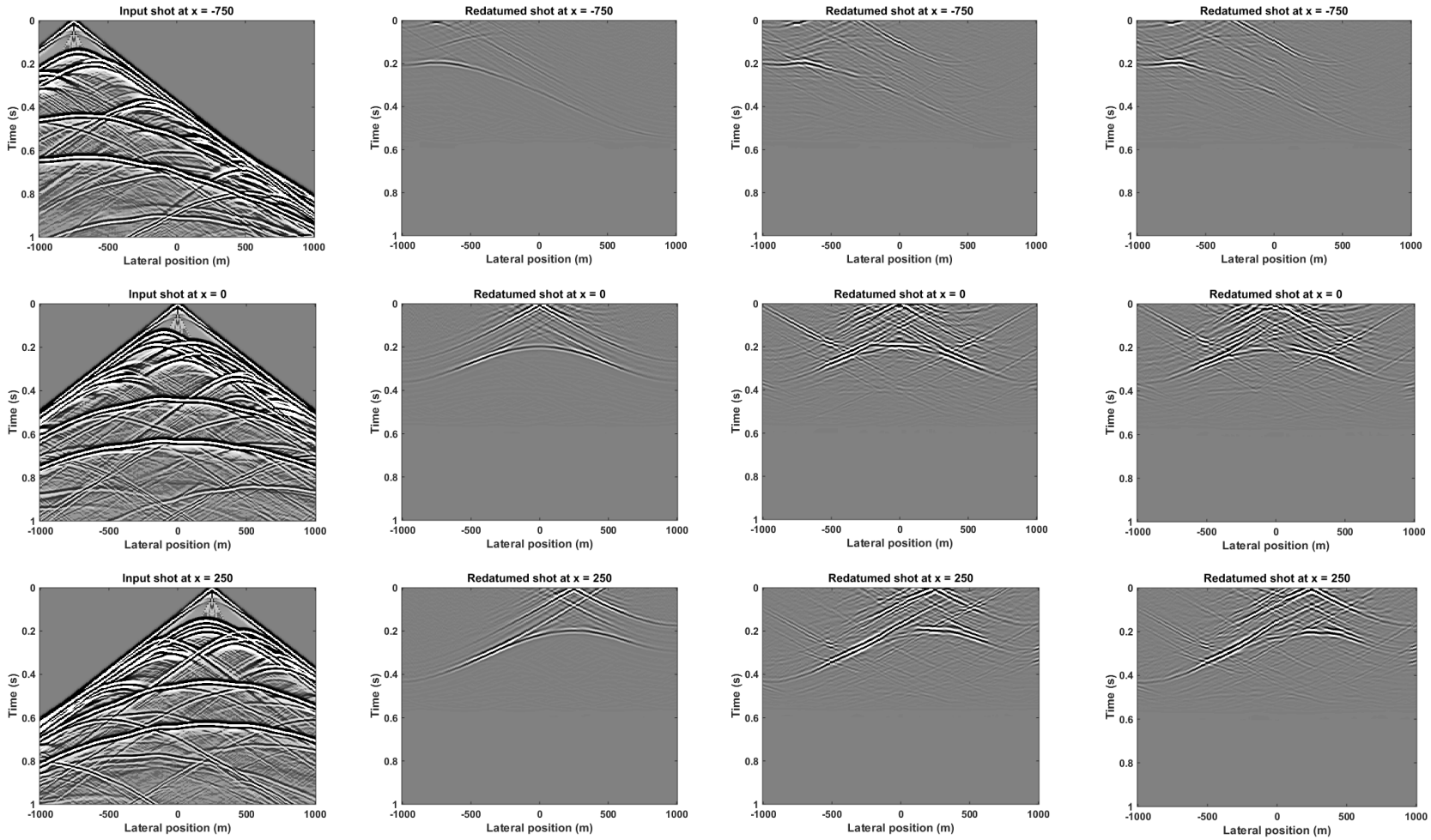

a) Synthetic data b) Accurate operator c) Full diffractor operator d) Interpolated diffractor operator

Figure 4-17: The comparison of results from CFP redatuming using b) an accurate operator, c) fully picked diffraction events, and d) partially picked diffraction events that are not covered by strong primary reflection events. a) shows the input synthetic raw shot gathers before redatuming.

4.5 Comparison of model- and data- driven method

In this section, I present a comparison of the two different redatuming methods, finite difference using backpropagation and the CFP method, which are discussed in Chapter 3 and 4. This work has been published as an extended abstract in the EAGE special issue journal (Ung and Bona, 2016).

The synthetic model used for this comparison is shown in Figure 4-18(a) where undulating and dipping interface was included to introduce distortion to the recorded data. The velocity used for this model ranges from 3000m/s to 6000m/s. The two flat reflector at depth 600m and 800m in this model is used as the reference reflector where sources and receivers will be redatumed to and the target reflector respectively. Synthetic data is gathered with a fixed receiver array from 200m to 1800m with a spacing of 10m while having a source located at every second receiver position. Both sources and receivers are located at the surface. Finite difference modelling was used with a voxel spacing of 2m and a sampling rate of 0.1ms. The central frequency for the source is 60Hz and total recording time is 600ms. The result is shown in Figure 4-18(b).

It is observed in the raw shot gather that the near surface undulations and dipping reflector distort the reflection of the deepest reflector. My aim is to apply both the model and data driven wave equation redatuming methods to improve the imaging quality of synthetic data by relocating the sources and receivers virtually to the first horizontal reflector that is 200m above the last reflector that was degraded as see in the synthetic data. Wave equation redatuming for the finite difference and CFP method will be performed using the accurate velocity model as an input model for backpropagation and to obtain the focusing operator respectively. These results will be used as a control to validate the feasibility of the method in an event the accurate velocity model is unavailable. For the feasibility test, a smoothed velocity model will be used as an input for the finite difference method and the focusing operator will be obtained from the CMP gathers. Figure 4-19 illustrates the process that I will employ to perform redatuming using the finite difference method, which is illustrated in panel (a) and (b), and the CFP method, as illustrated in panel (c) and (d).

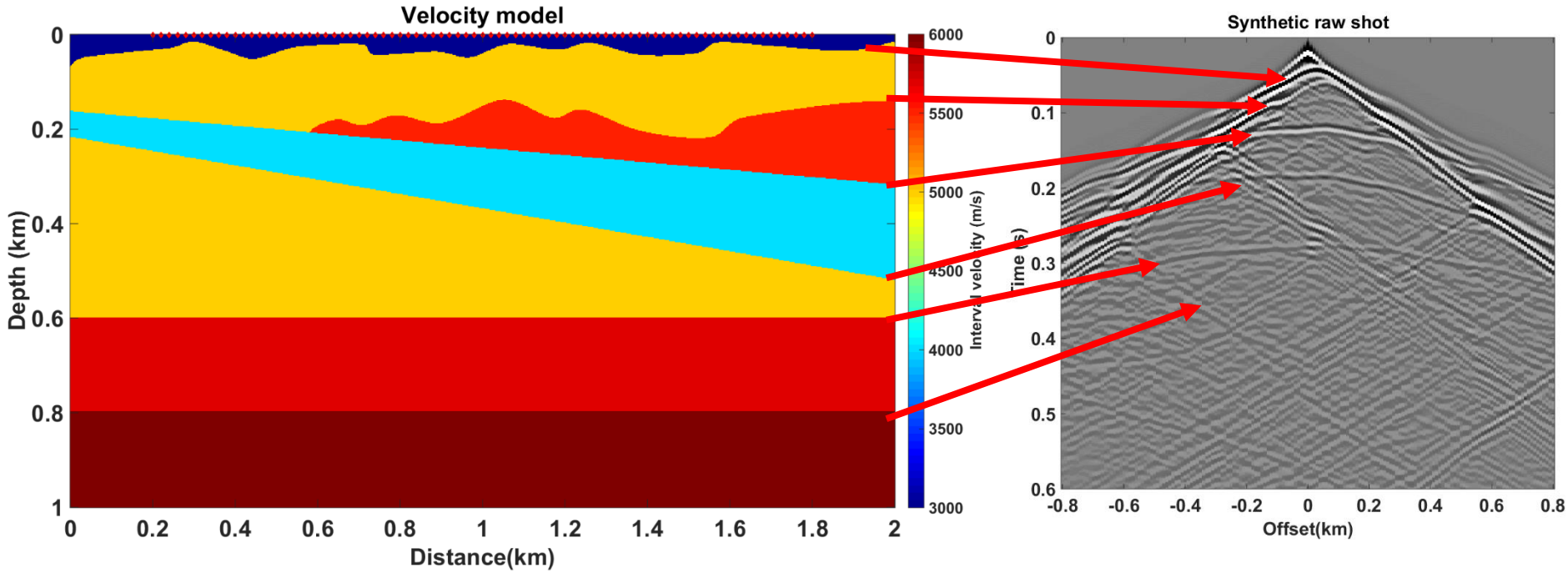

Figure 4-18: (a) Initial velocity model used to acquire synthetic data (b) example of synthetic shot record.

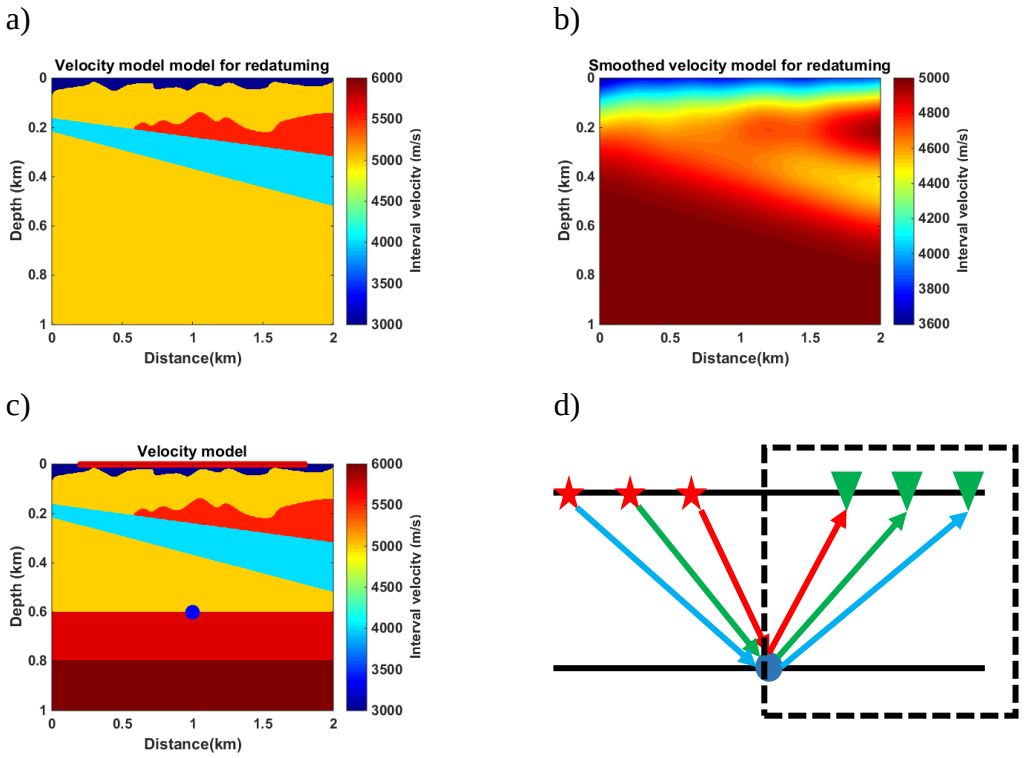

Figure 4-19: Input parameters for finite difference redatuming using (a) the accurate velocity model and (b) a smoothed velocity model. For CFP redatuming, the focusing operator is acquired using (c) modelling from the accurate velocity model and (d) estimated using CMP gathers.

The output datum for these experiments is to the first horizontal reflector at 600m. The redatumed result shows the reconstructed reflection from the horizontal reflector at 800m which is marked by the red arrow in Figure 4-20 (b) through 4-20 (e). Results of finite difference redatuming obtained using backpropagation with the accurate and smoothed velocity models as input are shown in Figure 4-20 (b) and 4-20 (c). Here we observe that there are a significant amount of finite difference dispersion noise as well as boundary artefacts being introduced. These artefacts can be reduced using a finer sampled velocity model, which can be accomplished with the availability of more computational resources. With the use of the smoothed velocity model, the hyperbola still exhibits minimal undulating characteristics from the near surface structures, however the position and general shape of the reflection hyperbola for the target reflector is accurate.

Figure 4-20 (d) and 4-20 (e) shows the result of CFP redatuming using operator acquired from accurate velocity model and also estimated from CMP gathers respectively. It is noted that redatuming using the CFP method shows less artefacts than using the finite difference method. The linear dipping artefacts from edges of the redatumed data are reduced using F-K filter. CFP redatuming using the CMP estimated operator also shows encouraging result which can be further improved by performing the iterative updating in the DTS panel as mentioned earlier in this chapter. We can clearly observe that the amplitude of the reflection hyperbola from the target reflector diminishes at the far offset. This is due to the aperture of the method.

Figure 4-21 (a) shows the stacked section of the finite difference redatuming with the accurate velocity model and Figure 4-21 (b) with the smoothed velocity model as the input. Figure 4-21 (c) is the stack result of applying the CFP redatuming using the accurate focusing operator and Figure 4-21 (d) is from using a focusing operator estimated from the CMP gathers. The noise generated from the finite difference method has been removed from the stacking process. The stacked result is converted from time domain to depth domain. It is observed in Figure 4-21 (a) through Figure 4-21 (d) that not only the reflection from the target reflector can be imaged (flat event at 200m) but also the weak reflection response from the bottom of the model (flat event at 400m) which proves strength of the imaging power of redatuming.

To summarise, wavefield extrapolation redatuming method is a promising technique for eliminating near-surface complexities to simplify hard rock seismic data. The finite difference and CFP redatuming method discussed shows good results in handling of both laterally and vertically varying velocities of the overburden and even in recovering week reflection amplitudes. Even the feasibility test with a smoothed velocity model and estimated focusing operator shows equally good results. That said, the accuracy of finite difference redatuming method relies heavily on the input velocity model of the overburden and the CFP method requires a continuous reference reflection surface to be performed. Table 4-1 shows a summary of the differences in the methodology of both redatuming methods. Due to computational power constrain and lack of accurate velocity model for the finite difference redatuming technique, the CFP method will be used in the following chapter, where I present several case study on field data.

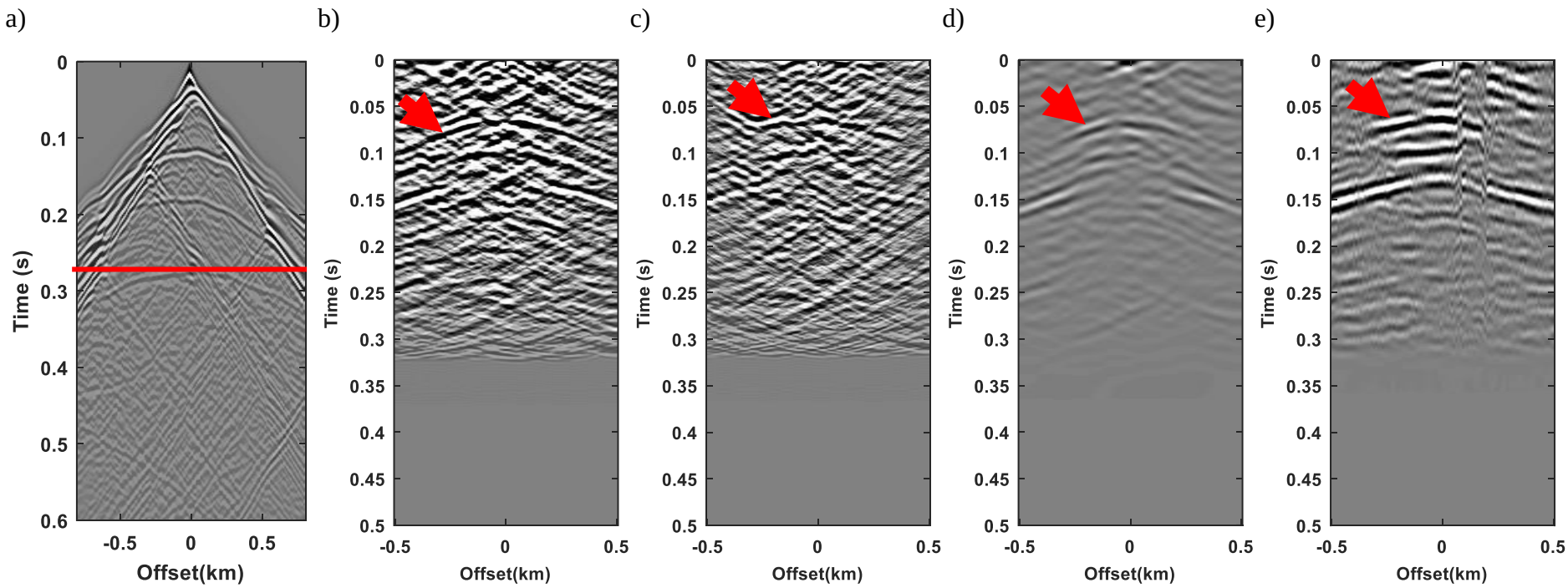

Figure 4-20: Synthetic data in common source gathers of (a) input data with the red line indicating the redatuming output location in time. The result of using finite difference redatuming using (b) accurate velocity and (c) using smoothed velocity as input. The CFP redatuming result (d) using a focusing operator from the accurate velocity model and (e) estimated from CMP gathers. The red arrow indicated the reconstructed target reflection.

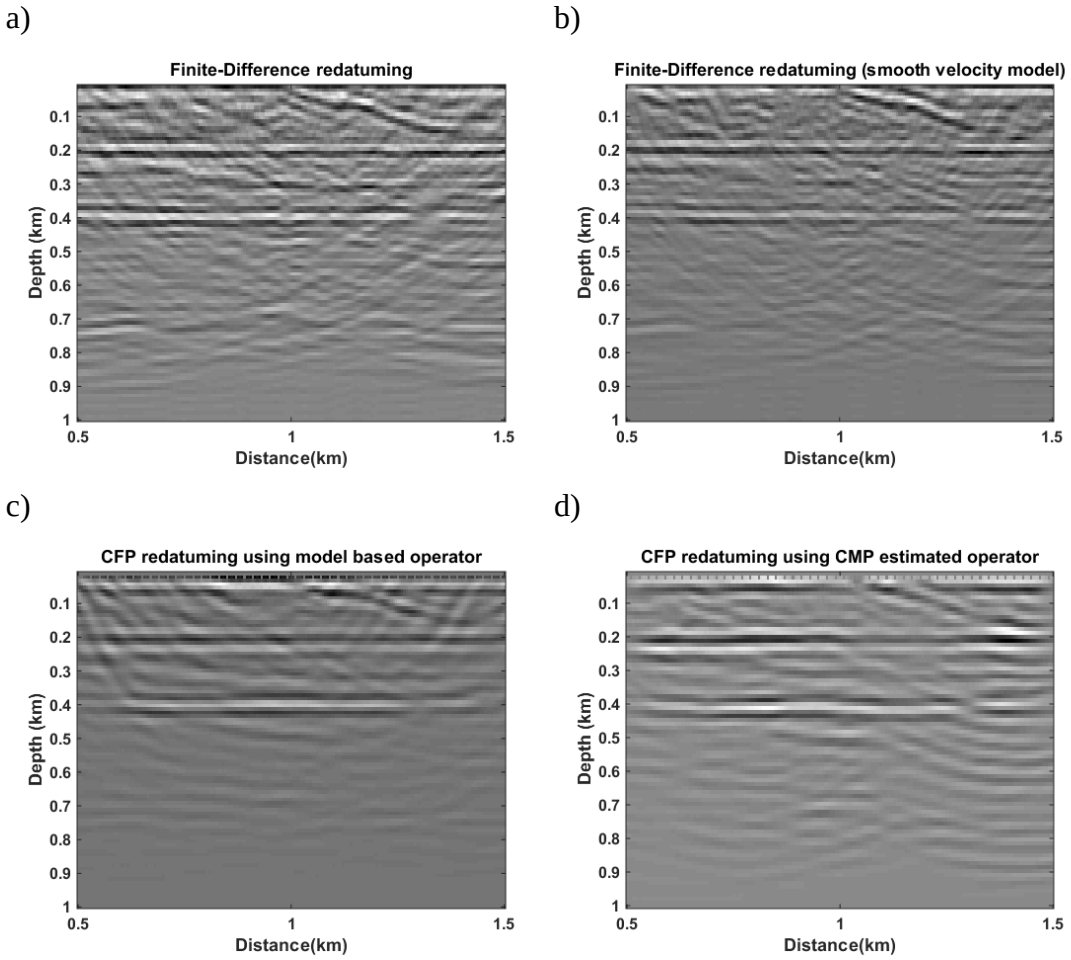

Figure 4-21: Depth domain stack section of finite difference redatuming using (a) the accurate velocity model and (b) the smoothed velocity model as input. CFP redatuming stack section produced using the focusing operator estimated by (c) the accurate velocity model and (d) CMP gathers.

Finite-difference method	Common Focus Point method
Methodology	
Extrapolation of wavefield.	Focusing of wavefield.
Advantageous	
Theoretically most accurate; Lateral and vertical varying velocities can be handled; Stable computation for steeply dipping events.	Velocity model independent; Lateral and vertical varying velocities can be handled; Uses less computational power; Operator can be iteratively updated to improve redatuming result.
Disadvantageous	
Complex subsurface requires denser grid to avoid spatial aliasing and finite difference dispersion; Computationally demanding; Velocity model cannot be easily updated.	Requires a continuous reference reflector or a set of diffractors; Determining and updating operators are not fully automated; Tracking of events in the DTS panel can be challenging for noisy data.

Table 4-1: Summary of comparison of finite difference vs CFP redatuming methods.

Chapter 5 Case studies

5.1 Harvey area, southern Perth Basin, Western Australia

In 2011, the Department of Exploration Geophysics at Curtin University re-acquired the 11GA_LL2 2D seismic line over the southern part of Perth Basin. The survey took place near Harvey, WA, which is approximately 140 km south of Perth, WA. The survey was part of the South West CO_2 Hub project that was initiated under the Federal Carbon Capture and Storage (CCS) program. To date, several 2D, 3D and borehole seismic datasets within this area were acquired since 1990. Table 5-1 shows the list of seismic survey lines obtained from the area along with the quality of the data from 1991 to 2011. In this case study, I look at the acquired line 11GA_LL2 specifically. The location of this line is shown in Figure 5-1. Herein, I attempt to improve the imaging of certain aspect of the processed data using the CFP redatuming technique, which can be potentially important for geosequestration. Here the focusing operator is estimated using the CMP gathers.

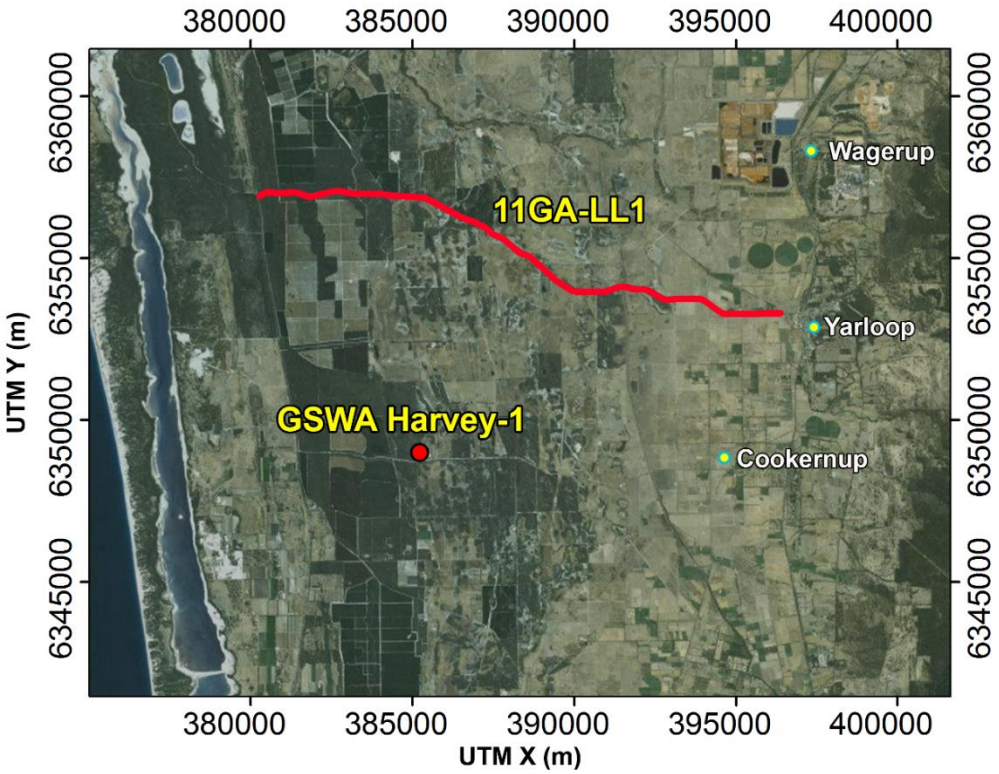

Figure 5-1: Location of survey line 11GA_LL2 that was re-acquired by the Department of Exploration Geophysics, Curtin University (Urosevic et al., 2014).

Survey	Line	Length (km)	Quality rating	Comments
GSWA Lower Leseure 2011 (Vibroseis)	11GA_LL1	17.5	1	Processed by Velseis in 2011
	11GA_LL2	14.6	1	
	11GA_LL3	14.8	1	
	11GA_LL4	25.9	1	
	11GA_LL5	15.6	1	
	11GA_LL6	10.5	1	
Wellesley 2008 (Vibroseis)	EW08_01	11.3	2	Processed by CGGVeritas in 2008
	EW08_02	5.8	2	
	EW08_03	11.1	2	
	EW08_04	10.4	2	
Korijekup 1991 (Vibroseis)	P91_101	31.8	3	Processed by Simon-Horizon in 1991
	P91_102	13.6	2	
	P91_103	44.0	1	
	P91_104	6.4	2	
	P91_105	6.7	2	
	P91_106	7.4	3	
	P91_107	8.2	3	
	P91_108	7.4	2	
	P91_109	9.4	2	
	P91_1010	8.4	2	
	P91_1011	7.2	2	
	P91_1012	7.9	2	
	P91_1013	7.0	3	
	P91_1014	7.9	2	
	P91_1015	9.4	2	
	P91_1016	5.6	4	
	P91_1017	10.6	2	

Table 5-1: List of seismic lines along the southern part of Perth basin from 2011 to 1991 (Zhan, 2014).

5.1.1 Processing procedure and initial results discussion

The Department of Exploration Geophysics from Curtin University applied standard seismic processing steps to the dataset. The 2D acquisition line is crooked due to the seismic crew's limited access to the area, as data was acquired along the road. A vibroseis source was utilised producing 537 shots fired at a 25 m spacing interval. A receiver array with 300 channels was used to record the data that moves along with the shot point in a split spread configuration (Figure 5-2) wherever possible. Receiver spacing was at 25 m as well. The shots were fired from the west direction to the east. The 2D seismic data was processed using nominal (straight line) geometry. The main focus during processing was on enhancing the data quality, denoising and stacking velocity analysis with the main challenges being the crooked line acquisition geometry and presence of steeply dipping reflection events from strongly dipping geological structures (Pevzner et al., 2013), such as fault planes. Table 5-2 shows the processing steps and parameters used.

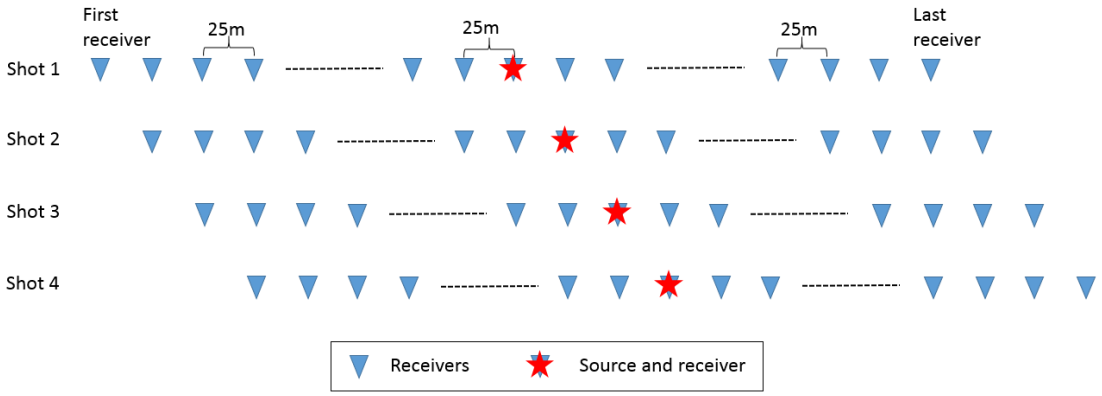

Figure 5-2: Split spread acquisition configuration used in acquiring the 2D seismic line with a source and receiver spacing of 25m. Receiver array of 300 channels moves along with each shot position.

Procedure	Parameters
Data Input	SEG-D data input
Geometry assignment	Applied from ASCII files
Binning	Bin size 12.5 m
Trace editing	Kill bad traces
Elevation statics	Final datum elevation - 0 m, Replacement velocity - 2250 m/s
True amplitude recovery	Time power constant 1.5
Air-blast attenuation	Attenuation mode for air velocity at 331 m/s
TFD noise rejection	Frequency range 0 - 125 Hz, aperture - 21
Spiking deconvolution	Zero phase, applied in at a gate Decon Operator length - 80 ms Operator 'white noise' level - 1%
Bandpass filtering	8-14-70-120 Hz
Trace muting	Top muting
Automatic gain control	50 ms, applied before FK filter and removed after
Linear movement correction	applied before F-K filter and removed after
FK filtering	Applied in a window
Bandpass filter	7-10-140-150 Hz
Interactive stacking velocity analysis	5 iterations
Residual static correction	2 - 3 iterations (Max power autostatics)
Normal moveout correction	30% - NMO muting
Common depth point stacking	Method of trace summing - mean, Power scalar for stack normalisation 0.5
FX-deconvolution	Wiener Levinson filter, 1 - 120 Hz
Time migration	Post-stack Phase shift, Pre-stack Kirchhoff

Table 5-2: Processing chart for seismic line 11GA_LL2 (Pevzner et al., 2013).

The key conclusion drawn from this project as discussed by Pevzner et al. (2013): (1) variation of the seismic data quality, particularly from the west side of the data to the east side of the data (2) inclusion of denser sources and receivers sampling with longer offsets along the east-west direction for optimal imaging of the major fault striking northwest–southeast, (3) Presence of shallow coastal limestone with strong variations of velocities that deteriorates imaging requires advanced processing techniques as static correction is insufficient, (4) Distortion of data from the crooked acquisition line creates false structures, (5) poststack depth migration (PSDM) improves imaging over larger steep-dip faults, major fault blocks, subtle internal faulting and weak reflections over poststack time imaging (PSTM).

An interpretation of the Kirchhoff stack section is shown in Figure 5-3. In this section, there are a number of faults, with the biggest fault being the Darling fault as marked. In addition to this, four distinct interfaces can be observed from this seismic section and are marked in red, green, blue and purple. Taking a closer look at this seismic section, it is observed that the quality of the seismic section appears to be of better resolution on the footwall wall (East side of the seismic section) compared to the resolution on the hanging wall side of the Darling fault. This is true especially between the blue and purple interfaces.

The purpose of applying CFP redatuming to this seismic data is to reconstruct and improve seismic reflection quality in the said low resolution area, which I will refer to as the low amplitude zone. Sources and receivers will be virtually relocated so that data is seen as recorded on the blue interface, above the low amplitude zone. This will remove any propagation effects from the subsurface above the blue interface and therefore increase the quality of seismic reflection in the area under this reflector.

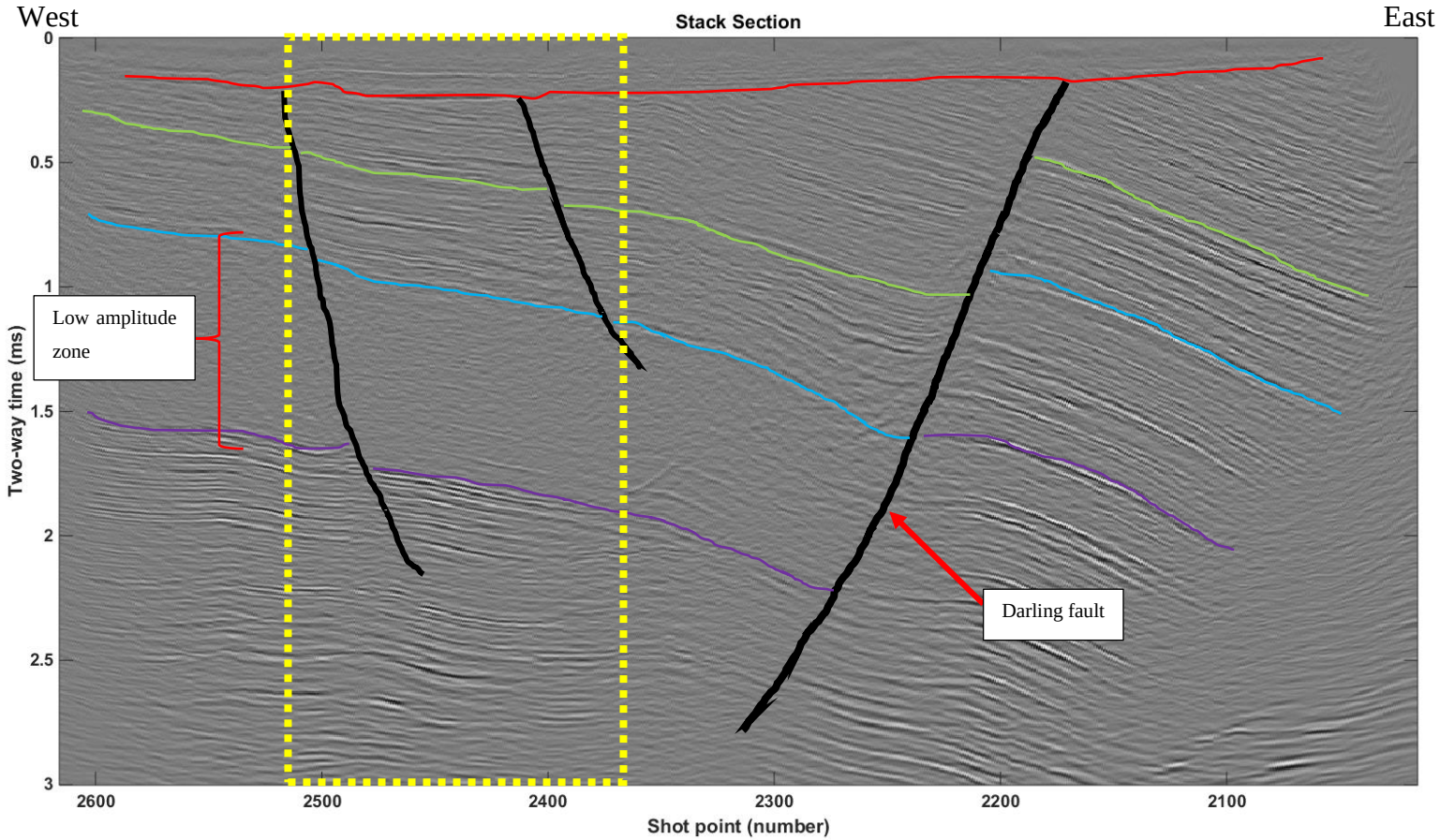

Figure 5-3: Interpretation of pre-stack Kirchhoff migration (Zhan, 2014). The black lines cutting across the interface represents the faults observed in the seismic data. As observed, there are four interfaces marked by the red, green, blue and purple lines. The yellow area marks the area of interest for CFP redatuming.

5.1.2 Application of redatuming

Since we do not have a sufficiently accurate velocity model to apply model-based redatuming techniques, CFP redatuming technique will be used to virtually relocate the sources and receivers from the surface into the subsurface. The key ingredient for applying the CFP redatuming technique lies in the focusing operator that will be used to remove the upgoing and downgoing wavefields between the receivers and sources and the new location of the receivers and sources respectively. As previously mentioned, in this survey the receiver arrays are moved with every shot location. This makes computing and applying the focusing operator a little more complicated. For example, if we have a standard survey with fixed receiver array locations, we just need to compute one Green's function with a fixed aperture for each focus point. However, in the event where the receiver array moves with the sources, we would have to compute the Green's function for each aperture of the receiver array for one focus point (See Figure 5-4 for illustration).

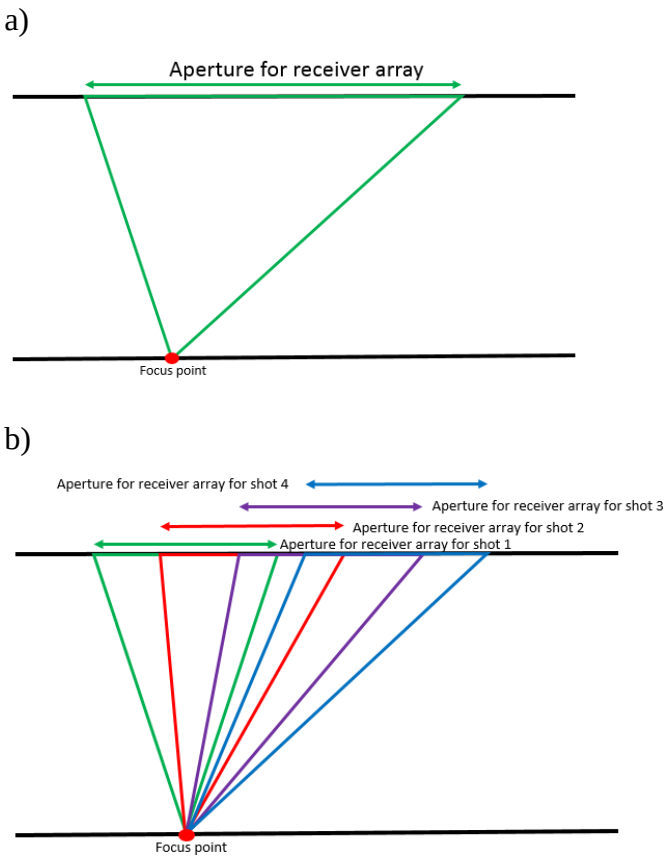

Figure 5-4: Aperture of Green's function for CFP redatuming with (a) Fix receiver array location; (b) Moving the receiver array location with each shot. In (b), the aperture of the Green's function describing the propagation path between the focus point moves with each different receiver array location.

To avoid having to construct multiple focusing operators for each receiver array aperture, I clipped and sorted the data in such a way that they share the same aperture for the receivers. In this dataset, we are only interested in the low-amplitude zone in the hanging wall side of the seismic section. We therefore clip the data to only the area in the yellow box in Figure 5-3. On the acquisition layout, as shown in Figure 5-5, the green area marks the selected receiver array location and the black marks the selected sources location that will be used for CFP redatuming. The total number of shots for this area is 150 with 25 m spacing and a total of 150 channels per shot with a 25 m spacing as well.

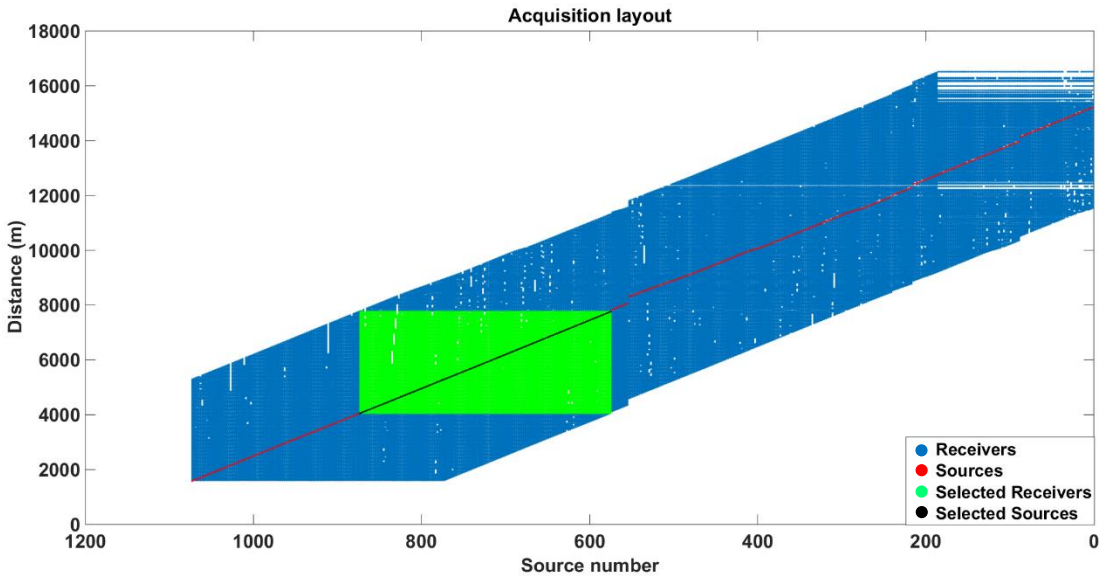

Figure 5-5: Acquisition layout of the 2D survey with selection of sources (black mark) and receiver arrays (green mark) that will be used for CFP redatuming.

Now that we have selected the area of interest and sorted the data to incorporate fixed receiver arrays for every shot covering the area of interest, we can start to look for the focusing operator. Ideally, we are looking for a focusing operator with the focus point on the blue horizon, with a two-way time of 0.8 s to 1.2 s, within the yellow box in Figure 5-3. With the absence of a sufficiently accurate velocity model and diffractions, we estimate the focusing operators in the CMP domain as shown in Figure 5-6. The stacked result of CFP redatuming using this estimated operator is shown in Figure 5-7.

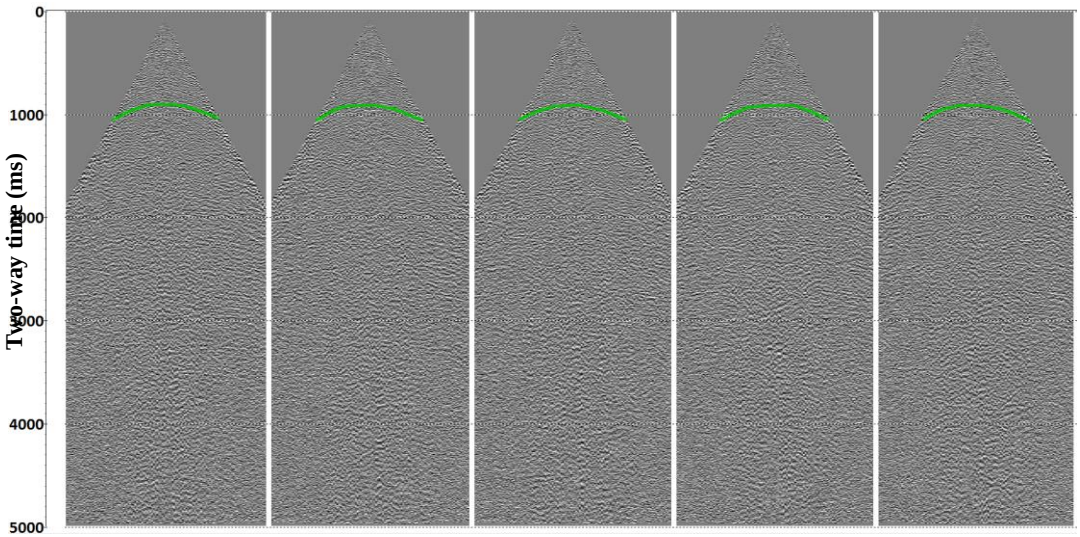

Figure 5-6: CMP data gathers. The green line indicates the picks of reflection from the blue horizon in Figure 4-4, which will be used as the focusing operator for CFP redatuming.

From the CFP redatumed stack section, strong linear events can be seen on both side of the section. These linear events are the result of the finite aperture (discussed in section 4.5) and can be removed using a spatial or F-K filter. For a comparison on how CFP redatuming has improved the data, we apply a F-K filter to the CFP redatumed section and also produce a stacked section with the original data that has been clipped to cover the same area as the redatumed output, which is shown in Figure 5-8. In the zoomed section (Figure 5-9), a better continuity of reflectors in the low-amplitude zone is revealed, as indicated by the red arrow. In addition, two reflection events can be observed after CFP redatuming has been applied to the data as indicated by the red circle in the zoomed section.

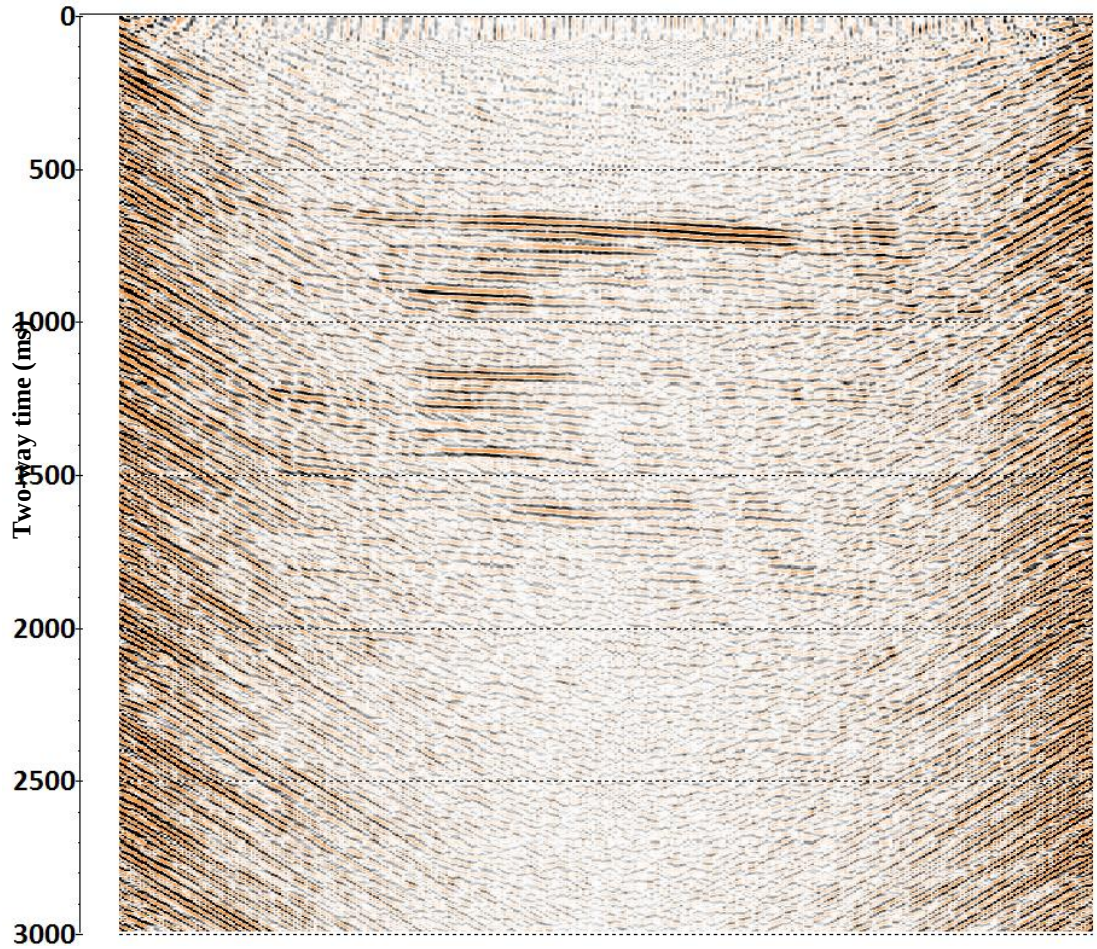

Figure 5-7: CFP redatuming stack section. Strong linear events seen on the side of the data are results of the finite aperture.

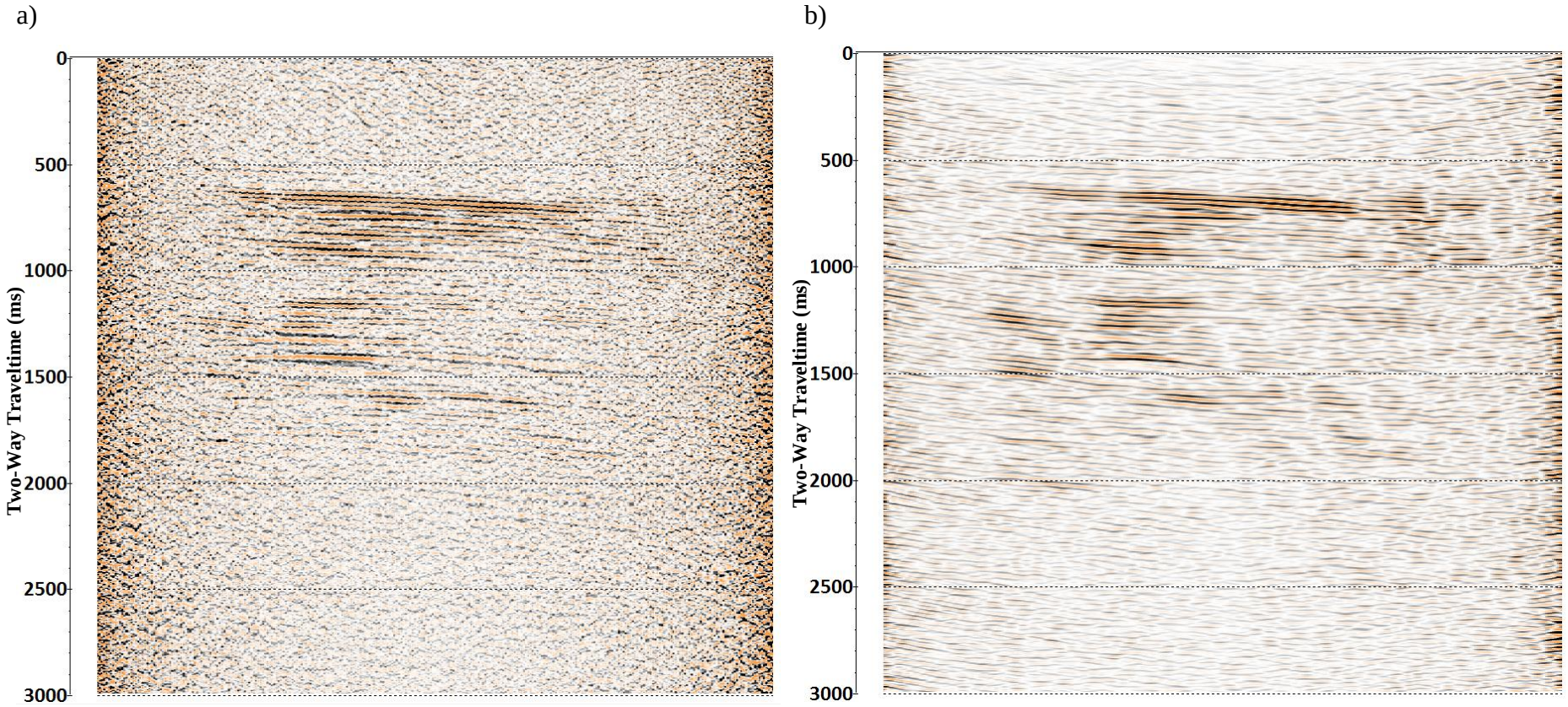

Figure 5-8: Stacked section of (a) initial input data with clipped sources and receivers and (b) CFP redatuming on clipped sources and receivers data with a F-K filter to remove linear events.

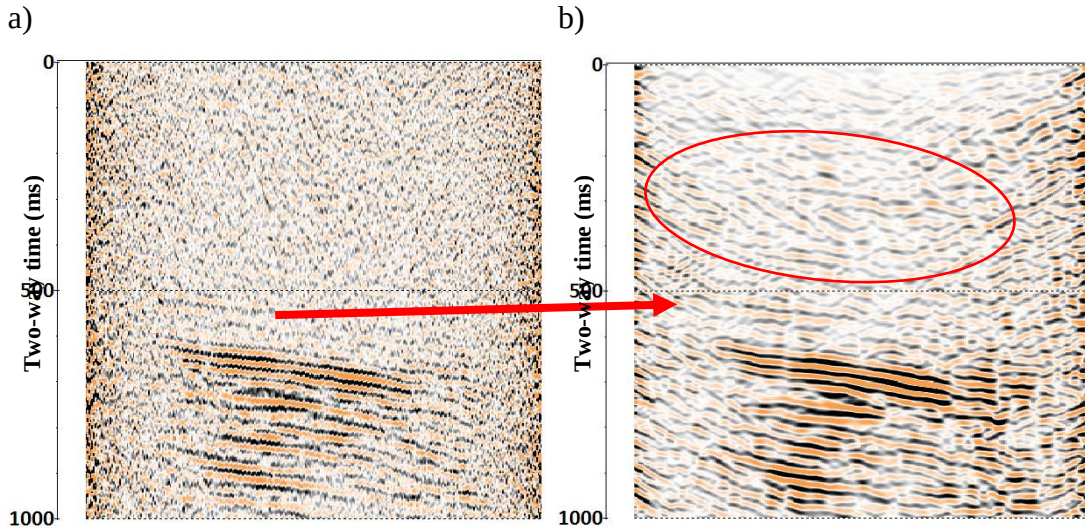

Figure 5-9: Stack section zoomed from 0 to 1000ms for (a) input data and (b) CFP redatumed data.

5.1.3 Discussion of result

CFP redatuming is a data-driven method that virtually relocates the sources and receivers from the surface to a new user-define datum in the subsurface. This transforms the recorded data by removing all the wave propagation between the new source and receiver locations and their initial locations. At the heart of CFP redatuming lies Green's function, also known as the focusing operator, which describes the downward/upward propagation response between the initial source/receiver locations and their new locations. In this case study, the absence of a sufficiently accurate velocity model or diffraction points leads to the estimation of the focusing operator in the CMP gathers as strong reflection events were observed above the area of interest. The CFP redatuming result suffers from finite apertures, which produces the linear artefacts and are reduced using F-K filter. In this dataset, the goal of redatuming is to illuminate the low-amplitude zone, which is observed between the blue and purple horizons in Figure 5-3. The redatuming results show better continuity of existing reflection events that can be identified on the data before redatuming. In addition, the redatumed stack revealed new reflectors that are otherwise difficult to detect before redatuming. This result shows the potential of the redatuming technique to improve seismic imaging in areas where seismic reflection may be weaker or distorted due to near-surface effects.

5.2 Mineral System Drilling Program surface seismic data

The Mineral System Drilling Program (MSDP) is a collaboration between the Deep Exploration Technology Cooperative Research Centre (DET CRC), Geological Survey of South Australia, Kingdom Resources and Minotaur Exploration, which was initiated in 2015 (McAvaney et al., 2017). Part of this exploration program took place in the southern side of Six Mile Hill area located in South Australia. The objective was to map mineralisation and geochemical footprints under cover in a regional scale over the southern margin of the Gawler Ranges on the northern Eyre Peninsula in South Australia. Deposits in this area consist of iron ore, copper and gold. In conjunction with drilling, several 2D seismic datasets were acquired to help with the imaging of the subsurface. In this section, I implement the CFP redatuming technique to improve seismic data imaging below a strong reflector, believed to be the basalt, where seismic resolution is poor. The seismic data (line MSDP01) was collected approximately 40 km northeast of Port Augusta, South Australia, as shown in the Figure5-10.

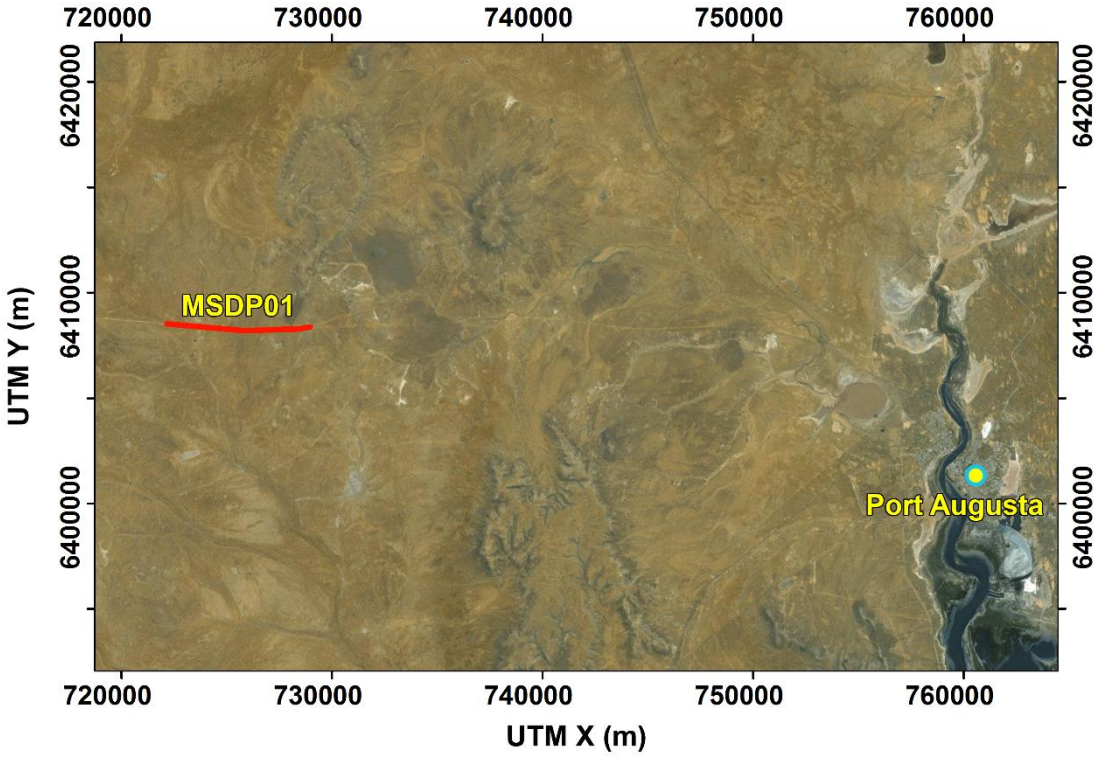

Figure 5-10: Location of 2D seismic survey MSDP01 marked in peach colour.

5.2.1 Seismic data acquisition and processing

The 2D seismic reflection data was collected by the Department of Exploration Geophysics of Curtin University. The objective of performing the seismic acquisition was to investigate and optimise the seismic reflection methodology for imaging of hard-rock environments. Seismic reflection data were acquired using a fixed receiver array with a moving source. The receiver array consisted of 300 channels with a 15 m spacing. A total of 299 shots were fired between every receiver. The source spacing was 15 m as well. The total recording time was 1.5 s with a 0.2 ms sampling rate. Figure 5-11 shows an example of the recorded data. We observe that the data is heavily contaminated with ground roll and air-waves with low S/N.

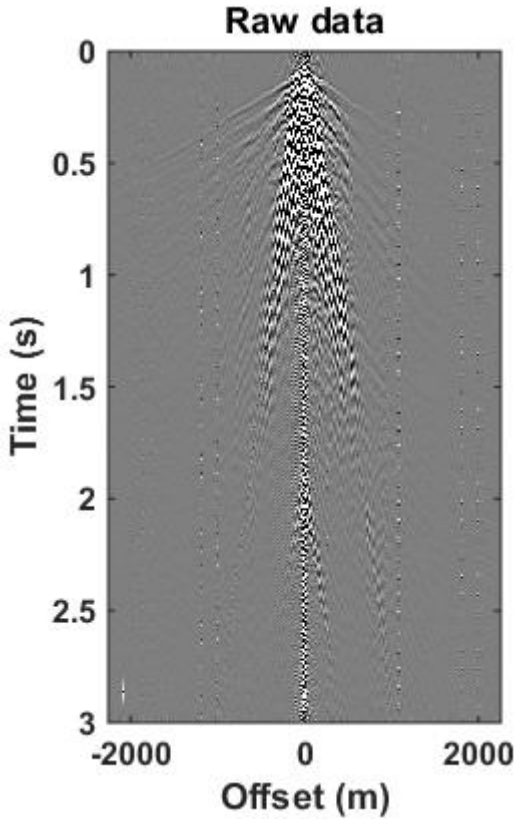

Figure 5-11: Recorded data from MSDP01 line. Data is heavily contaminated with ground roll and air-wave noise and has an overall low S/N.

The data was then processed in-house to improve the quality of seismic imaging (S. Ziramov, personal communication August 24, 2016). Standard seismic processing techniques were employed to improve the S/N of the dataset. Besides refraction statics to account for the elevation change in the acquisition surface, spatial filtering and air-blast attenuation was used in an effort to de-noise the data as best as possible. Table 5-3 shows the processing steps applied to the recorded data. The processing results are shown in Figure 5-12. The ground noise and air-wave have been removed at the expense of losing data in the near offsets. The overall S/N has also been improved thus revealing reflection events beneath 400 ms. Despite this, the resolution of the data is quite poor when compared to data collected over soft-rock environments as seen in the previous section. Figure 5-13 shows the brute stack of the data using a constant NMO velocity of 4500 m/s up to 400 ms and 5000 m/s for times longer than 400 ms.

Procedure	**Parameters**
Data Input	SEG-D data input
Geometry assignment	Applied from ASCII files
Binning	Bin size 7.5 m
Trace editing	Kill bad traces
Refraction statics	Final datum elevation – 130 m, Replacement velocity - 4500 m/s
2D spatial filtering	40% rejection for spatial filter
Air blast attenuation	Attenuation mode for air velocity at 340 m/s
Normal moveout correction	90% - NMO muting
Bandpass filter	1-70-90-140 Hz
Automatic Gain Control	350ms
Common depth point stacking	Method of trace summing - mean, Power scalar for stack normalisation 0.5
FX-deconvolution	Wiener Levinson filter, 5-100 Hz
Spectral shaping	Whiten in percentage
Bandpass filter	1-30-70-100 Hz

Table 5-3: Processing chart for seismic line MSDP01.

The stack section shows several of strong reflection events up to approximately 500ms. Coupled with the borehole data from this area, we have identified the basalt deposit at the right corner marked by the green arrow in Figure 5-13. The strong reflection event in the centre of the stack is identified as potential basalt, which is marked by the red arrow. Other than these reflections, the deeper recordings of the data show no strong reflections and it would be a waste to just discard this information. Here I apply CFP redatum of sources and receivers from the surface to the strong events in an attempt to recover the reflection events in deeper area.

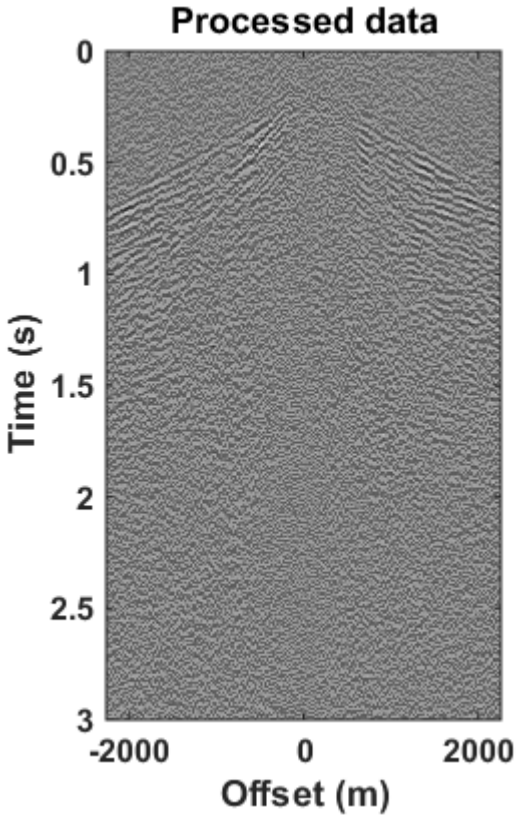

Figure 5-12: Processed common shot gather. S/N has been significantly improved and reflection responses can be observed.

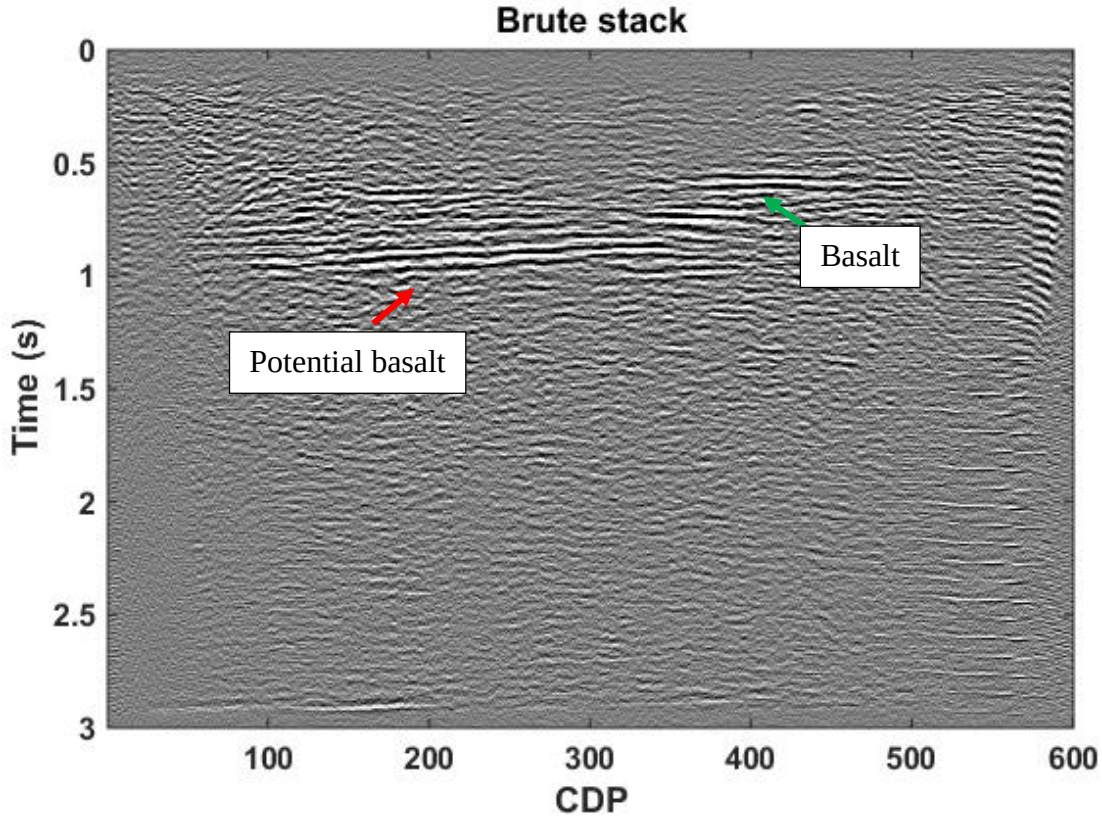

Figure 5-13: Brute stack of processed data. Strong reflection events marked by green arrow relate to the basalt deposit and the red arrow indicates the potential basalt.

5.2.2 CFP redatuming

As the seismic data does not have sufficient S/N, sorting the gathers to the common depth domain does not reveal strong reflection hyperboles. Therefore, this limits our options in deriving the focusing operator. Here, I estimate the focusing operator by using the strong event (potential basalt) observed in the stack section as the focusing point for CFP redatuming. This provides me with the required two-way time information of the peak of the hyperbola operator. By using the velocity used for the NMO and equation 5.1, we are able to compute the Green's function to be used as an operator to relocate the sources and receivers to the basement, as seen in the stack section.

$$t_i = \sqrt{t_0^2 + \left(\frac{s - r_i}{V}\right)^2}, \tag{5.1}$$

where t_0 is the zero-offset two-way traveltime from the surface to the basement, s is the source location, r_i is the receiver location and V is the NMO velocity. The result of applying this focusing operator to the processed data is shown in Figure 5-14 (b).

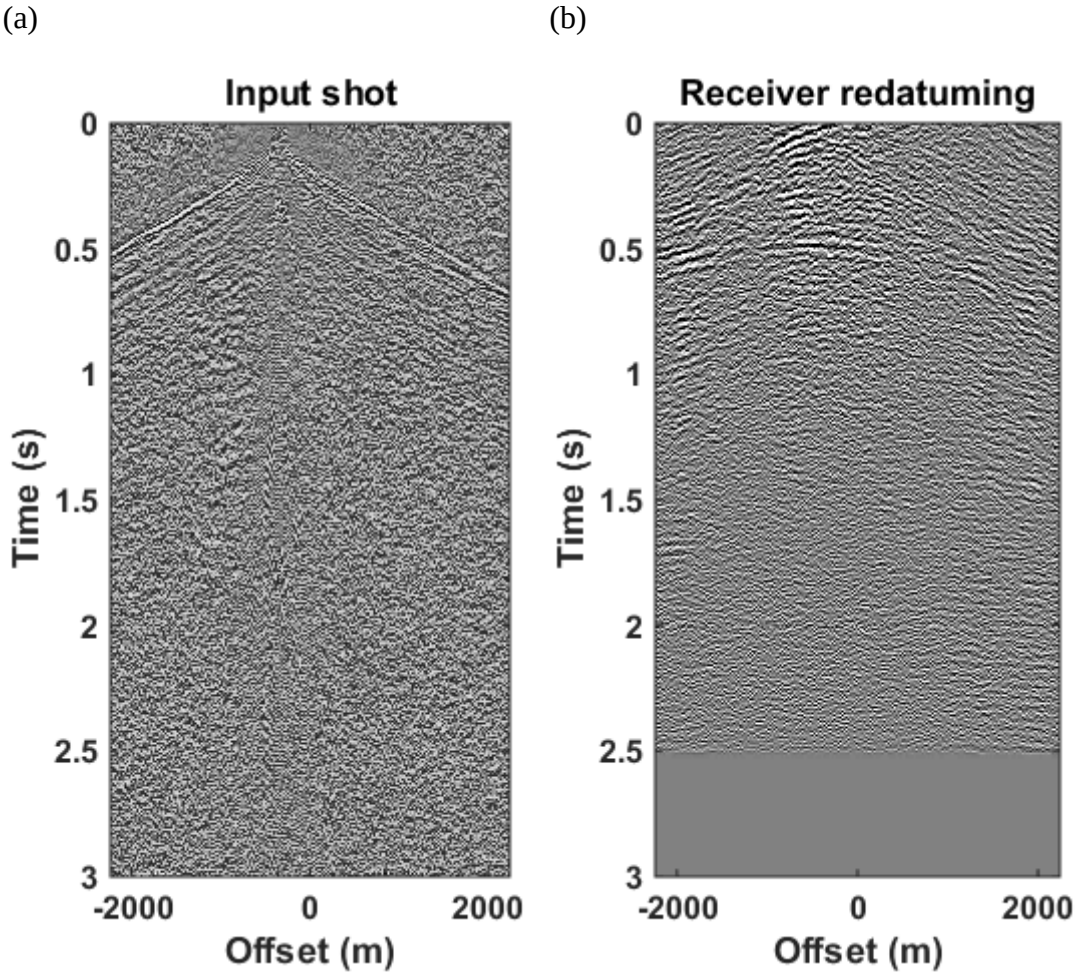

Figure 5-14: Comparison of (a) input and (b) receiver redatumed data in the common receiver domain.

After receiver redatuming, we can see a positive improvement in the data. Looking at the input data sorted in common receiver domain, as shown in Figure 5-14 (a), redatuming was able to improve the S/N and increase the resolution the reflection event, which is observed in Figure 5-14 (b). This reflector is the strong event seen on the stack section and has been classified as potential basalt, which is the reference reflector for this redatuming process. To determine whether our initial focusing operator is accurate, we obtain the DTS panel by convolving the receiver redatumed gathers with the focusing operator as shown in Figure 5-15. Here we note that the reference reflector has been transformed to a near-flat event at time zero as marked by the red arrow. This indicates that the focusing operator that we used was sufficiently accurate. Moving on from this, we apply the same focusing operator to the receiver redatumed data and obtained a result that has been source redatumed, as shown in Figure 5-16 (a). Strong linear events in the source and receiver redatuming output is attenuated using F-K filter as shown in Figure 5-16 (b).

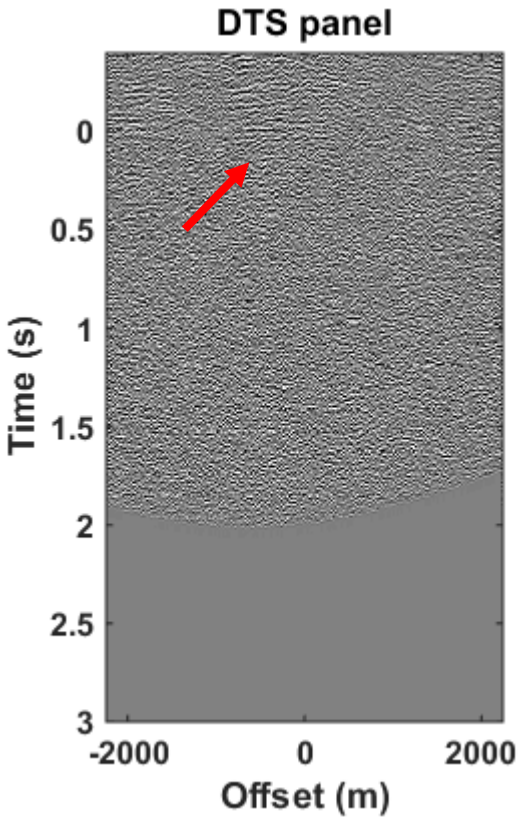

Figure 5-15: DTS panel. Flat event at time zero, as indicated by the red arrow, corresponds to the basement reflection, which is now our reference reflector.

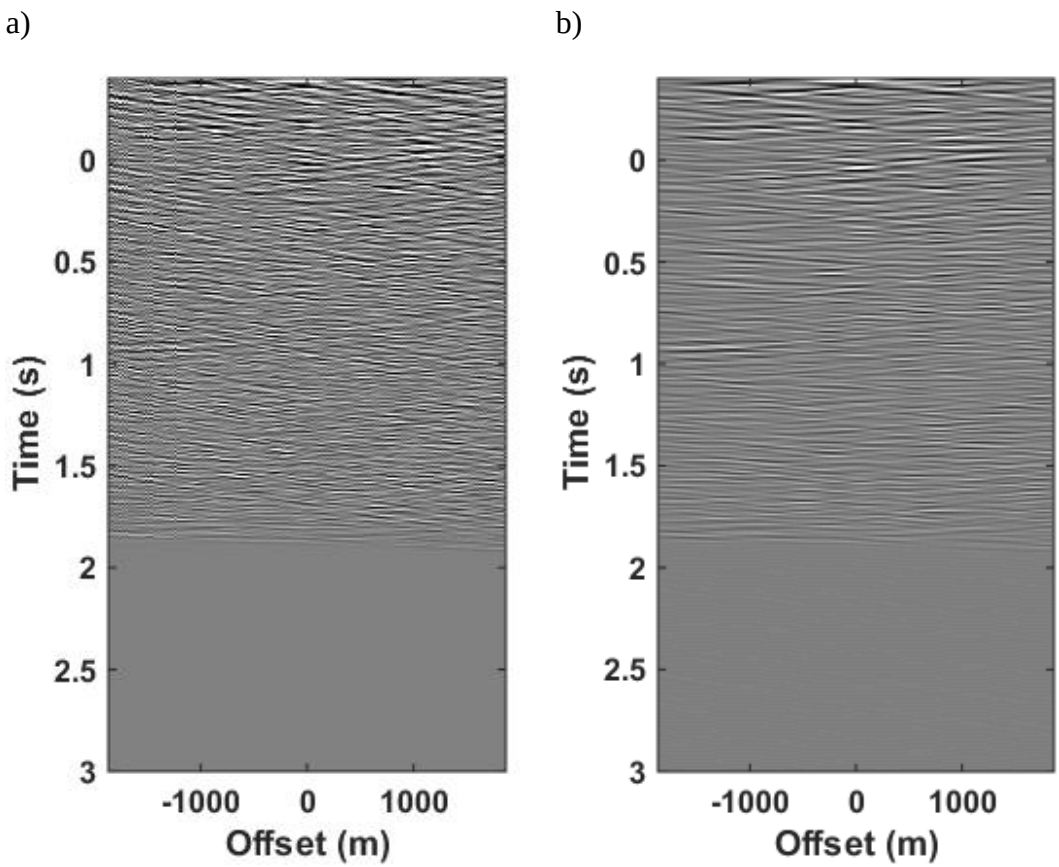

Figure 5-16: Source and receiver redatuming of input data (a) before F-K filter and (b) after FK filter.

5.2.3 Discussion

This CFP redatuming transforms the input data from the surface to a new datum in the subsurface, which in this case is the strong reflector at 1 s in the stack section. This event could not be identify in the gathers, therefore, the estimation of the focusing operator is calculated using the NMO velocities and the reflection event in the stack section. A good estimation of the kinematics for the focusing operator is obtained, which is indicated in the DTS panel as a flat event at time zero is observed. Despite this achievement, the result of both source and receiver redatuming, as shown in Figure 5-16 (a), is plagued with linear noise that dips downward from both edges of the output data. The application of the F-K filter to reduce this linear artefacts reveals weak near horizontal reflection events. This is likely due to the low S/N from the input, whereby the overwhelming noise has convolved with the focusing operator and therefore carried forward to the redatumed output. However in the receiver redatuming results, we notice the presence of possible reflections beneath the redatuming datum clearly,

which were not there in the input data. A possible way forward from here is to process and migrate just the receiver redatumed outputs. However, if a better quality hard-rock seismic data where present, we would be most likely able to achieve a better source and receiver redatuming result.

Chapter 6 Conclusion

6.1 Summary

In this thesis, I studied the application of wave equation redatuming mainly on synthetic dataset with complex subsurface and applied this technique to field data. Due to the low signal-to-noise ratio of the field data, redatuming result did not improve the imaging of events in noisy area. Hard-rock seismic data are often dominated by complex wave propagations generated in the geologically complex near surface. To resolve this challenge, the acquisition surface can be buried beneath the near-surface complexities but this is not a viable and economical option. However, we can virtually reposition the sources and receivers beneath this complex overburden. Redatuming aims to reconstruct seismic data from the recording surface to a new user-defined surface by virtually relocating the sources and receivers. This essentially removes the imprints from the near surface if the redatumed output is deeper in the subsurface. In essence, the redatuming framework requires detailed knowledge of the Green's function describing the one-way wave propagation between the acquisition surface and the new surface. This operator can be derived via a velocity model of the subsurface using the model-driven way or it can be derived in the data-driven way from the input data. The literature review (Chapter 2) summarises the existing methods to obtain the operator in the model- and data-driven methods.

There are several ways of estimating the Green's function. If the velocity of the overburden is known, then we can use the finite difference redatuming method presented in Chapter 3. Here, backpropagation is used to redatum the input data to remove the near-surface imprints with the use of the accurate velocity model. I have also verified the reciprocity theorem for different radiation pattern to allow for source redatuming, as presented in Section 3.3. As obtaining a detailed knowledge of the subsurface is challenging in a hard-rock environment, I investigate the feasibility of this method using a smoothed and RMS velocity models as an input. The results are comparable with the output from using the accurate velocity model; however, for the RMS velocity the method breaks down in far offsets and most of the imprints are unable to be removed from the data. In addition to that, this method can also produce finite difference artefacts that further contaminate the data.

With the challenges and limitations of the model-driven method in mind, I investigate the data-driven method on a synthetic dataset, which is presented in Chapter 4. I use the CFP method that uses a focusing operator, which is a time reverse of the Green's function between the recorded surface and new datum. Instead of requiring a detailed knowledge of the subsurface, this method requires the identification of a reference reflector to estimate the Green's function operator that can be updated, using the DTS panel, to achieve a better result. With the use of an accurate operator the results are comparable with the finite difference method. The operator for CFP redatuming is then estimated from the CMP gathers and with a few updates done, an accurate redatuming was achieved.

The CFP method does introduce some artefacts, which can be seen as the upward curving events above the direct wave and linear events dipping into the data from the edges. These artefacts are produced from the events above the reference reflector. To address this, I include an additional step in the conventional CFP method, which is a mute above the flat event seen in the DTS panel. After applying the mute, I transform the DTS panel back to the redatumed gathers and successfully remove these artefacts. Other artefacts in this method include the linear dipping events coming in from the edge of the data. The current CFP method does not account for the amplitude preservation, which contributes to the constructive interference of the linear artefacts and the reflection events. To rectify this, I apply an amplitude factor derived from the Kirchhoff migration, which further improves the quality of the redatuming.

The evaluation of these methods on synthetic data leads me to conclude that the CFP method has the best potential to be the most economical and efficient method in field data applications. However, in real hard-rock datasets, it would be difficult to pick a reference reflector due to all the scattering and diffraction of seismic energy from the near surface. I then investigate a novel approach to estimate the operator by using the kinematics of diffractions. Diffractors are used as they can be observed in the zero offset section and they also contain the information to estimate the Green's function. By picking these diffractions in the data and interpolating between them, I obtain an operator that produces a redatuming result that is comparable with the result from using the accurate focusing operator without performing any updating. Additionally,

the use of data collected over larger offset will provide a better estimation of the focusing operator and would also provide enough aperture to avoid the edge effects.

Based on the study of different wave equation redatuming techniques on synthetic data, I apply the CFP redatuming technique to field data using two case studies. In the first study, the CFP method is applied to soft-rock data whereby the data exhibits low resolution. The Green's function operator is estimated in the CMP domain and the redatumed results are promising, where a better continuation of reflections and reconstruction of a couple weak reflectors is achieved. Finally, I apply this method to hard-rock data with low signal-to-noise. Since weak reflection events are observed in the gathers and there are no prominent diffractors in the recorded data, operators are estimated from the brute stack section using the NMO velocities. Despite the redatuming result showing little observable improvement, a better-quality gather is obtained from the redatuming of the receivers only.

6.2 Discussion

CFP redatuming is a very versatile method that can be used to improve seismic imaging affected by near-surface complexities, as the focusing operator can be estimated through different approaches. Some of these estimation methods include the use of CMP gathers, diffractors and stack sections with NMO velocities as discussed in my thesis. We observe that redatuming works particularly well in data with good signal-to-noise; however, breaks down when a low signal-to-noise data is used, as the noise convolves with the focusing operator and creates strong artefacts. Although my work shows the potential of using wave equation redatuming to further improve seismic imaging in challenging near-surface conditions—such as in many hard rock situations—some issues still exist that would benefit from further investigation.

Firstly, I have addressed the amplitude preservation of the CFP technique by applying an amplitude factor derived from the Kirchhoff migration. This has improved the quality of redatuming by reducing the effects of the artefacts on reflection events. However, to fully account for the phase changes during the redatuming, one should also account for the phase shift analogous to the time derivative in the Kirchhoff migration.

The second issue to address is the iterative updating of focusing operator using the DTS panel. Currently, the processor would have to pick the events manually from the DTS panel in order to apply the correct kinematics to update the focusing operator, which can be a tedious task, especially with larger dataset. The next step would be to automate this process if possible. One possible approach could be to look at the cross-correlation of the traces in the DTS panels as a 3D volume to estimate the necessary time shifts.

As a final remark, the application of redatuming in this thesis is performed on complex 2D seismic field data. For a more reliable image of the subsurface, 3D seismic data would be useful as the effects from propagation from all directions will be accounted for.

Appendices

Appendix I – Copyright Consent

From: Pietro Guj <pietro.guj@uwa.edu.au>
Sent: Saturday, 24 September 2016 8:08 AM
To: Kai Fu Kevin Ung
Subject: Re: Copyright permission

Dear Kai

I see no impediments for you to use those figures subject to reference.

Best luck with your study.

Sent from my Samsung Galaxy smartphone.

-------- Original message --------
From: Kai Fu Kevin Ung <k.ung@postgrad.curtin.edu.au>
Date:23/09/2016 7:43 PM (GMT+08:00)
To: Pietro Guj <pietro.guj@uwa.edu.au>
Cc:
Subject: Copyright permission

Dear Dr. Pietro,

I am a PhD student at the Department of Exploration Geophysics of Curtin University, Perth, Western Australia. In my doctoral thesis entitled "Redatuming of Hard Rock Seismic", I would like to include Figure 6 and Figure 16 from the following publication:

"Schodde, R. C., and P. Guj. 2012. "Where Are Australia's Mines of Tomorrow." *Centre for Exploration Targeting, University of Western Australia, September.* "

Once completed, the thesis will be made available in the hard-copy format at Curtin Library and digital format on the website: http://library.curtin.edu.au/find-resources/theses/. The material will be provided strictly for educational purposes and on a non-commercial basis.

I would be grateful to you for your consent to the copying and republishing of the above-mentioned figures. I would be willing to use a specific form of acknowledgement that you may require and to communicate any conditions related to the use of the material.

If you are not the copyright owner of the referred material, I would be grateful for any information you can provide as to who is likely to hold the copyright. I look forward to hearing from you and thank you in advance for your consideration of my request.

Kind Regards,
Kevin Kai Fu, Ung
PhD Candidate
Department of Exploration Geophysics | Western Australia School of Mines
[Postal Address: GPO Box U1987, Perth, Western Australia School of Mines] (Bld 613, Rm 4H23)
[Street Address: ARRC/CSIRO Building, H Block, Level 4, 26 Dick Perry Avenue, Kensington 6151, WA]

Curtin University
Tel | +61 8 9266 3521


Rightslink® by Copyrigh
Secure | https://s100.copyright.com/AppDispatchServlet#formTop
Copyright Clearance Center
RightsLink®
Home
Create Account
Help
Taylor & Francis
Taylor & Francis Group
Title: Time reversal in acoustics
Author: M. Fink
Publication: Contemporary Physics
Publisher: Taylor & Francis
Date: Mar 1, 1996
Copyright © 1996 Taylor & Francis
LOGIN
If you're a copyright.com user, you can login to RightsLink using your copyright.com credentials. Already a RightsLink user or want to learn more?
Thesis/Dissertation Reuse Request
Taylor & Francis is pleased to offer reuses of its content for a thesis or dissertation free of charge contingent on resubmission of permission request if work is published.
BACK
CLOSE WINDOW
Copyright © 2017 Copyright Clearance Center, Inc. All Rights Reserved. Privacy statement. Terms and Conditions.
Comments? We would like to hear from you. E-mail us at customercare@copyright.com

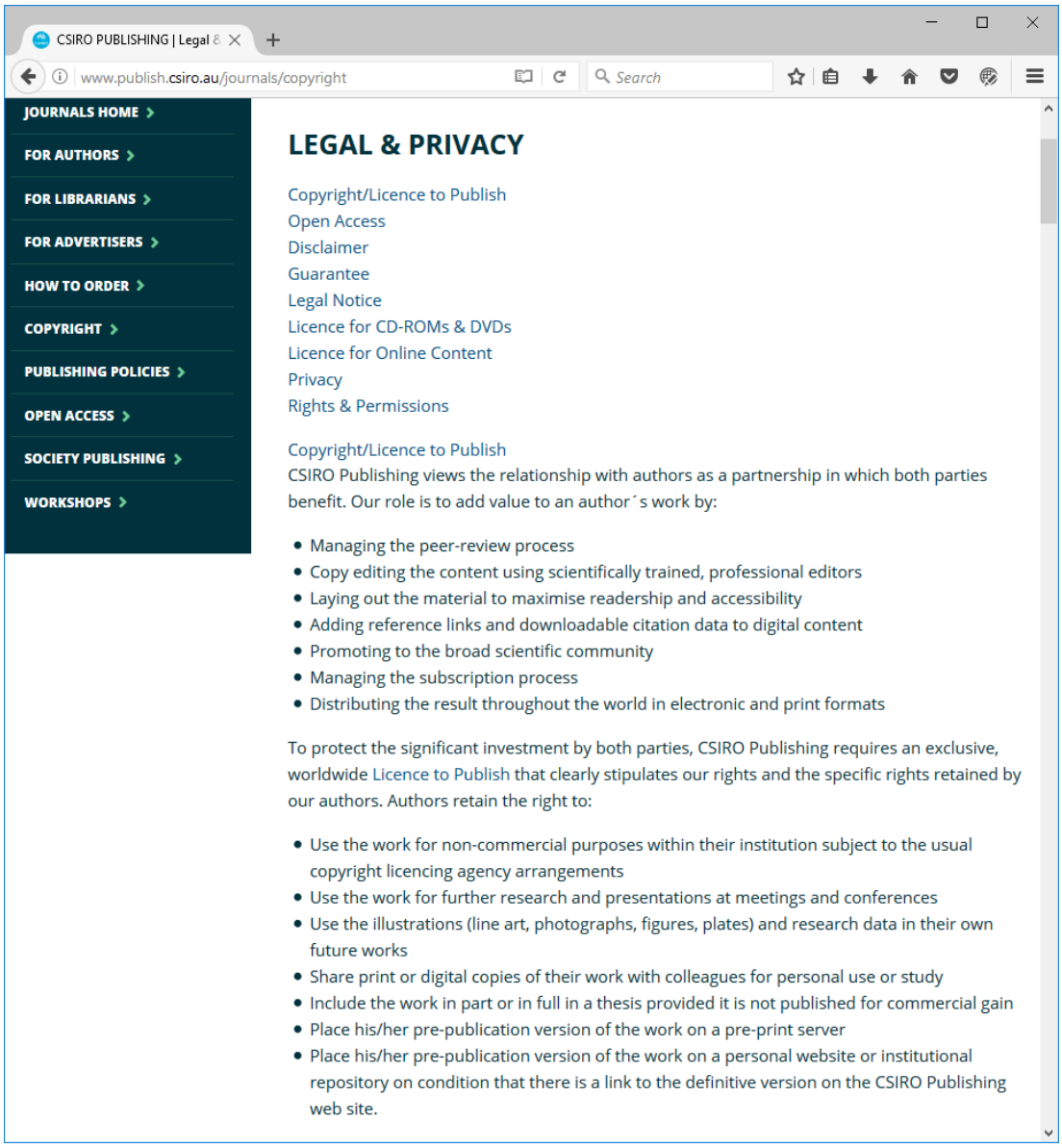
CSIRO PUBLISHING | Legal &
www.publish.csiro.au/journals/copyright
Search
JOURNALS HOME
FOR AUTHORS
FOR LIBRARIANS
FOR ADVERTISERS
HOW TO ORDER
COPYRIGHT
PUBLISHING POLICIES
OPEN ACCESS
SOCIETY PUBLISHING
WORKSHOPS
LEGAL & PRIVACY
Copyright/Licence to Publish
Open Access
Disclaimer
Guarantee
Legal Notice
Licence for CD-ROMs & DVDs
Licence for Online Content
Privacy
Rights & Permissions
Copyright/Licence to Publish
CSIRO Publishing views the relationship with authors as a partnership in which both parties benefit. Our role is to add value to an author´s work by:
Managing the peer-review process
Copy editing the content using scientifically trained, professional editors
Laying out the material to maximise readership and accessibility
Adding reference links and downloadable citation data to digital content
Promoting to the broad scientific community
Managing the subscription process
Distributing the result throughout the world in electronic and print formats
To protect the significant investment by both parties, CSIRO Publishing requires an exclusive, worldwide Licence to Publish that clearly stipulates our rights and the specific rights retained by our authors. Authors retain the right to:
Use the work for non-commercial purposes within their institution subject to the usual copyright licencing agency arrangements
Use the work for further research and presentations at meetings and conferences
Use the illustrations (line art, photographs, figures, plates) and research data in their own future works
Share print or digital copies of their work with colleagues for personal use or study
Include the work in part or in full in a thesis provided it is not published for commercial gain
Place his/her pre-publication version of the work on a pre-print server
Place his/her pre-publication version of the work on a personal website or institutional repository on condition that there is a link to the definitive version on the CSIRO Publishing web site.

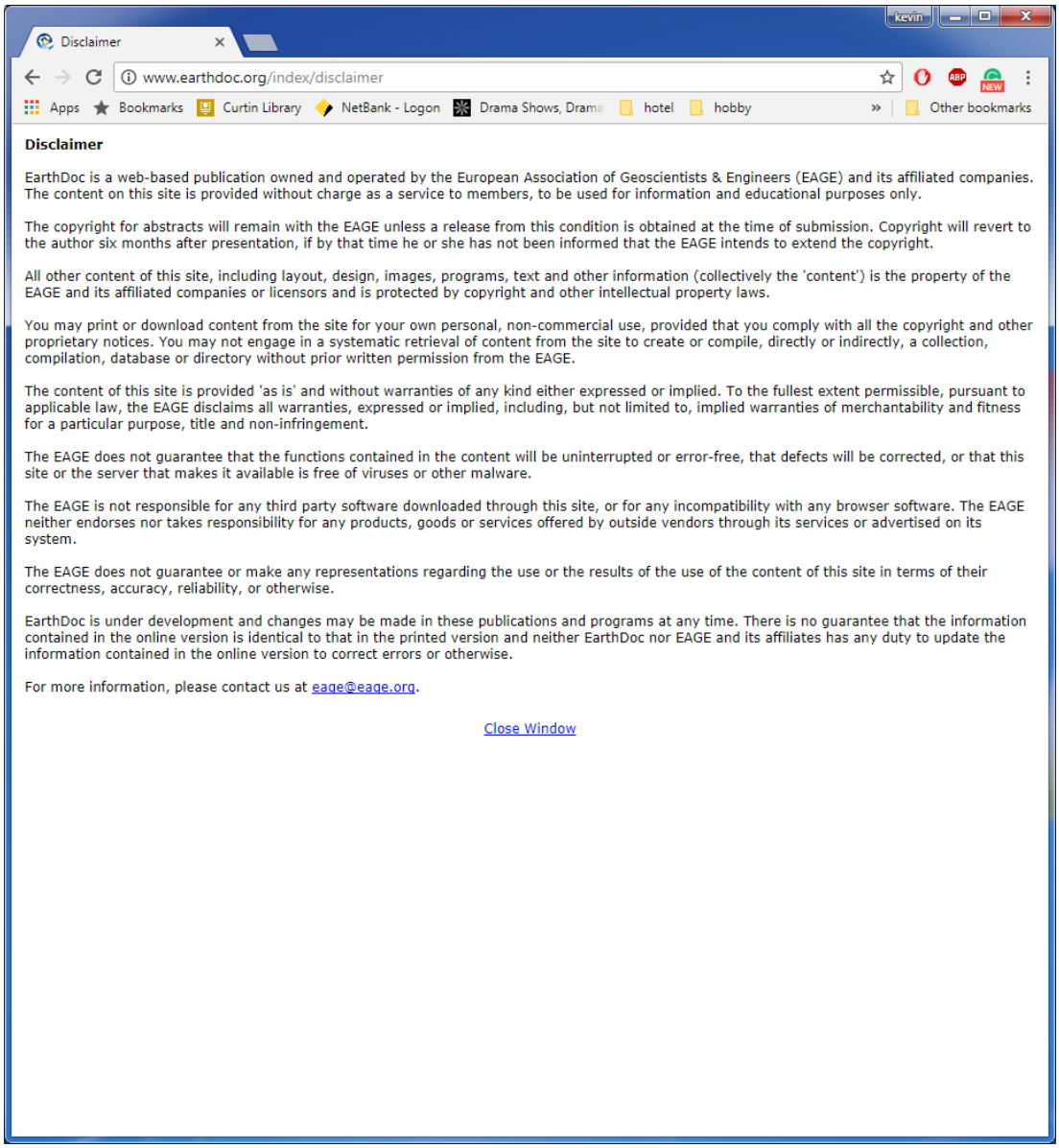
kevin
Disclaimer
www.earthdoc.org/index/disclaimer
Apps
Bookmarks
Curtin Library
NetBank - Logon
Drama Shows, Drama
hotel
hobby
Other bookmarks
Disclaimer
EarthDoc is a web-based publication owned and operated by the European Association of Geoscientists & Engineers (EAGE) and its affiliated companies. The content on this site is provided without charge as a service to members, to be used for information and educational purposes only.
The copyright for abstracts will remain with the EAGE unless a release from this condition is obtained at the time of submission. Copyright will revert to the author six months after presentation, if by that time he or she has not been informed that the EAGE intends to extend the copyright.
All other content of this site, including layout, design, images, programs, text and other information (collectively the 'content') is the property of the EAGE and its affiliated companies or licensors and is protected by copyright and other intellectual property laws.
You may print or download content from the site for your own personal, non-commercial use, provided that you comply with all the copyright and other proprietary notices. You may not engage in a systematic retrieval of content from the site to create or compile, directly or indirectly, a collection, compilation, database or directory without prior written permission from the EAGE.
The content of this site is provided 'as is' and without warranties of any kind either expressed or implied. To the fullest extent permissible, pursuant to applicable law, the EAGE disclaims all warranties, expressed or implied, including, but not limited to, implied warranties of merchantability and fitness for a particular purpose, title and non-infringement.
The EAGE does not guarantee that the functions contained in the content will be uninterrupted or error-free, that defects will be corrected, or that this site or the server that makes it available is free of viruses or other malware.
The EAGE is not responsible for any third party software downloaded through this site, or for any incompatibility with any browser software. The EAGE neither endorses nor takes responsibility for any products, goods or services offered by outside vendors through its services or advertised on its system.
The EAGE does not guarantee or make any representations regarding the use or the results of the use of the content of this site in terms of their correctness, accuracy, reliability, or otherwise.
EarthDoc is under development and changes may be made in these publications and programs at any time. There is no guarantee that the information contained in the online version is identical to that in the printed version and neither EarthDoc nor EAGE and its affiliates has any duty to update the information contained in the online version to correct errors or otherwise.
For more information, please contact us at eage@eage.org.
Close Window

Reference List

Achenbach, J. D., 2006, Reciprocity and Related Topics in Elastodynamics: Applied Mechanics Reviews, **59**, no. 1, 13-32, doi: 10.1115/1.2110262.

Aki, K., and P. G. Richards, 2002, Quantitative Seismology Second Edition: Sausalito, California, University Science Books.

Bakulin, A., and R. Calvert, 2004, Virtual Source: New Method for Imaging and 4d Below Complex Overburden: In Seg Technical Program Expanded Abstracts 2004, 2477-2480.

Barison, Erika, Giuseppe Brancatelli, Rinaldo Nicolich, Flavio Accaino, Michela Giustiniani, and Umberta Tinivella, 2011, Wave Equation Datuming Applied to Marine Obs Data and to Land High Resolution Seismic Profiling: Journal of Applied Geophysics, **73**, no. 3, 267-277, doi: https://doi.org/10.1016/j.jappgeo.2011.01.009.

Bean, Christopher J., and Francesca Martini, 2010, Sub-Basalt Seismic Imaging Using Optical-to-Acoustic Model Building and Wave Equation Datuming Processing: Marine and Petroleum Geology, **27**, no. 2, 555-562, doi: https://doi.org/10.1016/j.marpetgeo.2009.09.007.

Berkhout, A. J., 1980, Seismic Migration, Imaging of Acoustic Energy by Wave Field Extrapolation, A. Theoretical Aspects: Elsevier. Science Publishing Co.

Berkhout, A. J., 1982, Imaging of Acoustic Energy by Wave Field Extrapolation: Amsterdam, Elsevier.

Berkhout, A. J., 1996, Seismic Processing between Two Focusing Steps: In Seg Technical Program Expanded Abstracts 1996, 403-406.

Berkhout, A. J., 1997a, Pushing the Limits of Seismic Imaging, Part I: Prestack Migration in Terms of Double Dynamic Focusing: Geophysics, **62**, no. 3, 937-953, doi: 10.1190/1.1444201.

Berkhout, A. J., 1997b, Pushing the Limits of Seismic Imaging, Part Ii: Integration of Prestack Migration, Velocity Estimation, and Avo Analysis: Geophysics, **62**, no. 3, 954-969, doi: 10.1190/1.1444202.

Berkhout, A. J., and D. J. Verschuur, 2005, Removal of Internal Multiples with the Common-Focus-Point (Cfp) Approach: Part 1 — Explanation of the Theory: Geophysics, **70**, no. 3, V45-V60, doi: 10.1190/1.1925753.

Berkovitch, A., I. Belfer, Y. Hassin, and E. Landa, 2009, Diffraction Imaging by Multifocusing: Geophysics, **74**, no. 6, WCA75-WCA81, doi: 10.1190/1.3198210.

Berryhill, J., 1979, Wave-Equation Datuming: Geophysics, **44**, no. 8, 1329-1344, doi: doi:10.1190/1.1441010.

Berryhill, J., 1984, Wave-Equation Datuming before Stack: Geophysics, **49**, no. 11, 2064-2066, doi: doi:10.1190/1.1441620.

Bevc, D., 1995, Imaging under Rugged Topography and Complex Velocity Structure: PhD, Stanford University, Ann Arbor.

Bohlen, T., 2002, Parallel 3-D Viscoelastic Finite Difference Seismic Modelling: Computers & Geosciences, **28**, no. 8, 887-899, doi: http://dx.doi.org/10.1016/S0098-3004(02)00006-7.

Britt, A. F., D. Summerfield, A. Whitaker, P. Kay, D.C. Champion, D. Huston, A. B. Senior et al., 2015, Australia's Identified Mineral Resources 2015, Canberra, Australia. doi: http://dx.doi.org/10.11636/1327-1466.2015.

Claerbout, J. F., and S. M. Doherty, 1972, Downward Continuation of Moveout-Corrected Seismograms: Geophysics, **37**, no. 5, 741-768, doi: 10.1190/1.1440298.

Cox, B. E., and D. J. Verschuur, 2001, Data-Driven Tomographic Inversion of Focusing Operators: In Seg Technical Program Expanded Abstracts 2001, 722-725.

Cox, M., 1999, Static Corrections for Seismic Reflection Surveys, Static Corrections for Seismic Reflection Surveys: Tulsa, Okla, Society of Exploration Geophysicists.

Fink, M., 1992, Time Reversal of Ultrasonic Fields. I. Basic Principles: IEEE Transactions on Ultrasonics, Ferroelectrics, and Frequency Control, **39**, no. 5, 555-566, doi: 10.1109/58.156174.

Fink, M., 1996, Time Reversal in Acoustics: Contemporary Physics, **37**, no. 2, 95-109, doi: 10.1080/00107519608230338.

Fokkema, J. T., and P. M. van den Berg, 1993, Seismic Application of Acoustic Reciprocity: Amsterdam, Elsevier.

Fomel, S., E. Landa, and M. T. Taner, 2007, Poststack Velocity Analysis by Separation and Imaging of Seismic Diffractions: Geophysics, **72**, no. 6, U89-U94, doi: 10.1190/1.2781533.

Fouque, J-P, J. Garnier, G. Papanicolaou, and K. Sølna, 2007, Wave Propagation and Time Reversal in Randomly Layered Media: Springer New York.

Gangi, A. F., 1970, A Derivation of the Seismic Representation Theorem Using Seismic Reciprocity: Journal of Geophysical Research, **75**, no. 11, 2088-2095, doi: 10.1029/JB075i011p02088.

Gazdag, J., 1978, Wave Equation Migration with the Phase-Shift Method: Geophysics, **43**, no. 7, 1342-1351, doi: 10.1190/1.1440899.

Gazdag, J., and P. Sguazzero, 1984, Migration of Seismic Data by Phase Shift Plus Interpolation: Geophysics, **49**, no. 2, 124-131, doi: 10.1190/1.1441643.

Green, A. G., and J. A. Mair, 1983, Subhorizontal Fractures in a Granitic Pluton; Their Detection and Implications for Radioactive Waste

Disposal: Geophysics, **48**, no. 11, 1428-1449, doi: 10.1190/1.1441428.

Gupta, I. N., 1965, Note on the Use of Reciprocity Theorem for Obtaining Radiation Patterns: Bulletin of the Seismological Society of America, **55**, no. 2, 277-281.

Gupta, I. N., 1966, Use of Reciprocity Theorem for Obtaining Rayleigh Wave Radiation Patterns: Bulletin of the Seismological Society of America, **56**, no. 4, 925-936.

Hecht, E., 1987, Optics, 2nd ed: Reading, Mass, Addison-Wesley Pub. Co.

Hindriks, C. O. H., and D. J. Verschuur, 2001, Common Focus Point Approach to Complex near Surface Effects: In SEG Technical Program Expanded Abstracts 2001, 1863-1866, doi: 10.1190/1.1816495.

Joseph, A. Olowofela, D. Akinyemi Olukayode, and O. Ajani Olumide, 2016, Effect of Grid Step Sizes on Computational Time Using Finite-Difference Method for Seismic Wave Modeling: Applied and Computational Mathematics, **5**, no. 2, 56-63, doi: 10.11648/j.acm.20160502.14.

Kabir, M., M. Nurul, and D. J. Verschuur, 1996, Migration Velocity Analysis Using the Common Focus Point Technology: In Seg Technical Program Expanded Abstracts 1996, 407-410.

Kelamis, P. G., K. E. Erickson, T. Taner, D. J. Verschuur, and A. J. Berkhout, 2000, Cfp-Based Redatuming: Synthetic and Field Data Examples: In Seg Technical Program Expanded Abstracts 2000, 509-512.

Kelamis, P. G., K. E. Erickson, D. J. Verschuur, and A. J. Berkhout, 2002, Velocity-Independent Redatuming: A New Approach to the near-Surface Problem in Land Seismic Data Processing: The Leading Edge, **21**, no. 8, 730-735, doi: 10.1190/1.1503185.

Kelamis, P. G., E. Verschuur, A. J. Berkhout, and K. E. Erickson, 1999, Velocity-Independent Datuming of Seismic Data: In Seg Technical Program Expanded Abstracts 1999, 441-444.

Klokov, A., and S. Fomel, 2012, Separation and Imaging of Seismic Diffractions Using Migrated Dip-Angle Gathers: Geophysics, **77**, no. 6, S131-S143, doi: 10.1190/geo2012-0017.1.

Knopoff, L., and A. Gangi, 1959, Seismic Reciprocity: Geophysics, **24**, no. 4, 681-691, doi: doi:10.1190/1.1438647.

Larkin, Steven P., and Alan Levander, 1996, Wave-Equation Datuming for Improving Deep Crustal Seismic Images: Tectonophysics, **264**, no. 1, 371-379, doi: https://doi.org/10.1016/S0040-1951(96)00137-0.

Mahapatra, M., and S. Mahapatra, 2009, Seismic Diffraction Tomography Technique Using Very Fast Simulated Annealing Method for Delineating Small Subsurface Features: Journal of Applied Geophysics, **67**, no. 2, 125-129, doi: https://doi.org/10.1016/j.jappgeo.2008.10.004.

Malehmir, A., R. Durrheim, G. Bellefleur, M. Urosevic, C. Juhlin, D. J. White, B. Milkereit, and G. Campbell, 2012, Seismic Methods in Mineral Exploration and Mine Planning: A General Overview of Past and Present Case Histories and a Look into the Future: Geophysics, **77**, no. 5, WC173–WC190, doi: 10.1190/GEO2012-0028.1.

Maxwell, J. C., 1864, A Dynamical Theory of the Electromagnetic Field: Proceedings of the Royal Society of London, **13**, 531-536, doi: 10.2307/112081.

McAvaney, S. O., C. B. E. Krapf, M. Werner, M. J. Pawley, B. E. Nicolson, and J. A. Irvine, 2017, Six Mile Hill Mapping Provides New Insights into the Southern Gawler Craton: Accessed 27th August 2017, http://www.minerals.statedevelopment.sa.gov.au/knowledge_centre/mesa_journal/previous_feature_articles/six_mile_hill_mapping_reveals_new_insights_into_the_southern_gawler_craton.

McKay, A.D., Y. Miezitis, K. Porritt, A.F. Britt, D.C. Champion, S. Cadman, R. Towner et al., 2014, Australia's Identified Mineral Resources 2013, Canberra, Australia. http://dx.doi.org/10.11636/1327-1466.2013.

Morton, S. A., and J. Thorbecke, 1996, Automating Prestack Migration Analysis Using Common Focal Point Gathers: In Seg Technical Program Expanded Abstracts 1996, 411-414.

Mulder, W. A., 2005, Rigorous Redatuming: Geophysical Journal International, **161**, no. 2, 401-415, doi: 10.1111/j.1365-246X.2005.02615.x.

Papanicolaou, G., K. Solna, and L. Ryzhik, 2004, Statistical Stability in Time Reversal: SIAM Journal on Applied Mathematics, **64**, no. 4, 1133-1155, doi: doi:10.1137/S0036139902411107.

Pevzner, R., D. Lumley, M. Urosevic, B. Gurevich, A. Bóna, S Ziramov, V. Rasouli et al., 2013, Advance Geophysical Data Analysis at Harvey-1: Storage Site Characterization and Stability Assessment.

Pretorius, C. C., A. Jamison, and C. Irons, 1989, Seismic Exploration in the Witwatersrand Basin, Republic of South Africa: Proceedings of Exploration '87, Ontario Geol. Surv., Spec, **3**, 241-253.

Rickett, J., and J. Claerbout, 1999, Acoustic Daylight Imaging Via Spectral Factorization: Helioseismology and Reservoir Monitoring: The Leading Edge, **18**, no. 8, 957-960, doi: doi:10.1190/1.1438420.

Salisbury, M. H., M. Bernd, G. Ascough, R. Adair, L. Matthews, D. R. Schmitt, J. Mwenifumbo, D. W. Eaton, and J. Wu, 2000, Physical Properties and Seismic Imaging of Massive Sulfides: Geophysics, **65**, no. 6, 1882-1889, doi: 10.1190/1.1444872.

Salisbury, M., and D. Snyder, 2007, Application of Seismic Methods to Mineral Exploration in Mineral Deposits of Canada: A Synthesis of Major Deposit-Types, District Metallogeny, the Evolution of Geological Provinces, and Exploration Methods, edited by W.D. Goodfellow, 971–982. Geological Association of Canada, Mineral Deposits Division, Special Publication No. **5**.

Salisbury, Matthew H., Craig W. Harvey, and Larry Matthews, 2003, The Acoustic Properties of Ores and Host Rocks in Hardrock Terranes: In Hardrock Seismic Exploration, 9-19.

Schneider, W. A., 1978, Integral Formulation for Migration in Two and Three Dimensions: Geophysics, **43**, no. 1, 49-76, doi: 10.1190/1.1440828.

Schodde, R. C., and P. Guj, 2012, Where Are Australia's Mines of Tomorrow: Centre for Exploration Targeting, University of Western Australia.

Schuster, G. T., J. Yu, J. Sheng, and J. Rickett, 2004, Interferometric/Daylight Seismic Imaging: Geophysical Journal International, **157**, no. 2, 838-852, doi: 10.1111/j.1365-246X.2004.02251.x.

Schuster, G., and M. Zhou, 2006, A Theoretical Overview of Model-Based and Correlation-Based Redatuming Methods: Geophysics **71**, no. 4, SI103-SI110, doi: doi:10.1190/1.2208967.

Shtivelman, V., and A. Canning, 1988, Datum Correction by Wave-Equation Extrapolation: Geophysics, **53**, no. 10, 1311-1322, doi: 10.1190/1.1442409.

Sølna, K., 2002, Focusing of Time-Reversed Reflections: Wave Random Media, **12**, 365-385.

Tinivella, U., M. Giustiniani, and I. Vargas-Cordero, 2017, Wave Equation Datuming Applied to Seismic Data in Shallow Water Environment and Post-Critical Water Bottom Reflection: Energies, **10**, no. 9, 1414, doi: http://dx.doi.org.dbgw.lis.curtin.edu.au/10.3390/en10091414.

Ung, K., and A. Bona, 2016, Comparison on Finite-Difference and Common Focusing Point Redatuming Technique for Hard Rock Seismic. in Near Surface Geoscience 2016 - First Conference on Geophysics for Mineral Exploration and Mining. , Barcelona,Spain.

Ung, K., A. Bona, and M. Madadi, 2015, Reciprocity Principle in Finite Difference Modelling of Waves in Elastic Media: ASEG Extended Abstracts, 1-4, doi: https://doi.org/10.1071/ASEG2015AB266.

Urosevic, M., and C. Juhlin, 2007, An Analysis of Seismic Information Obtained from Crooked Line Seismic Survey in Crystalline Rocks, Australia: In Eage 69th Conference & Exhibition. London UK.

Urosevic, M., A. Kepic, E. Stolz, and C. Juhlin, 2007, Seismic Exploration of Ore Deposits in Western Australia: Proceedings of Exploration 07: Fifth Decennial International Conference on Mineral Exploration,

Urosevic, M., S. Ziramov, R. Pevzner, and A. Kepic, 2014, Harvey 2d Test Seismic Survey - Issues and Optimisations.

van Borselen, R., J. Fokkema, and P. van den Berg, 2013, Wavefield Decomposition Based on Acoustic Reciprocity: Theory and Applications to Marine Acquisition: Geophysics, **78**, no. 2, WA41-WA54, doi: doi:10.1190/geo2012-0332.1.

Wapenaar, K., D. Draganov, J. Thorbecke, and J. Fokkema, 2002, Theory of Acoustic Daylight Imaging Revisited: In Seg Technical Program Expanded Abstracts 2002, 2269-2272.

White, J., 1960, Use of Reciprocity Theorem for Computation of Low-Frequency Radiation Patterns: Geophysics, **25**, no. 3, 613-624, doi: doi:10.1190/1.1438742.

Yilmaz, O., 2001, Seismic Data Analysis: Processing, Inversion, and Interpretation of Seismic Data, Edited by Stephen M. Doherty: Tulsa, OK, Society of Exploration Geophysicists.

Zhan, Y., 2014, 2d Seismic Interpretation of the Harvey Area, Southern Perth Basin, Western Australia, Geological Survey of Western Australia, Record 2014/7, 25p.